AN INVESTIGATION INTO THE MECHANISM OF TOXICITY OF ZINC OXIDE NANOPARTICLES

Vyom Sharma BSc, MSc

Submitted for the degree of
Doctor of Philosophy

School of Life Sciences
University of Bradford

United Kingdom

2011

Abstract

The wide scale use of ZnO nanoparticles (NPs) in the world consumer market has resulted in likelihood of exposure to human beings. The present study was aimed to assess the *in vitro* and *in vivo* interactions of ZnO NPs in the mammalian system and to elucidate the possible mechanism of their toxicity.

Our *in vitro* results using human epidermal cells (A431), primary human epidermal keratinocytes and human liver cells (HepG2) demonstrated that cells exposed to ZnO NPs exhibit a decrease in cell viability which was independent of NP dissolution. ZnO NPs also induced oxidative DNA damage as evidenced by an increase in the Fpg sensitive sites. The reactive oxygen species triggered a decrease in mitochondrial membrane potential and an increase in the ratio of Bax/Bcl2 leading to apoptosis through the intrinsic pathway. In addition, ZnO NPs induced phosphorylation of JNK, P38 and $P53^{ser15}$. The results from our *in vivo* studies using a mouse model showed that ZnO NPs induce lipid peroxidation, oxidative DNA damage and apoptosis in liver which further confirmed our *in vitro* findings.

The data from the present study provide valuable insights into the cellular interactions of ZnO NPs and the underlying molecular mechanism of their toxicity. The results also stress the need for a comprehensive environmental health and safety assessment of engineered nanomaterials to ensure safer nanotechnology based products.

Acknowledgements

I would like to convey my deepest regards and gratitude to my supervisors Professor Alok Dhawan, Indian Institute of Toxicology Research, India and Professor Diana Anderson, University of Bradford, United Kingdom for their guidance, support and constant encouragement throughout this study.

This work would not have been possible without the generous financial support and collaborative research opportunity provided under the UK-India Education and Research Initiative (UKIERI) program.

I wish to acknowledge my colleagues and members of the Nanomaterial Toxicology Group, Indian Institute of Toxicology Research, India and the School of Life Sciences, University of Bradford, United Kingdom for their cooperation and help whenever required.

I would like to thank my family for their unconditional love, care and encouragement.

Finally, I thank God for providing me this opportunity as well as faith and strength.

CONTENTS

Abstract ii

Acknowledgement iii

Contents 1

Abbreviations 5

List of figures 8

List of tables 14

Chapter 1. Introduction 15

1.1. Nanoparticles 16

1.1.1. Different types of nanoparticles 16

1.2. Nanoparticle/ nanomaterial toxicity 19

1.3. Biological responses to nanomaterials exposure 22

1.4. Exposure to nanoparticles 27

1.4.1. Exposure sources 27

1.4.1.1. Occupational exposure at work place 27

1.4.1.2. Exposure through consumer product 27

1.4.1.3. Exposure through unintentional Release 27

1.4.2. Exposure routes 27

1.4.2.1. Inhalation exposure 28

1.4.2.2. Dermal exposure 29

1.4.2.3. Gastrointestinal exposure 30

1.5. Characterization of nanoparticles 31

1.5.1. Brunauer-Emmett-Teller (BET) method 32

1.5.2. Electron microscopy 33

1.5.3. Dynamic light scattering 33

1.6. Nanoparticle internalization in biological systems 34

1.6.1. Electron microscopy 36

1.6.2. Inductively coupled plasma mass spectroscopy 37
1.6.3. Flow cytometry 37
1.7. Agglomeration and dispersion 40
1.8. Oxidative stress 43
1.8.1. Effect on DNA 44
1.8.2. Effect on apoptosis 45
1.8.3. Effect on cell membrane 45
1.8.4. Measurement of oxidative stress in cells 45
1.8.4.1. ROS generation 45
1.8.4.2. Lipid peroxidation 46
1.8.4.3. Glutathione 46
1.8.4.4. Superoxide dismutase 47
1.8.4.5. Catalase 47
1.9. Genotoxicity 48
1.9.1. Types of DNA damage 48
1.9.2. Nanoparticle induced DNA damage 49
1.9.2.1. Direct interactions with the DNA 49
1.9.2.2. Oxidative DNA damage 51
1.9.3. Comet assay/ Single cell gel electrophoresis 52
1.9.3.1. Principle 52
1.9.3.2. Advantages 53
1.10. Apoptosis 53
1.10.1. Intrinsic apoptotic pathway 54
1.10.2. Extrinsic apoptotic pathway 54
1.11. Mitogen activated protein kinase (MAPK) signalling pathways 56
1.11.1. Extracellular-signal-regulated kinase pathway 57
1.11.2. JNK pathway 58
1.11.3. p38 pathway 58

1.12. Zinc oxide nanoparticles 59
1.13. Aims and objectives of the study 62
Chapter 2. Materials and Methods 63
2.1. Chemicals 66
2.2. Characterization of nanoparticles 66
2.2.1. Dynamic light scattering 67
2.2.2. Transmission electron microscopy 67
2.3. Cellular uptake of nanoparticles 67
2.3.1. Flow cytometry 67
2.3.2. Electron microscopy 67
2.4. Cytotoxicity assays 68
2.4.1. MTT assay 68
2.4.2. Neutral red uptake assay 69
2.4.3. Lactate dehydrogenase release assay 69
2.5. Assays for oxidative stress markers 70
2.5.1. Reactive oxygen species measurement 70
2.5.2. Lipid peroxidation assay 71
2.5.3. Catalase assay 72
2.5.4. Superoxide dismutase assay 74
2.5.5. Glutathione estimation 75
2.6. Cell viability using Trypan blue 75
2.7. Comet assay/ Single cell gel electrophoresis (SCGE) 76
2.7.1 Standard alkaline Comet assay 76
2.7.2. Fpg-modified Comet assay 77
2.8. Detection of apoptosis 78
2.8.1. AnnexinV/PI staining 78
2.8.2. Hoechst staining 79
2.9. Assessment of mitochondrial membrane potential 80
2.10. Western blot analysis 81

2.11. *In vivo* studies 84

2.11.1. Animals and treatment 84

2.11.2. Zn content analysis in tissues 85

2.11.3. Biochemical assays in serum 85

2.11.4. Lipid peroxidation assay 85

2.11.5. Histopathology 86

2.11.6. TUNEL assay 87

2.12. Statistical analysis 88

Chapter 3. Toxic responses to ZnO nanoparticles in human epidermal cells 89

3.1. Introduction 90

3.2. Materials and methods 92

3.3. Results 94

3.4. Discussion 99

Chapter 4. Mechanism of toxicity of ZnO nanoparticles 113

4.1. Introduction 114

4.2. Materials and methods 118

4.3. Results 122

4.4. Discussion 128

Chapter 5. *In vivo* toxicity of ZnO nanoparticles in mice 153

5.1. Introduction 154

5.2. Materials and methods 156

5.3. Results 158

5.4. Discussion 160

Chapter 6. General Discussion 169

6.1. General discussion 169

6.2. Future work 171

References 172

Presentations and publications originating from this study 196

ABBREVIATIONS

AAS: Atomic absorption spectroscopy

ALP: Alkaline phosphatase

ALT: Alanine aminotransferase

BET: Brunauer-Emmett-Teller

BSE-SEM: Back scattered electron-scanning electron microscopy

BSI: British standards Institution

BUN: Blood Urea nitrogen

CMEM: Complete minimal essential medium

CNT: Carbon nanotubes

COC: Committee on carcinogenicity

COM: Committee on mutagenicity

COT: Committee on toxicity

DAPI: 4, 6-diamidino-2-phenylindole

DCFDA: 2,7-Dichlorofluorescein diacetate

DLS: Dynamic light scattering

DMEM: Dulbecco's modified eagle medium

DNA: Deoxyribonucleic acid

EDTA: Ethylenediaminetetraacetic acid

EHS: Environmental health and safety

EMS: Ethyl methane-sulphonate

ERK: Extracellular signal- regulated protein kinase

EtBr: Ethidium bromide

FBS: Foetal bovine serum

FPG: Formamidopyrimidine DNA glycosylage

GSH: Glutathione

JC-1: 5,5′,6,6′-tetrachloro-1,1′,3,3′-tetraethylbenzimidazolcarbocyanine iodide

JNK: c-Jun N-terminal kinase

KGM2: Keratinocyte growth medium 2

LDH: Lactate dehydrogenase release

LMA: Low melting agarose

LPO: Lipid peroxidation

MAPK: Mitogen activated protein kinase

MEM: Minimal essential medium

MMP: Mitochondrial membrane potential

MTT: 3-(4,5-dimethylthiazoyl-2-yl)-2,5-diphenyltetrazolium bromide

MWCNT: Multiwalled carbon nanotube

NAC: N-acetylcysteine

NF-kB: Nuclear factor kappa B

NMA: Normal melting agarose

NP: Nanoparticle

NRU: Neutral red uptake

OECD: Organization for economic cooperation and development

OTM: Olive tail moment

PBS: Phosphate buffer saline

PI: Propidium iodide

QD: Quantum dot

REACH: Registration, Evaluation, Authorisation and Restriction of Chemicals

ROS: Reactive oxygen species

RS/RAE: Royal Society and Royal Academy of Engineering

SAPK: Stress activated protein kinase

SEM: Standard error of mean

SCENIHR: Scientific Committee on Emerging and Newly Identified Health Risks

SCCP: Scientific Committee on Consumer Products

SCGE: Single cell gel electrophoresis

SOD: Superoxide dismutase

SWCNT: Single walled carbon nanotube

TEM: Transmission electron microscopy

TiO_2: Titanium dioxide

TUNEL: Terminal deoxynucleotidyl transferase dUTP nick end labeling

USEPA: United States Environmental Protection Agency

ZnO: Zinc oxide

LIST OF FIGURES

Figure 1.1. Applications of engineered nanoparticles in the consumer products.

Figure 1.2. Surface molecules as a function of particle size.

Figure 1.3. Size- surface area- reactivity paradigm for nanoparticles (Downward and upward arrow points to a decrease and increase respectively in concerned properties).

Figure 1.4. Possible exposure to nanoparticles. (Source: Nanosciences and nanotechnologies: Opportunities and Uncertainties, Royal Society/Royal Academy of Engineering, 2004).

Figure 1.5. Inferred pathways of nanoparticle uptake. (1) Clathrin mediated endocytosis; (2) Caveolae-mediated endocytosis; (3) Clathrin and caveolae-independent endocytosis. Early-endo- early endosome; endo-lyso- late endosome-lysosome; recy-endo- recycling endosome; ER- endoplasmic reticulum; NPC- nuclear pore complex.

Figure 1.6. Analysing nanoparticle (NP) uptake in cells by flow cytometry- (A) Light scattering by a cell having no association with any nanoparticle; (B) Nanoparticles adhered to cell surface leading to increase in forward scatter (FSC) and side scatter (SSC); (C) Nanoparticle internalization by cell leading to increase in SSC alone; (D) Fluorescent nanoparticle internalization by cell leading to increase in SSC and fluorescent intensity (FL).

Figure 1.7. Schematic showing the phenomenon of agglomeration of nanoparticles.

Figure 1.8. Spectrum of DNA damage induced by physical and chemical agents (adapted from Casserette and Doull;s “Toxicology: the basic science of poison” Genetic Toxicology, pp 326).

Figure 1.9. The intrinsic and extrinsic apoptotic pathway.

Figure 1.10. Mammalian MAPK cacades. There are four major mammalian MAPKKK–MAPKK–MAPK protein kinase cascades. The ERK pathway is commonly activated by growth factors, the JNK, p38 and ERK5 pathways are activated by environmental stress.

Figure 1.11. Scattering of light for 100nm and 200nm ZnO particles. (Source: www.nanosense.org).

Figure 1.12. Interaction of visible light with different sized particles of ZnO (A) Large particles (>200nm) scatter visible light (B) Nanoparticles (<100nm) do not scatter visible light and let it interact with melanin (Source: www.nanosense.org).

Figure 2.1. Cell marked with comet parameters.

Figure 3.1. Characterization of ZnO NPs (A-B) Hydrodynamic diameter and zeta potential in DMEM medium (C-D) Hydrodynamic diameter and zeta potential in KGM-2 medium (E) TEM microphotograph of ZnO NPs.

Figure 3.2. TEM microphotographs of human epidermal cells (A431) (A) Control cells (B) Cells treated with ZnO NPs depicting intracellular localization of ZnO NPs (black arrow).

Figure 3.3. Cytotoxic effect of ZnO NPs in human epidermal cells (A431) as assessed by (a) MTT assay; (b) Neutral red uptake assay; (c) Lactate dehydrogenase release assay. Data are expressed as the percentage viability of cells exposed to ZnO NPs relative to control cells and are mean ± S.E.M. of triplicates.*$p < 0.05$, compared to control.

Figure 3.4. Morphology of human epidermal cells (A431) (A) normal, and ZnO NP treated (B) 8µg/ml for 6h, (C) 8µg/ml for 24h, (D) 8µg/ml for 48h. Magnification X100.

Figure 3.5. Effect of ZnO NPs on the oxidative stress markers in human epidermal cells (A431) (A) lipid peroxidation, (B) glutathione content, (C) catalase activity and (D) superoxide dismutase activity. Data represent mean± S.E.M. of three experiments. *$p < 0.05$, compared to control.

Figure 3.6. Scanning electron microscopy (back scattered electron imaging) microphotographs of primary human epidermal keratinocytes. (A) Control cells (B) Cells treated with ZnO NPs (14 µg/ml) for 6 h showing ZnO NP agglomerates *(white arrow)* inside cells.

Figure 3.7. Transmission electron microscopy microphotographs of primary human epidermal keratinocytes. (A) Control cells (B) Cells treated with ZnO NPs (14µg/ml) for 6h depicting intracellular localization ZnO NPs *(black arrow)* (C) High power view shows localization of these nanoparticles in the filopodia.

Figure 3.8. Concentration and time dependent cytotoxicity of ZnO NPs in primary human epidermal keratinocytes. Data are expressed as the percentage viability of cells exposed to ZnO NPs relative to control cells and are mean ± S.E.M. of triplicates.*p < 0.05, compared to control.

Figure 3.9. Morphology of primary human epidermal keratinocytes (A) Control cells and (B) Cells treated with ZnO NPs (20µg/ml) for 6 h. Magnification X100.

Figure 3.10. A representation of results from this study depicting the ZnO NPs induced cellular toxicity.

Figure 4.1. Schematic diagram of the study design.

Figure 4.2. Characterization of ZnO NPs; (A) Hydrodynamic diameter; (B) Zeta potential.

Figure 4.3. Cellular uptake of ZnO NPs in HepG2 cells as assessed by the flow cytometry (A) Control (B-D) ZnO NPs exposed cells.

Figure 4.4. Cytotoxic effect of ZnO NPs in HepG2 cells as assessed by (A) MTT assay; (B) Neutral red uptake assay; (C) Lactate dehydrogenase.

Figure 4.5. Photomicrographs showing generation of the intracellular reactive oxygen species using DCFDA dye in HepG2 cells (A) Control cells; (B) Cells exposed to ZnO NPs for 6h showing increase in fluorescence (Magnification X200).

Figure 4.6. Effect of N-acetyl cysteine (NAC) on ZnO NP induced oxidative DNA damage in HepG2 cells; Data represents mean ± S.E.M. of three experiments.*$p < 0.05$ when compared to control using one way ANOVA in Fpg-modified Comet assay. $^{\alpha}p < 0.05$ using when compared to "(-) NAC" at the same concentration using the Student 't' test.

Figure 4.7. HepG2 cells treated with ZnO NPs showing oxidative DNA damage (magnification X400) (A) Control cells in standard alkaline Comet assay; (B) Control cells in Fpg-modified Comet assay; (C) ZnO NPs (20µg/ml) treated HepG2 cell in standard Comet assay; (D) ZnO NPs (20µg/ml) treated HepG2 cell in Fpg-modified Comet assay.

Figure 4.8. ZnO NPs induced apoptosis in HepG2 cells - (A) Control cells; (B) Cells treated with 14µg/ml ZnO NPs; (C) Cells treated with 20µg/ml ZnO NPs. Quadrants: Q1- necrotic cells; Q2- necrotic cells or late phase of apoptotic cells; Q3- unstained live cells, Q4- Early apoptotic cells. Representative dot plots of three independent experiments are presented. Data represent mean ± S.E.M. of three experiments.

Figure 4.9. Fluorescence images of cells stained with Hoechst 33342. ZnO NP treated cells show apoptotic cells with condensed or fragmented nuclei (indicated by arrows).

Figure 4.10. ZnO NPs induced mitochondrial membrane potential (MMP) changes in HepG2 cells - (A) Control cells; (B) Cells exposed to 14µg/ml ZnO NPs; (C) Cells exposed to 20µg/ml ZnO NPs.

Figure 4.11. Fluorescence images of ZnO NP induced changes in MMP in HepG2 cells. The first (extreme left) column showing only green fluorescence (aggregated form of JC-1), the second (middle) column showing only red fluorescence (monomeric form of JC-1), the third (extreme right) column showing overlay (red-green fluorescence).

Figure 4.12. Western blot analysis of proteins involved in apoptosis: (A) Bax, Bcl2, NF-kβ expression levels, caspase-9 activation and $p53^{Ser15}$ phosphorylation. β-actin was used as internal control to normalize the data. (B-C) Relative quantification of protein expression levels. Data represent mean ± S.E.M. of three experiments.*$p < 0.05$, compared to control.

Figure 4.13. Western blot analysis of proteins involved in MAPK signalling in HepG2 cells - (A) Effect of ZnO NPs exposure. (B) Relative quantification of protein expression levels. Quantification was done using scion image software. Data represent mean ± S.E.M of three experiments.*$p < 0.05$, compared to control.

Figure 4.14. Effect of NAC on ZnO NP induced MAPK signalling.

Figure 4.15. Effect of MAPK inhibition and N-acetylcysteine on ZnO NPs induced cytotoxicity in HepG2 cells. Data represent mean±S.E.M. of three experiments.*$p < 0.05$, compared to cell treated with ZnO NPs only.

Figure 4.16. Effect of N-acetylcysteine on mitochondrial mediated apoptosis (A) Effect of N-acetylcysteine on ZnO NPs induced loss of MMP. Data represent mean ± S.E.M. of three experiments. *$p<0.05$ when compared to control. $^{\alpha}p<0.05$ using when compared to “without NAC” at the same concentration. (B) Effect of N-acetylcysteine on ZnO NPs induced Bax, Bcl_2

and p53 phosphorylation. β-actin was used as internal control to normalize the data. Blots shown are representative of three different experiments.

Figure 4.17. Effect of dissolution on ZnO NPs induced cytotoxicity (A) Assessment of cytotoxicity of Zn^{2+} released into the medium from ZnO NPs. (B) Assessment of Zn^{2+} released from ZnO NPs. (C) Assessment of cytotoxicity of released Zn^{2+} using $ZnCl_2$ as the reference standard. The cytotoxicity was assessed by the MTT assay after 6, 12, and 24h exposure. Data represent mean ± S.E.M. of three experiments.

Figure 4.18. Possible mechanisms involved in ZnO NPs induced toxicity in human liver cells.

Figure 5.1. Zinc content in selected tissue of the mice (n=3) after oral administration of ZnO NPs (300mg/Kg) for 14 consecutive days. Data represent mean ± S.E.M. of three animals.*$p < 0.05$, compared to control.

Figure 5.2. Histopathology of liver and kidney tissues in mice treated with ZnO NPs for 14 consecutive days (A-B) Control group showing normal liver and kidney (B-C) Pathological alterations in the liver and kidney of ZnO NPs (300mg/Kg) treated group (indicated by arrow); Magnification (X200).

Figure 5.3. ZnO NPs induced apoptosis in the liver cells of mice as detected by the TUNEL assay. Representative images (X400) of TUNEL positive cells (green fluorescence) in the liver sections of (A) Control mice (B-C) Mice exposed to ZnO NPs (300 and 50 mg/Kg) through oral route for 14 consecutive days.

LIST OF TABLES

Table 1.1. Toxicological effects of some widely used nanoparticles (NPs).

Table 2.1. The techniques used in the present study.

Table 3.1. DNA damage by ZnO NPs after 6h exposure to human epidermal cells (A431) as evident by the comet parameters.

Table 3.2. DNA damage by ZnO NPs after 6 h exposure to primary human epidermal keratinocytes as evident by the comet parameters.

Table 4.1. Effect of ZnO NPs on the ROS generation and lipid peroxidation in HepG2 cells after 6h exposure.

Table 4.2. Induction of DNA strand breaks and oxidative DNA damage in human liver cells after 6h exposure to ZnO nanoparticles as evident by the Comet parameters.

Table 5.1. Body weights and organ weights of mice after oral exposure to ZnO nanoparticles.

Table 5.2. Serum biochemistry parameters in mice after oral exposure to ZnO nanoparticles (300mg/kg) for 14 consecutive days.

Table 5.3. Effect of ZnO NPs on lipid peroxidation (LPO)[a] in different organs of mouse.

Table 5.4. Effect of ZnO NPs on Comet parameters in liver and kidney cells of mice after oral exposure to ZnO nanoparticles for 14 consecutive days.

CHAPTER – 1

Introduction

1.1. Nanoparticles

Nanotechnology holds great potential for creating new materials with enhanced properties. A number of nanotech based products are finding applications in industries, medical devices, imaging, sports, biosensing, electronics, drugs, environmental cleanup, cosmetics and sunscreens etc (NCPI 2011; USEPA 2007). The global economy will be increasingly influenced by nanotechnology as more products containing nanomaterials move from research and development into production and commerce (Figure 1.1).

A nanometre (nm) is one billionth of a metre (10^{-9} m) — about half the size of the diameter of DNA. The prefix *nano* is derived from the Greek word for 'dwarf'. The definition for the 'Nanoparticle' given in the new PAS71 document developed by the UK's National Standards Body- British Standards Institution (BSI) is: "A particle having one or more dimensions of the order of 100nm or less" (PAS71 2005). Nanoparticles are also called as ultrafine particles by some toxicologists (USEPA 2007), aitken mode and nucleation mode particles by atmospheric scientists (Kulmala 2004; NRC 1983), and engineered nanoparticles by the materials scientists (NNI 2004).

1.1.1. Different types of nanoparticles: Nanoparticles can be classified into two main categories: natural and anthropogenic nanoparticles. Natural nanoparticles existed in the environment long before the nanotechnology era started. Examples of natural nanoparticles include soil colloids, airborne nano-crystals of sea salts, fullerenes, carbon nanotubes, biogenic magnetite, etc. (Buffle 2006; Nowack and Bucheli 2007). Soils contain many kinds of inorganic and organic nanoparticles, namely clay minerals, metal oxides and

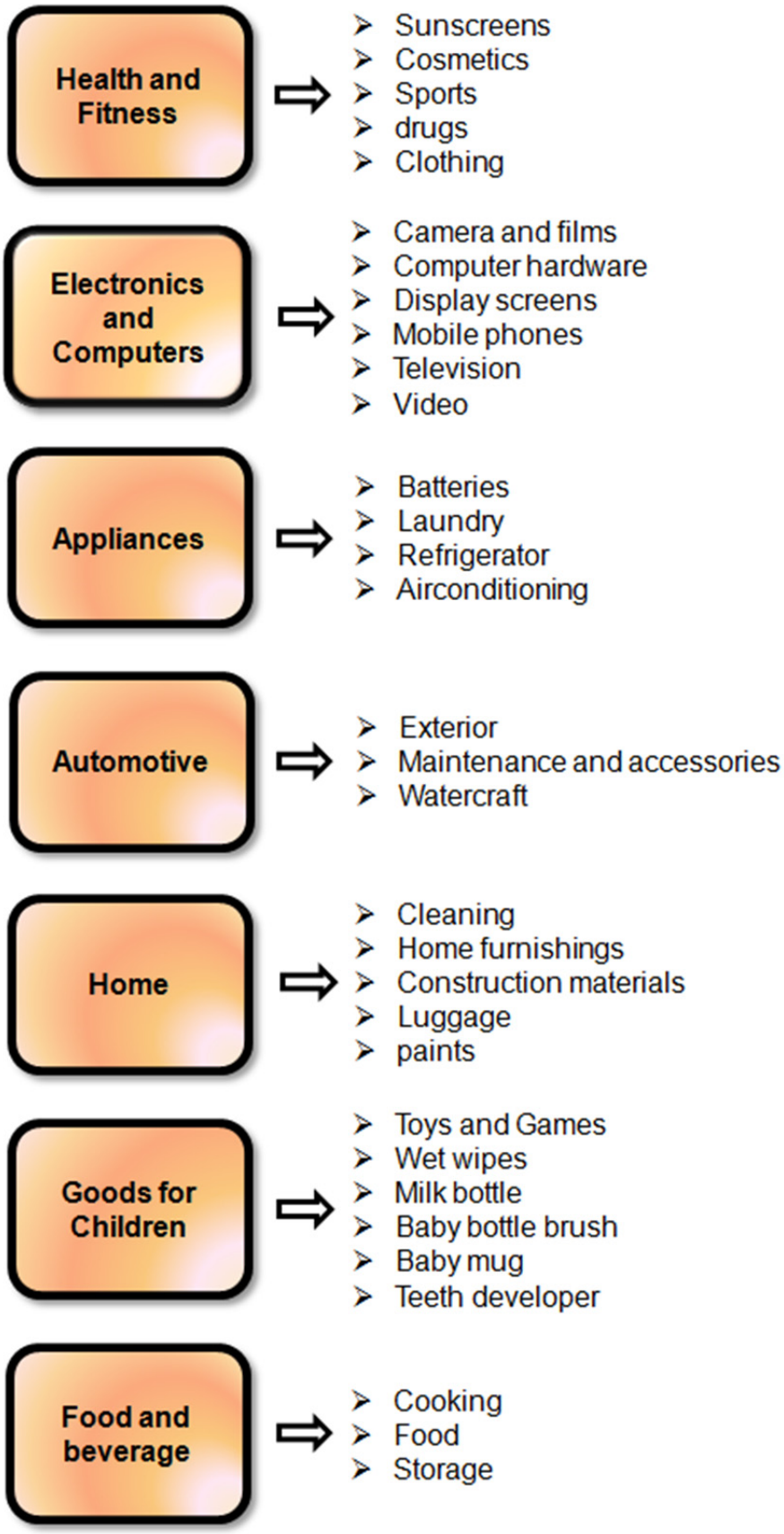

Figure 1.1. Applications of engineered nanoparticles in the consumer products.

hydroxides, humic substances, allophane, and imogolite (Theng and Yuan 2008). Organic nanoparticles can also be found in natural vegetation (Xia et al. 2010). Anthropogenic nanoparticles can be further divided into two categories: incidental, which are nanoparticles produced unintentionally in manmade processes (e.g., carbon black, carbon nanotubes and fullerenes, platinum- and rhodium-containing nanoparticles from combustion by-products (Nowack and Bucheli 2007), and engineered/manufactured, which are nanoparticles that are produced intentionally due to their nano-specific properties.

A variety of engineered nanomaterials are already known and more novel materials are being engineered. The different ways to produce engineered nanoparticles can be categorised in two different classes: “top-down” or “bottom-up”. Top down techniques involve etching or milling down a block of material to desired shape whereas bottom up involves arranging smaller subunits into more complex assemblies (RS/RAE 2004).

Some of the most widely used nanomaterials are listed below:

Carbon-based nanomaterials- These nanomaterials are composed mostly of carbon, in the shape of a hollow spheres or tubes. Spherical carbon nanomaterials are referred to as fullerenes, while cylindrical ones are called carbon nanotubes (CNT). There are two types of CNT- single-walled carbon nanotube (SWCNT) or multi-walled carbon nanotube (MWCNT). Both of these are typically a few nanometres in diameter and several micrometres to centimetres long (RS/RAE 2004).

Metal/ Metal oxide nanoparticles/ nanomaterials- Metal oxide nanoparticles have applications in cosmetics, textiles, fuels, drug delivery

and paints. Examples include silver, gold, zinc oxide aluminium oxide, cerium oxide and titanium dioxide nanoparticles.

Quantum dots – Quantum dots (QD) are semiconductor nanocrystals used extensively in biomedical imaging. Fluorescent QDs can be conjugated with bioactive moieties (e.g., antibodies, receptor, ligands) to target specific biologic events and cellular structures (Hardman 2006).

Dendrimers- Dendrimers are spherical polymeric molecules, formed through a nanoscale hierarchical self-assembly process. Dendrimers can act as nanoscale carrier molecules and as such could be used in drug delivery (RS/RAE 2004).

1.2. Nanoparticle/ nanomaterials toxicity

At the nanoscale, the materials have a high surface area to volume ratio compared to the same mass of material produced in larger form, as the ratio of surface to total atoms or molecules increases exponentially with decreasing particle size (Figure 1.2) (Oberdorster et al. 2005). This leads to high surface reactivity which affects their strength and physical properties.

Although the small size and subsequent larger surface area of nanoparticles endow them with some highly useful and specific properties, it also renders them biologically more active (Figure 1.3) leading to unexpected and unanticipated consequences on interaction with biological systems. Smaller size also imparts a different biokinetic behaviour and ability to reach more distal regions of the body compared to their larger counterparts (Oberdorster et al. 2005). The occupational exposure will also increase with the growing production and use of nanomaterials in society. Environmental contamination is yet another concern. All these apprehensions have

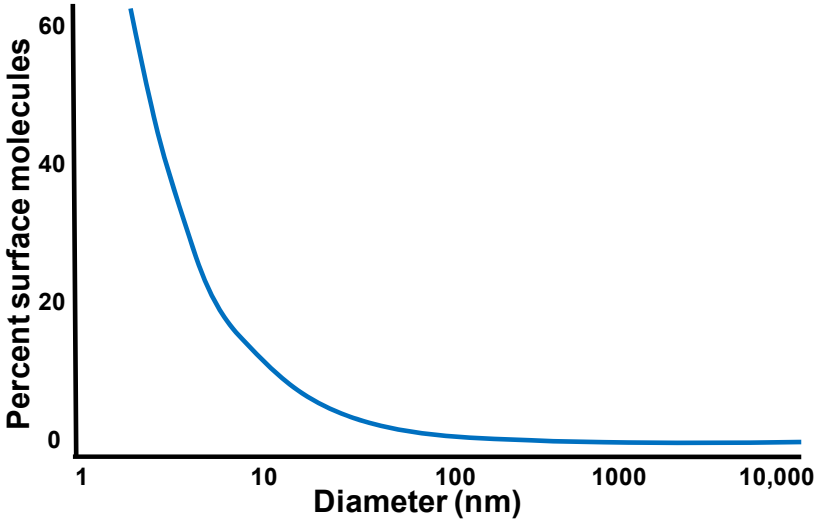

Figure 1.2. Surface molecules as a function of particle size (Oberdorster et al. 2005)

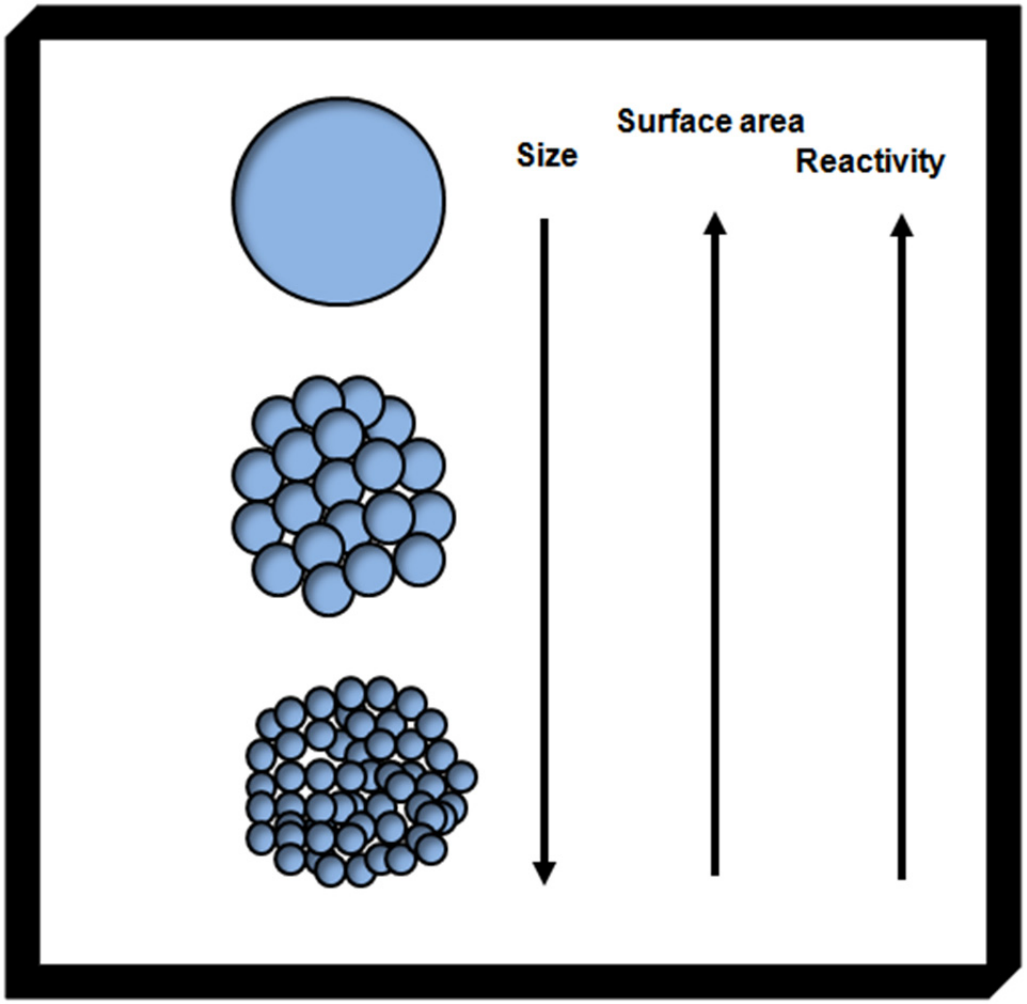

Figure 1.3. Size- surface area- reactivity paradigm for nanoparticles (Downward and upward arrow points to a decrease and increase respectively in concerned properties).

generated a public debate over understanding and managing the potential adverse effects of engineered nanomaterials on human health and the environment.

Government/ regulatory authorities regarding EHS of nanotechnology: Governments and scientific authorities all over the world are realizing the importance of nanomaterials risk assessment and have undertaken efforts in the area. In June 2003, the UK Government commissioned The Royal Society and The Royal Academy of Engineering to look into the ethical, health and safety issues related to nanotechnology. In their report "Nanoscience and Nanotechnologies: Opportunities and Uncertainties" published in 2004, The Royal Society recommended that "chemicals in the form of nanoparticles or nanotubes should be treated as new substances under the existing Notification of New Substances (NONS) regulations and in the Registration, Evaluation, Authorisation and Restriction of Chemicals (REACH)" to trigger additional testing for these nanomaterials (RS/RAE 2004). Committees on the Toxicity, Carcinogenicity and Mutagenicity of Chemicals in Food, Consumer Products and the Environment have also identified the risk assessment of nanomaterials as an area of interest in their 'Joint Statement on Nanomaterials Toxicology'(COT;COM;COC 2005). United States Environmental Protection Agency (USEPA) while recognizing the potential benefits of nanotechnology has also stressed on the need for a responsible development of nanotechnology and a proactive approach. In its document- EPA 100/B-07/001 (Nanotechnology White Paper) published in 2007, it stated **"***as the use of nanomaterials in society increases, it is reasonable to assume that their presence in environmental media will*

increase proportionately, with consequences for human and environmental exposure" (USEPA 2007). The European Commission's Scientific Committee on Emerging and Newly Identified Health Risks (SCENIHR) has also reviewed the existing literature and issues to be considered in conducting risk assessment on nanomaterials (SCENIHR 2009). European Commission's Scientific Committee on Consumer Products (SCCP) issued a document titled "Opinion On Safety of Nanomaterials in Cosmetic Products" and raised a concern about large data gaps, inappropriateness of existing methodologies for nanoparticle risk assessment and inadequate information regarding nanoparticles skin absorption in both normal and abnormal (diseased) skins (SCCP 2007). Guidance documents on safe handling of nanomaterials are also being drafted by researchers (Dhawan et al. 2011). The non-governmental organisations like the Friends of the Earth warned against nanotechnology in cosmetic and sunscreen products, since they may produce a possible uptake of particles by human skin: *if nanoparticles penetrate the skin, they can join the bloodstream and circulate around the body with uptake by cells, tissues and organs* (FOE 2006).

1.3. Biological responses to nanomaterials exposure

The concerns and awareness related to health and safety aspects of nanoparticles have culminated in a number of scientific publications concerning toxicological evaluation of nanomaterials. Some of the major biological effects exhibited by different categories of nanomaterials have been summarized in Table 1.1.

Table1.1. Toxicological effects of some widely used nanoparticles (NPs).

Type of NPs	Toxic effects	References
MWCNT	*In vitro* studies: DNA damage, oxidative stress, apoptosis in mammalian cells; disrupt actin filament integrity and VE-cadherin distribution in human aortic endothelial cells.	(Cheng et al. 2009a; Cveticanin et al. 2010; Patlolla et al. 2010a; Ravichandran et al. 2009; Reddy et al. 2010; Walker et al. 2009)
	In vivo studies: Pulmonary toxicity-asbestos-like, length-dependent, pathogenic behaviour; induce inflammation, formation of granuloma, cytotoxicity and rapid development of fibrosis in lungs; apoptosis of alveolar macrophages.	(Crouzier et al. 2010; Elgrabli et al. 2008; Han et al. 2010; Ma-Hock et al. 2009; Poland et al. 2008; Porter et al. 2010)
	Promote allergic response in mice; increased chromosomal aberrations and micronuclei frequency; suppression of systemic immune function through activation of cyclooxygenase enzymes in the spleen; spotty necrosis, inflammatory cell infiltration in portal region, hepatocyte mitochondria swelling and altered gene expression in liver.	(Ji et al. 2009; Mitchell et al. 2009; Nygaard et al. 2009; Park et al. 2009; Patlolla et al. 2010b)
	Negative effect on reproduction potential, phenotypic defects, apoptosis, delayed hatching and formation of abnormal spinal cords in zebrafish embryo (Danio rerio); toxic effects on bacteria.	(Asharani et al. 2008; Cheng et al. 2009b; Kang et al. 2008)
Gold NPs	Effect on cellular micromotility; mitochondrial damage; oxidative stress, autophagy in *in vitro* studies.	(Li et al. 2010; Pan et al. 2009; Tarantola et al. 2009)
	In vivo studies: Bioaccumulation in important body organs; acute inflammation and apoptosis in the liver; adverse effect on human sperm motility; penetration of gold nanoparticles in sperm head and tail.	(Cho et al. 2009b; Lasagna-Reeves et al. ; Wiwanitkit et al. 2009)
	Adverse effects on rainbow trout hepatocytes.	(Farkas et al. 2010)
Silver NPs	*In vitro* studies: Cytotoxicity and chromosome instability, oxidative stress, apoptosis, intracellular calcium	(Asharani et al. 2009a; AshaRani et al. 2009b; Foldbjerg et al. 2010; Hsin et al.

	transients, cell cycle arrest, interference with DNA replication fidelity, JNK activation in mammalian cells.	2008; Kawata et al. 2009; Miura and Shinohara 2009; Yang et al. 2009b)
	In vivo studies: Free radical-induced oxidative stress and alteration of gene expression; blood-brain barrier destruction and astrocyte swelling, neuronal degeneration; induce brain edema formation.	(Rahman et al. 2009; Sharma et al. 2010; Tang et al. 2009)
	Cytotoxicity and genotoxicity in fish cells; NPs accumulation in gill tissue; adverse effects on embryonic development of oyster, lysosomal destabilization of adult oysters; oxidative stress, double-strand break marker gamma-H2AX and the expression of p53 protein, embryonic morphological malformations in zebrafish.	(Bar-Ilan et al. 2009; Choi et al. 2009a; Ringwood et al. 2009b; Scown et al. 2010; Wise et al. 2010)
	Induce heat shock stress, oxidative stress, DNA damage and apoptosis with up-regulation of p53 and p38 proteins in *Drosophila melanogaster.*	(Ahamed et al. 2010)
	Decrease in reproduction potential, toxicity, oxidative stress in *Caenorhabditis elegans.*	(Roh et al. 2009)
Quantum Dots	*In vitro* studies: Cytotoxic, induce inflammatory response, oxidative stress in various types of cell culture systems	(Cho et al. 2007; Li et al. 2009; Ryman-Rasmussen et al. 2007; Su et al. 2009; Tang et al. 2008; Wang et al. 2008b; Zhang et al. 2007)
	In vivo studies: Transfer of quantum dots from pregnant mice to pups across the placental barrier; negative impact of CdSe-core quantum dots on mouse oocyte development; ability to penetrate intact and UV radiation compromised skin barrier	(Chu et al. 2010; Hsieh et al. 2009; Mortensen et al. 2008)
	Phototoxic in *Daphnia magna* under environmentally relevant UV-B light	(Kim et al. 2010b)
SWCNT	*In vitro* studies: Impair human macrophage engulfment of apoptotic cell corpses; fibrogenic effects in lung cells; suppress inflammatory mediator responses in human lung epithelium; disrupt actin filament integrity and VE-	(Cveticanin et al. 2010; Herzog et al. 2009; Lindberg et al. 2009; Migliore et al. 2010; Murray et al. 2009; Pacurari et al. 2008; Walker et al. 2009; Wang et al. 2010b; Witasp et al.

	cadherin distribution in human aortic endothelial cells; activate MAPKs, AP-1, NF-kappaB, and Akt in normal and malignant human mesothelial cells; cause cytotoxicity, oxidative stress, apoptosis, induction of micronuclei and double strand breaks of the DNA, inflammatory response in various mammalian cells.	2009; Zhang et al.)
	In vivo studies: Lung inflammation and genotoxicity; increased levels of 8-oxodG in liver and lung; activate platelets and accelerate thrombus formation in the microcirculation; promote allergic response in mice.	(Bihari et al. 2010; Folkmann et al. 2009; Nygaard et al. 2009; Yang et al. 2008)
	Microbial inactivation of diverse microbial communities of river water and wastewater effluent; locomotor impairment and mortality in *Drosophila melanogaster.*	(Kang et al. 2009; Liu et al. 2009)
Fullerenes	*In vitro* studies: Oxidative stress and DNA damaging potential in different mammalian cells.	(Dhawan et al. 2006; Jacobsen et al. 2008; Zhang et al. 2009)
	In vivo studies: Increase in pro-inflammatory cytokines and Th1 cytokines in BAL fluid, stronger gene expression of the MHC class II molecule than MHC class I and an increase in T cell distribution in lungs; elevated levels of 8-oxodG in the liver and lung.	(Folkmann et al. 2009; Park et al. 2010)
	Antibacterial activity through reactive oxygen species production.	(Brunet et al. 2009; Cho et al. 2009a)
	Adverse effects on embryonic development in oysters; oxidative stress and growth inhibition in the freshwater fish *Carassius auratus* after chronic exposure; long-term exposure caused significant cellular damage in the alimentary canal of Daphnia magna; upon sub-lethal exposure, the mortality rates of gestating daphnids increased with time and developmental stage, maturation of daughter daphnids negatively impacted; extracellular oxyradical and nitric oxide production, inflammatory response in marine bivalve *Mytilus* hemocytes.	(Canesi et al. 2010; Ringwood et al. 2009a; Tao et al. 2009; Yang et al. 2009c; Zhu et al. 2008)

Metal oxide NPs	Cytotoxicity, membrane damage, inflammatory response, oxidative stress, apoptosis, lysosomal membrane destabilization, DNA damage, alteration of calcium homeostatis and gene expression in diverse mammalian systems as reported in a wide array of *in vitro* and *in vivo* toxicity studies; reports of inhibitory effect of superparamagnetic iron oxide nanoparticle on osteogenic differentiation; disturbance of the ionic homeostasis and the physiological functions in hippocampal CA3 pyramidal neurons by ZnO NPs.	(Chen et al. 2010; Choi et al. 2009b; Eom and Choi 2009; Fahmy and Cormier 2009; Falck et al. 2009; Huang et al. 2010; Hussain et al. 2010; Karlsson et al. 2008; Karlsson et al. 2009; Kim et al. 2010a; Midander et al. 2009; Ogami et al. 2009; Tsaousi et al. 2010; Zhao et al. 2009)
	Toxic to *Saccharomyces cerevisiae*, bacteria, nematode *Caenorhabditis elegans* and aquatic species like fish, phytoplanktons, zebrafish.	(Gaiser et al. 2009; Jiang et al. 2009; Kasemets et al. 2009; Ma et al. 2009; Miller et al. 2010; Zhu et al. 2009)

Some of the studies mentioned in the above table have not done a proper characterization of the nanoparticles before assessing their toxicity. Correlating the toxicity of nanoparticles to their physicochemical properties becomes difficult in the absence of characterization. Therefore, the results from such studies should be carefully considered before reaching any firm conclusions.

1.4. Exposure to nanoparticles

1.4.1. Exposure sources

The exposure of general population to the nanoparticles can occur either directly or indirectly (Figure 1.4).

1.4.1.1. Occupational exposure at work place: In the production processes there is a likelihood of exposure during synthesis and recovery phases. The nature and probability of the exposure would differ according to the specific stage of process. Nanoparticle synthesis and manufacturing can also contribute to environmental contamination from industrial effluents or spillage during shipping and handling.

1.4.1.2. Exposure through consumer products: Nanoparticles are being used in personal care products such as cosmetics and sunscreens. This provides a direct source of exposure to humans and can also enter the environment from washing off of consumer products.

1.4.1.3. Exposure through unintentional release: Nanoparticles being used in electronics, tyres, fuel additives and many other products may reach the environment either through accidental leakage or during their disposal (Simonelli et al. 2007).

1.4.2. Exposure routes

Depending on the exposure source, nanoparticles can enter the organism through different routes and can have varied health effects. If nanoparticles contaminate the air, they will mainly enter the organism by inhalation and they will interact with the respiratory system. In the case of dermal exposure, nanoparticles have to pass through the skin. When soils or waters are

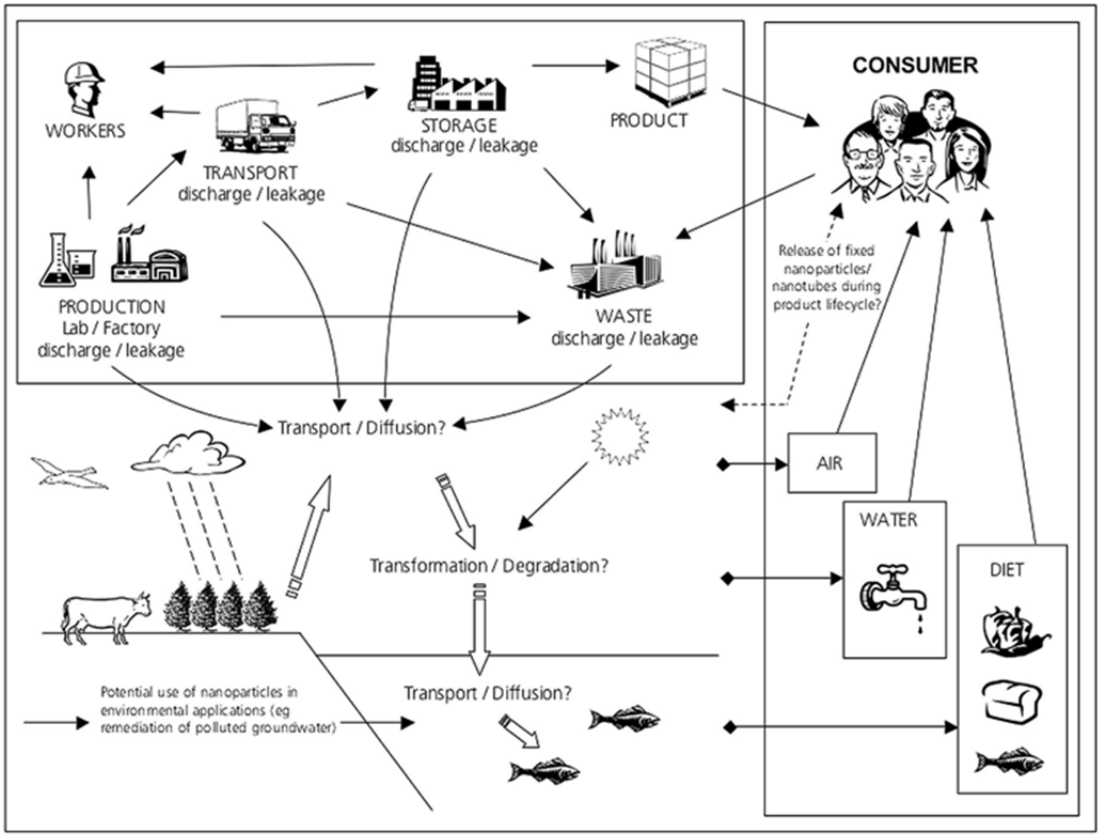

Figure 1.4. Possible exposure to nanoparticles. [Source: Nanosciences and nanotechnologies: Opportunities and Uncertainties, Royal Society/Royal Academy of Engineering, 2004 (RS/RAE 2004)]

contaminated or nanoparticles are deliberately injected or swallowed, their absorption is mainly through the circulatory or gastro-intestinal route.

1.4.2.1. Inhalation exposure: The most common route of exposure is through inhalation. This involves intake of airborne nanoparticles through the respiratory system. Inhalation exposure may occur while processing and packaging the dry powder during nanomaterials synthesis.

Some previous studies in rats have indicated that for the same material, nanometer particles are more potent than the micrometer particles in inducing pulmonary toxicity (Oberdorster et al. 2005). The inhaled nanoparticles can target all three regions of the human respiratory tract- the nasopharyngeal, tracheobronchial, and alveolar regions. Any foreign body in

the respiratory tract may face several clearance mechanisms. The mucociliary escalator dominates the clearance from upper airways (nasopharyngeal and tracheobronchial region); while clearance from the deep lung is predominantly by macrophage phagocytosis. The alveolar macrophage is the most important defense mechanism in the alveolar region for fine and coarse particles, yet inhaled singlet nanoparticles are not efficiently phagocytized by alveolar macrophages (Oberdorster et al. 2005).

A study based on the inhalation exposure of rats to ultrafine (20nm) and fine (200nm) titanium dioxide particles, demonstrated that the ultrafine particles cleared significantly slower, showing more translocation to interstitial sites and to regional lymph nodes when compared to the fine titanium dioxide particles (Oberdorster et al. 1994). The nanoparticles can be introduced into the blood circulation from the pulmonary interstitial sites. From the blood circulation the particles can be distributed to other target organs like liver and spleen.

1.4.2.2. Dermal exposure: Dermal exposure to nanomaterials has received much attention, perhaps due to concerns with occupational exposure and the introduction of nanomaterials in cosmetics (Wiesenthal et al. 2011). Dermal exposure may also occur during the equipment cleaning and maintenance.

Skin is the largest organ of the body and structured in three layers: the epidermis, the dermis, and the subcutaneous layer. It functions as a strict barrier to exogenous toxicants and micron sized particles. However, the efficiency of dermal barrier against nanoparticles is still to be investigated completely. The possible routes for nanoparticle entry through the skin are:

inter-cellular, trans-cellular and trans-appendageal (Baroli et al. 2007; Crosera et al. 2009). In the intercellular route- the lipid-soluble particles may move through lipid medium passing between skin cells whereas in the trans-cellular route the substance enters the skin cells. The trans-appendageal route is through the sweat glands and hair follicles which are scattered all over the skin in different densities and may become portals for nanoparticles to get through deeper parts of the skin (Zhao et al. 2007).

1.4.2.3. Gastrointestinal exposure: Nanoparticles can be ingested directly when used in food, food packaging, drug delivery and cosmetics. Workers can be exposed by unintentional hand-to-mouth transfer of materials. Moreover, as they are being used in a wide array of consumer products, they may enter the environment by a variety of routes such as discharge of industrial waste water and disposal of nanoparticles containing products. From the environment they can enter the human body through food chain. In addition, some of the nanoparticles can be swallowed into the gastrointestinal tract when they are expelled from the mucociliary system of the lungs after inhalation exposure (Oberdorster et al. 2005). Nanoparticles could be translocated from the lumen of the intestinal tract into different organs. Jani et al. (1990) found a particle size-dependent uptake (6.6% of the administered 50 nm particles, 5.8% of the 100 nm particles, 0.8% of 1 μm particles, and 0% for 3 μm particles) of polystyrene particles (ranging from 50 to 3,000 nm) by the gastrointestinal mucosa. The particles then translocated from the Peyer's patches into the mesenteric lymph and then to systemic organs (i.e., liver, spleen, blood, bone marrow, and kidney).

Bockmann et al also found the uptake of the TiO_2 nanoparticles from the gastrointestinal tract into the blood (Bockmann et al. 2000).

1.5. Characterization of nanoparticles

An initial characterization of the test substance is imperative before any toxicity screening is initiated. However, nanomaterials demand comprehensive characterization, unlike chemical toxicants, where the characterization is usually confined to chemical composition and purity determination. This is to determine the correct correlation between their physicochemical properties and the biological effects they elicit. Proper characterization prior to the experiments ensures better repeatability and hence greater reliability of results (Berhanu et al. 2009; Powers et al. 2007; Sayes and Warheit 2009; Warheit 2008). In addition, the characteristics of commercially available particles that are specified by the manufacturer sometimes differ from those found by the researcher (Sayes et al. 2007). However, since the facilities in most toxicology laboratories are not fully comprehensive, the complete characterization of nanoparticles is often difficult. In the absence of an elaborate laboratory set-up with all of the instruments and skilled manpower required, researchers are compelled to exploit the techniques available to them. Therefore, sometimes it is the availability of facilities that determines the type of characterization performed rather than the study design or experimental needs. Among all of the parameters that should be considered for characterization, size is the most important, and it is critical for determining the interactions of nanoparticles with living systems. Although a variety of methods are available for size determination of nanoparticles, most commonly employed techniques are

Brunauer-Emmett-Teller (BET), dynamic light scattering (DLS) and transmission electron microscopy (TEM). However, another challenge that arises here is the disagreement between average sizes and size distributions given by different methods. This is obviously not surprising in view of the different principles behind the techniques involved. In addition, variations in sample preparation methods and instrument operating procedures also contribute to measurement differences. However, this may lead to confusion about the actual nanoparticle size and size distribution if one is not well versed with the principles and technical details of the measurement methods involved, as is often the case.

1.5.1. BET Method: The nanoparticle surface area is an important factor in nanoparticle toxicity, as the interaction of the nanoparticles with biological systems takes place at their surfaces. The BET method is typically used to calculate the surface areas of solids by the physical adsorption of gas molecules on to the solid surface. It involves adsorbing a liquid nitrogen monolayer on to the surfaces of particles and then measuring the amount of nitrogen released upon vaporizing that layer. Thus, the BET surface represents the surface area that is freely accessible to gases. The primary particle diameter (assumed to be the equivalent sphere diameter) is then calculated from the specific surface area and the density of the particles - data that are already available. Though the merit of this method lies in the fact that it provides two parameters simultaneously (size as well as surface area), it does have a drawback in that it assumes a monodisperse system of average-sized spheres, so it does not account for the size distribution of the

particles, which is a key parameter in size-dependent toxicity assessment (Powers et al. 2007; Weibel et al. 2005).

1.5.2. Electron Microscopy: Electron microscopy is the simplest and most widely used technique that directly measures particle size, size distribution and morphology. However, it is time consuming and requires a sufficient number of particles containing the fields to be analyzed before a sound statistical assessment can be made. Moreover, it measures a sample in dry form, not as a suspension, and requires the drying of samples in vacuum, which may alter their properties. Another drawback of this technique is that it fails to measure the properties of the sample in the form of a dispersion, which is used for experimental exposure (Powers et al. 2007).

1.5.3. Dynamic light scattering: Among the commonly employed techniques for particle characterization, DLS is unique in its ability to provide the important parameters of size and size distribution in relevant solvents used for exposure risk assessment. It measures time-dependent fluctuations in scattering intensity produced by particles in Brownian motion and yields size of the particle by applying Stokes-Einstein relationship. The size obtained by DLS is usually more than the size measured by TEM or BET. For size characterization of nanoparticles during toxicity studies, DLS may be considered indispensable compared to TEM or BET as it can measure size under conditions that mimic more to the exposure conditions. It can provide an idea of the particle suspension stability with respect to time and medium. Although the choice of a particular characterization technique depends on the type of particle being analyzed and the final application of the nanoparticles, it is advisable to perform multi-technique analysis in order

to get a broader perspective and a more reliable picture of the particle characteristics.

1.6. Nanoparticle internalization in biological systems

It has been shown that size plays a critical role in cellular uptake of nano-structures (Chithrani and Chan 2007). A thorough understanding of the mechanisms of nanoparticles entering and leaving the cells could lead to a better understanding of NP toxicity as well as improvement in their bio-medical applications.

Earlier studies have demonstrated that when nanoparticles are exposed to cells at 4^{o}C or in ATP-depleted conditions, the nanoparticles entry into the cells is inhibited (Chithrani and Chan 2007; Torchilin et al. 2001). Therefore, endocytosis has been proposed as the inferred pathway for cellular uptake of nanoparticles than the free diffusion. It can be clathrin mediated endocytosis (Panyam et al. 2002), caveolae mediated endocytosis or clathrin and caveolae independent endocytosis (Rejman et al. 2004) (Figure 1.5).

Accumulation of nanoparticles in the perinuclear region or internalization via caveolae-mediated endocytosis to reach endoplasmic reticulum may facilitate physical contact of nanoparticles with nuclear pore complexes and subsequent transport into the nucleus (Chen and Mikecz 2007). The phagocytosis is unlikely to contribute to the nanoparticles uptake into the cells. This is evident from the fact that even non-phagocytic cells can efficiently internalize nanoparticles and the lower size cut-off described for phagocytosis is 500nm (Rupper and Cardelli 2001).

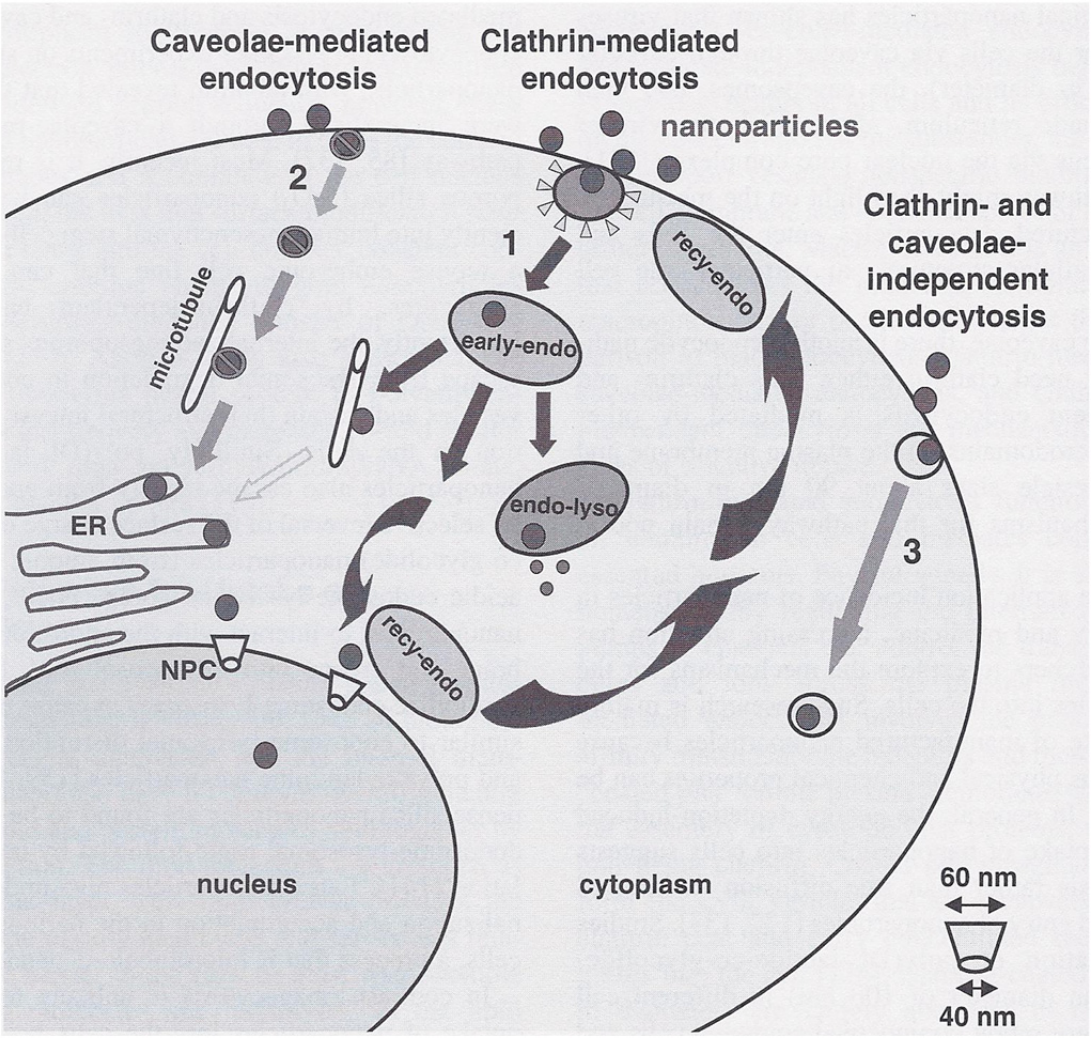

Figure 1.5. Inferred pathways of nanoparticle uptake. (1) Clathrin mediated endocytosis; (2) Caveolae-mediated endocytosis; (3) Clathrin and caveolae-independent endocytosis. Early-endo- early endosome; endo-lyso- late endosome-lysosome; recy-endo- recycling endosome; ER- endoplasmic reticulum; NPC- nuclear pore complex (Chen and Mikecz 2007).

Tracking nanoparticle internalization in cellular systems is of utmost importance for understanding and correlating the biological effects elicited by these nanoparticles. However, the challenge lies in detecting the uptake of nanoparticles, the mode of uptake, and the fate of nanoparticles inside the cells due to their small size and quantity.

1.6.1. Electron microscopy: Transmission electron microscopy has been the preferred method of studying the cellular uptake of nanoparticles. Apart from detecting the intracellular localization, it provides a detailed view of the interaction of nanoparticles with cell structures. Due to its high resolution, transmission electron microscopy enables the imaging of membrane invaginations, vesicle formation, and organelles (Motskin et al. 2009). This makes it possible to study the mode of nanoparticle uptake, which is of primary importance for understanding the influence of size, shape, surface chemistries, coatings, and other factors on nanoparticle uptake (Xia et al. 2008; Zhang et al. 2009). It also aids in understanding the ultrastructural changes that occur in cells subsequent to nanoparticle uptake (Song et al. 2010; Xie et al. 2009). However, transmission electron microscopy is only a qualitative tool for assessing nanoparticle uptake, and is usually confined to imaging a few cells due to the complicated sample preparation and image analysis involved.

A scanning electron microscope (SEM) can also be used to observe nanoparticles inside cells. For this, backscattered electron detection is used instead of the normal secondary electron mode of detection. Backscattered electrons (BSE) are high-energy electrons that are reflected or backscattered out of the specimen following elastic scattering interactions

with specimen atoms (Baroli et al. 2007; Pelka et al. 2009). This enables bright nanoparticles to be seen against the cellular dark background, since high atomic number elements backscatter electrons more strongly than low atomic number elements. In addition to visualizing the specimen, elemental analysis of the sample can be achieved by energy-dispersive X-ray spectroscopy (EDS) (Bastian et al. 2009; Kuhnel et al. 2009). The staining procedures generally used for electron microscopic preparations can introduce electron-dense artefacts that may be mistaken for nanoparticles.

1.6.2. Inductively coupled plasma mass spectroscopy (ICPMS): Sometimes very small amounts of nanoparticles in the environment or in living systems make it difficult to perform a qualitative assessment by microscopic tools. Moreover, electron microscopic techniques become ineffective when it comes to the analytical quantification of nanoparticles. In this case, ICPMS can be used as a sensitive and quantitative tool for the determination of even trace amounts of nanoparticles. ICPMS becomes especially important in the context of an *in vivo* scenario, where it identifies the target organs for nanoparticles (Tang et al. 2009). Using this technique, even trace amounts of nanoparticles that enter through a different route can be detected in various body organs. However, the digestion step involved in the sample preparation method for ICPMS may lead to contamination and dilution, and it makes it difficult to differentiate between ions formed as a result of nanoparticle dissolution and nanoparticles *per se* (Allabashi et al. 2009; Marquis et al. 2009).

1.6.3. Flow cytometry: Flow cytometry is yet another technique that can be used to study nanoparticle uptake in mammalian cells (Missirlis and Hubbell

2009; Suzuki et al. 2007; Wang and Wu 2006; Xu et al. 2009). It is not only simple, easy and sensitive, but it is also a cost-effective and non-invasive approach. In this method, a laser beam is made to strike a hydrodynamically focused stream of fluid containing a single cell suspension, and a number of detectors then collect information on how the light interacts with the cells. Some of the photons that hit the edge of the cell are deflected slightly, and this forward scattered light corresponds to the size of the cells. Photons scattered at right angle to the laser beam (side scatter) indicate the inner complexity or granularity of the cells. Fluorescence emitted by the structures present inside the cells or attached to the cells is also picked up by the detector, providing an array of useful information (Figure. 1.6). Thus, flow cytometry can be used for the detection of fluorescent as well as non-fluorescent nanoparticles inside the cells. In fluorescent nanoparticles, the forward-scattered light remains constant in exposed and unexposed cells, while the intensity of side-scattered light increases in proportion to the concentration of nanoparticles inside the cells. The sensitivity of side scattering should be kept low in order to detect a broad range of changes in uptake (Suzuki et al. 2007). Sample preparation for flow cytometry analysis is much simpler than for other analytical techniques. Cells exposed to nanoparticles are washed, trypsinized and then re-suspended in buffer for flow cytometry acquisition. Suzuki et al. (2007) used flow cytometry to show that the TiO2 nanoparticles were taken up by the cultured mammalian cells in a dose-, time- and size dependent manner (Suzuki et al. 2007). In addition, they also revealed a change in the uptake potential on a surface coating, which was shown by the intensity of the side-scattered light

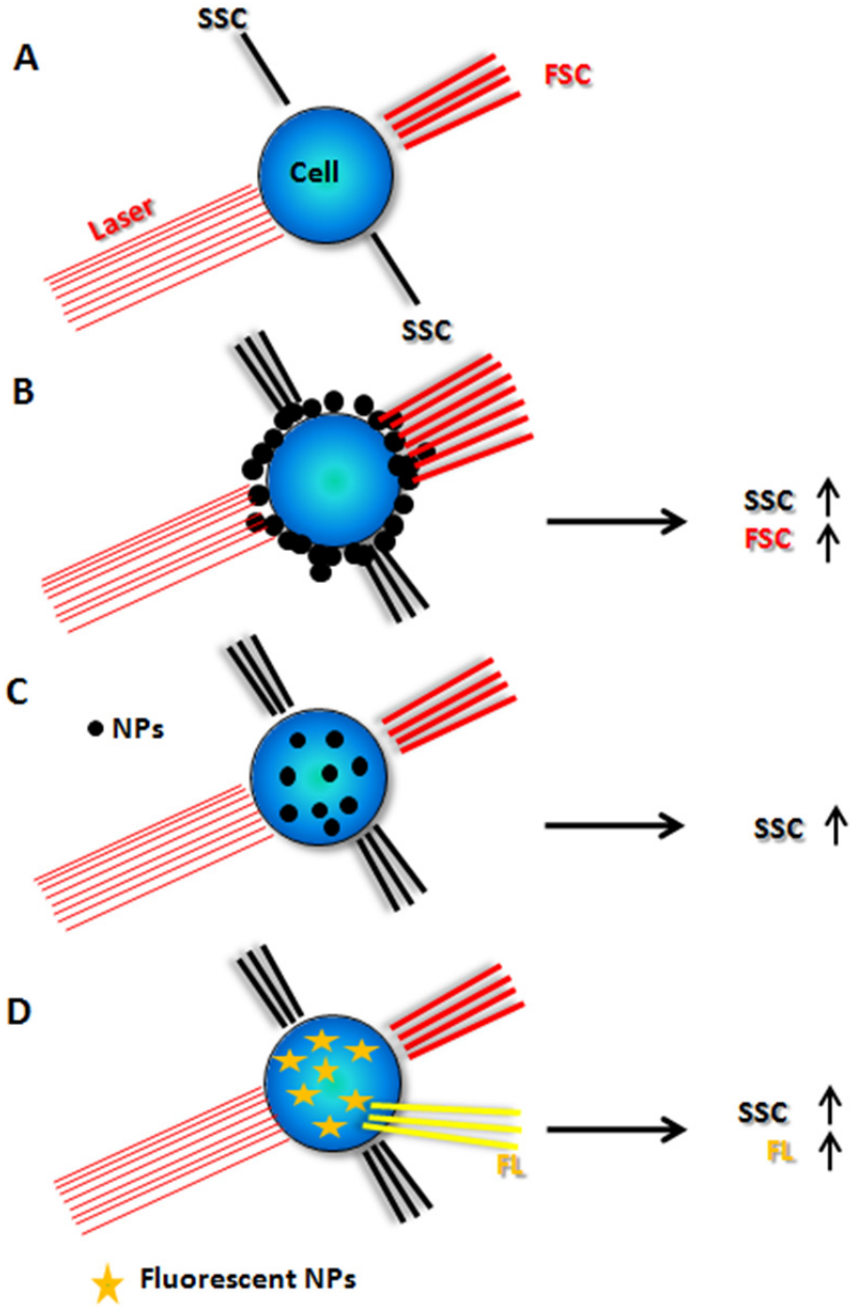

Figure 1.6. Analysing nanoparticle (NP) uptake in cells by flow cytometry- **(A)** Light scattering by a cell having no association with any nanoparticle; **(B)** Nanoparticles adhered to cell surface leading to increase in forward scatter (FSC) and side scatter (SSC); **(C)** Nanoparticle internalization by cell leading to increase in SSC alone; **(D)** Fluorescent nanoparticle internalization by cell leading to increase in SSC and fluorescent intensity (FL).

(Suzuki et al. 2007). The uptake of fluorescent amphiphilic hydrogel nanoparticles by a murine macrophage cell line (J774A.1) was demonstrated by determining the fluorescent intensities of exposed cells (Missirlis and Hubbell 2009). The uptake mechanism was also elucidated by selectively inhibiting cellular internalization processes with a variety of inhibitors and then analyzing the cells by flow cytometry (Missirlis and Hubbell 2009). The applicability of flow cytometry for studying the cellular internalization of nanoparticles was also utilized in an *in vivo* study investigating the phagocytic uptake of nanoparticles by mouse peritoneal macrophages (Wang and Wu 2006). Flow cytometric analysis of nanoparticle uptake in cells can be further supported by fluorescent spectroscopy or microscopy data in the case of fluorescent nanoparticles. Despite its many advantages, the main drawback of flow cytometry in nanoparticle uptake studies is that it can only show the association of nanoparticles with cells but does not indicate their localization and fate inside the cells.

1.7. Agglomeration and dispersion

The tendency of nanoparticles to agglomerate both in dry as well as in wet state is another significant technical challenge encountered while dealing with nanomaterials. The phenomenon of agglomeration involves adhesion of particles to each other mainly due to Van der Waal's forces which become quite prominent at nanoscale due to increased surface area to volume ratio (Powers et al. 2007) (Figure 1.7). The challenge for synthetic chemists is to prevent surface particle interactions to ensure that the nanoparticles do not agglomerate, especially in biologically relevant fluids. Brownian motion, in combination with Van der Waal's forces, also contributes significantly to the

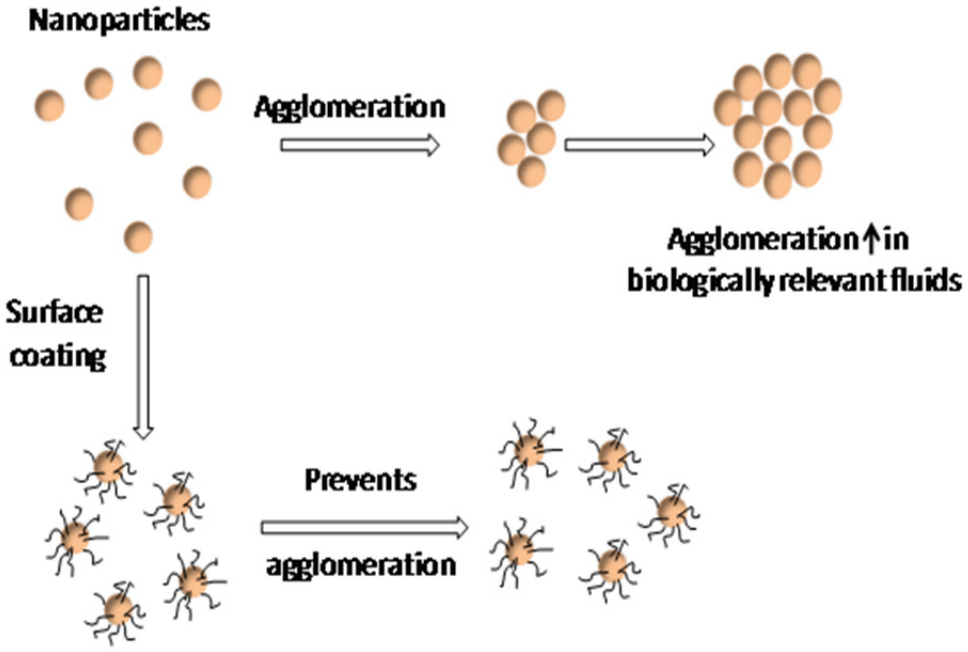

Figure 1.7. Schematic showing the phenomenon of agglomeration of nanoparticles.

agglomeration of nanoparticles, which ultimately settle down due to gravitational forces. Due to agglomeration, the physicochemical properties and the number concentration of the nanoparticles get altered. The major properties affected are their size, size distribution, surface-to-volume ratio, and hence their surface reactivity. Since these parameters play a major role in the toxicity of nanoparticles, and are altered due to agglomeration, it is prudent to account for these changes in the study design (Borm et al. 2006; Teeguarden et al. 2007).

It is well known that nanoparticles can traverse through biological barriers due to their size. Hence, agglomeration could alter biological responses due to a decrease in the total available surface area, leading to an underestimation of toxic potential (Sager et al. 2008). The rate and extent of agglomeration of nanoparticles could vary after they enter cells, due to their interaction with macromolecules (Balbus et al. 2007). Though different methods are available to deagglomerate nanoparticles (sonication, detergents, lung surfactants, polyethylene glycol, serum, etc.), sonication is the most preferable and widely used method. It disperses nanoparticles in a liquid by cavitation and does not have much effect on the properties of the particles.

Agglomeration is a challenge to the accurate interpretation of the biological response to any given nanomaterial. This is evidenced by an increase in the cytotoxicity when mesothelioma cells (MSTO-211H) are exposed to micron-sized agglomerates of carbon nanotubes rather than well-dispersed carbon nanotubes (dispersed with a non-ionic biocompatible surfactant, PS80). This is because the structural characteristics of the material change after

agglomeration; it becomes stiffer and behaves like asbestos particles (Wick et al. 2007).

Another important method of preventing the agglomeration of nanoparticles and homogeneously dispersing them in liquids is surface modification (Figure 1.7). This can be achieved in various ways, depending on the application. The particles can be coated with polymers or dispersed in ionic or nonionic surfactants or alveolar surfactants (Farah et al. 2008; Sager et al. 2008; Skebo et al. 2007; Wick et al. 2007). While surface modifications allow the particles to be stabilized and avoids agglomeration, it also raises concern that they may shield or influence the effects of nanomaterials on biological systems (Derfus et al. 2004; Warheit 2008; Warheit et al. 2005). The durability or stability of such surface coatings inside a biological environment is another critical issue that needs to be understood in order to unravel the toxicological consequences of nanoparticles. Quantum dot (QD) cores possess unique optical and electrical properties, but these cores are coated with different materials to make them biologically compatible/active (Hardman 2006). However, Hoshino et al. (2004) reported that the exposure of QD surface coatings to the acidic and oxidative environments of endosomes may cause their decomposition and subsequent release into cytoplasm. This can in turn expose the metalloid core, which may be toxic or pave the way for unforeseen reactions of the QD inside the cellular environment.

1.8. Oxidative stress

Oxidative stress has been proposed as a possible mechanism involved in the toxicity of nanoparticles (Nel et al. 2006). Oxidative stress can be defined

as a disturbance in the pro-oxidant–antioxidant balance in favour of the former, leading to cellular damage (Halliwell and Whiteman 2004). Oxidative stress is induced in cells as a result of one of two factors: 1) an increase in reactive oxygen species (ROS) generation, or 2) a decrease in antioxidant protection. ROS are either free radicals, reactive anions containing oxygen atoms, or molecules containing oxygen atoms that can either produce free radicals or are chemically activated by them. Examples are hydroxyl radical (•OH), superoxide, hydrogen peroxide etc (Vigneron and Vousden 2010). Some of those molecules are extremely reactive, such as the hydroxyl radical, while some are less reactive (superoxide and hydrogen peroxide).

A beneficial physiological use of ROS in cells is in intracellular signalling (Forman 2010; Thannickal and Fanburg 2000). However, at high levels cellular damage occurs which results from the ROS-induced alteration of macromolecules such as polyunsaturated fatty acids in membrane lipids, essential proteins, and DNA (Roberts et al. 2010).

1.8.1. Effect on DNA: ROS attack on DNA generates a huge range of base and sugar modification products. A number of alterations in DNA (e.g., cleavage of DNA, DNA-protein cross links, oxidation of purines, etc.) are due to reactions with ROS, especially hydroxyl radical (Marnett 2000). It is known that oxidised bases such as 8-oxoguanine (8-oxoGua) are potentially mutagenic, because of alteration in the base pairing properties (8-oxoGua pairs with adenine instead of cytosine) (Collins 2009). If the DNA repair systems are not able to immediately regenerate intact DNA, a mutation will result from erroneous base pairing during replication. This is the reason for

high prevalence of cancer in individuals exposed to oxidative stress (Mates et al. 1999).

1.8.2. Effect on apoptosis: Moderate oxidative stress induces apoptosis, whereas necrosis occurs at higher levels of oxidative stress. Signalling pathways that are activated by ROS and leads to apoptosis are the activation of JNK and p53 (Circu and Aw 2010) (Figure 1.8). ROS production causes dimerisation of Bax in the cytosol by generating disulfide bridges between critical cysteine residues (Neuzil et al. 2006). This changes the conformation of Bax, exposing the docking motif which then moves to the mitochondrial outer membrane where Bax dimers aggregate to form pores (D'Alessio et al. 2005). This results in release of pro-apoptotic factors and subsequently apoptotic cell death.

1.8.3. Effect on cell membrane: The lipids present in the cell membrane can be oxidized by ROS. Polyunsaturated fatty acids because of their multiple double bonds are excellent targets for free radical attacks. This leads to membrane damage and further production of free radicals as well as mutagenic compounds (Negre-Salvayre et al. 2010).

1.8.4. Measurement of oxidative stress in cells

Apart from measurement of ROS directly and oxidatively damaged DNA, measurement of some other biomarkers can also predict the state of oxidative stress in cells.

1.8.4.1. ROS generation: The intracellular generation of ROS can be measured by dichlorofluorescin diacetate (DCFDA). DCFDA is deacetylated by esterases to dichlorofluorescin (DCFH). This non-fluorescent product is converted by ROS into DCF, which can easily be visualized by strong

fluorescence at around 525nm when excited at around 488 nm (Halliwell and Whiteman 2004).

1.8.4.2. Lipid peroxidation: Lipid peroxidation refers to the oxidative degradation of lipids. Lipid peroxidation generates a complex variety of products, many of which are reactive electrophiles. Some of these are toxic and mutagenic and react with protein and DNA. ROS such as hydroxyl radical acts as initiator of lipid peroxidation by combining with a hydrogen atom (in methylene group of polyunsaturated fatty acids) to make water and a fatty acid radical. The later being an unstable species reacts with another free fatty acid producing a different fatty acid radical and a lipid peroxide (Catala 2010). These fatty acid radicals are neutralized in the cell membrane by either another molecule of fatty acid or vitamin E.

1.8.4.3. Glutathione: Glutathione (GSH) is the most abundant intracellular thiol-based antioxidant, synthesized in the body from the amino acids L-cysteine, L-glutamic acid and glycine (Lu 2009). Glutathione exists in reduced (GSH) and oxidized (GSSG) states. In the reduced state, the thiol group of cysteine is able to donate a proton to other unstable molecules, such as ROS. In donating a proton, glutathione itself becomes reactive, but reacts with another reactive glutathione to form glutathione disulphide (GSSG). GSH can be regenerated from GSSG by the enzyme glutathione reductase (Biswas and Rahman 2009; Franco and Cidlowski 2009). Oxidized glutathione (GSSG) is reduced by the NADPH-dependent flavoenzyme glutathione reductase (GR). Glutathione S-transferases (GST) catalyze the conjugation of glutathione with other molecules, thereby

functioning as an intermediate step in the detoxification of miscellaneous toxic substances (Van Bladeren 2000).

1.8.4.4. Superoxide dismutase: Superoxide dismutases (SOD) are the superoxide metabolizing enzyme. In eukaryotes, there are two SOD isoenzymes Mn-SOD present in mitochondria, and the Cu/Zn-SOD present in the cytosol (McCord and Fridovich 1969) The formation of superoxide takes place as a result of leakage of electrons from electron transport chain present in the mitochondrial inner membrane. They are also produced endogenously by flavoenzymes and by activated phagocytes. The superoxide dismutases (SOD) catalyze the conversion of superoxide anion into hydrogen and oxygen. The superoxide anion is created from molecular oxygen by the addition of an electron. In spite of being a free radical, it is not highly reactive. It lacks the ability to penetrate lipid membranes and is therefore enclosed in the compartment where it was produced. However, the Fenton reaction can facilitate the conversion of superoxide anion and hydrogen peroxide to hydroxyl radical.

1.8.4.5. Catalase: Catalases of many organisms are mainly heme-containing enzymes (Vlasits et al. 2010). Their predominant subcellular localization in mammalian cells is in peroxisomes. The catalases carry out a dismutation reaction in which one molecule of H_2O_2 oxidizes another such that the one is converted to O_2 and the other to two molecules of water (Zamocky et al. 2008). Hydrogen peroxide is not a free radical itself but can give rise to highly reactive hydroxyl radical via oxidation of transition metals often bound in complex with different proteins or other molecules. Thus

catalase lowers the risk of hydroxyl radical formation (Nordberg and Arner 2001).

1.9. Genotoxicity

Genotoxicity refers to the ability of a test substance to induce DNA damage. The incidence of DNA damage is likely to be more in cells subjected to unfavourable conditions such as inflammation or tobacco smoke exposure.

1.9.1. Types of DNA damages

Alteration of bases: Alkylating agents include nitrogen and sulfur mustards, methyl and ethyl methane sulfonate (MMS and EMS) and nitrosoguanodine. These chemicals donate alkyl groups to other molecules and induce mutations (Figure 1.8) (Gocke et al. 2009). For example, EMS causes ethylation of the bases in DNA at the 7-N and the 6-O positions. When 7-ethylguanine is produced, it base pairs with thymine to cause G: C to A: T transition mutation.

Absorption of the ultraviolet radiation causes the adjacent thymine residues in a DNA strand to be joined by formation of the bond resulting in thymine dimer formation (Narayanan et al. 2010).

Single strand breaks: A variety of agents can break phosphodiester bonds. Among the more common chemicals are peroxides, sulfhydryl containing compounds (Driessens et al. 2009). Ionizing radiation can produce strand breaks by action of secondary electrons produced by β- particle or an X- ray photon (Ayene et al. 2007; Rakhorst et al. 2006; Stap et al. 2008).

Double strand breaks: If a DNA molecule receives a sufficiently large number of randomly located single strand breaks, two situated opposite to one another results in breakage of double helix. Double strand breaks result

from exposure to highly ionizing radiation (e.g. χ- rays and γ -rays, electron beams etc.) (Bassing et al. 2002).

DNA crosslinks: Some antibiotics i.e. mitomycin C and reagents (nitrite ion) can form covalent linkages between a base in one strand and an opposite base in the complementary DNA strand (Hlavin et al. 2010). This prevents strand separation during DNA replication and also causes local distortion of the helix.

In general, some main sources of DNA damage are DNA- adducts forming molecules, intercalating agents and reactive oxygen species (ROS). In addition to these two major sources of DNA damage, another well recognized source is the ultraviolet (UV) component of sunlight, which is the key risk factor for malignant melanoma. The DNA damage induced by UV is primarily in the form of pyrimidine dimers. An example of DNA-adduct forming molecule is benzo[*a*]pyrene-7,8-diol-9,10-epoxide (BPDE).

1.9.2. Nanoparticle induced DNA damage

Genotoxicity is a central element of risk assessment for any chemical compound that humans may be routinely exposed to (e.g. in foods or personal care products). Information about genotoxicity is vital as DNA damage can not only initiate cancer development, but can also have an impact upon fertility and the health of subsequent generations if disturbances arise in reproductive cells (Singh et al. 2009). Nanoparticles have been demonstrated to possess genotoxic potential (Karlsson 2010) which may be attributed to following main reasons:

1.9.2.1. Direct interactions with the DNA: Nanoparticles may gain direct access to DNA after transport into the nucleus

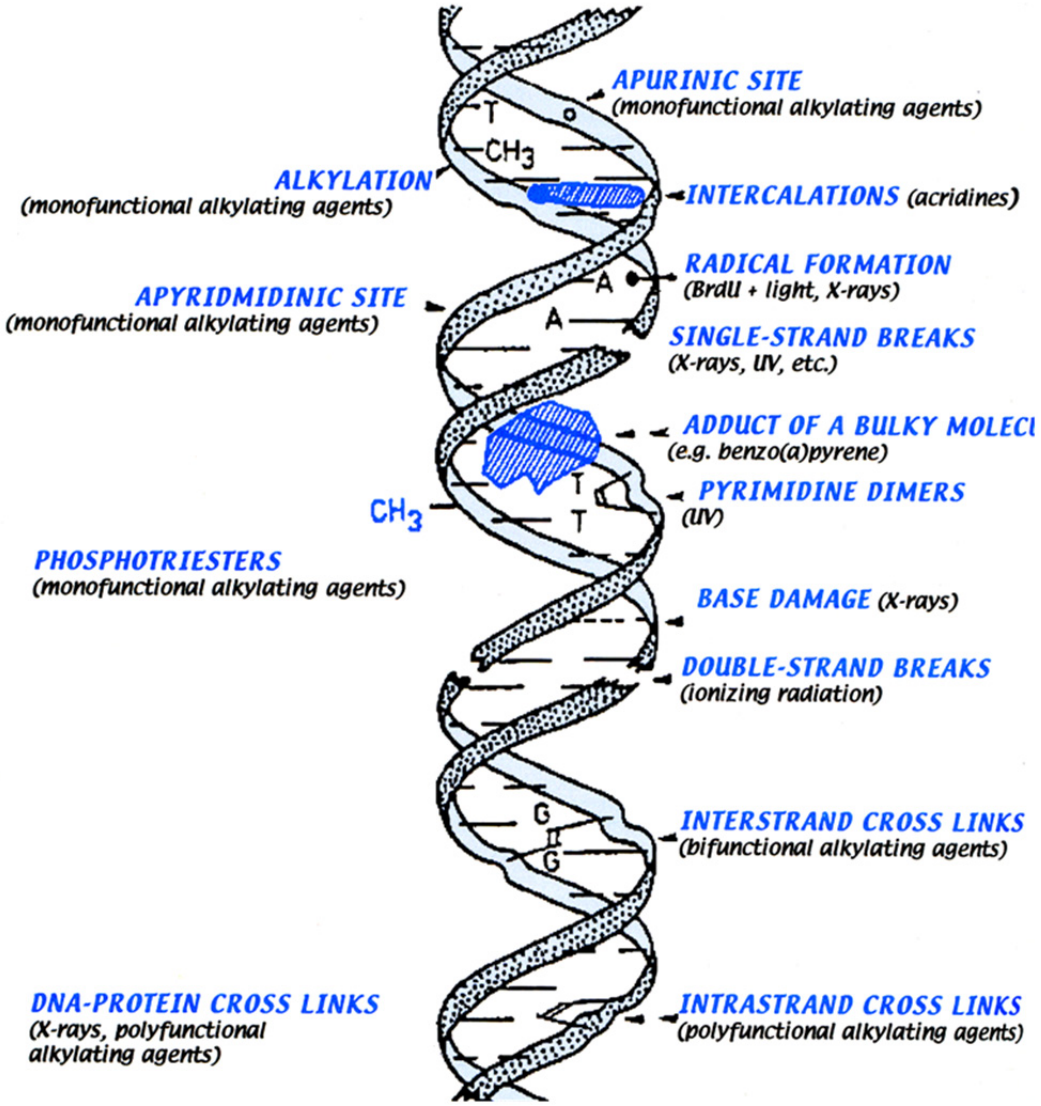

Figure 1.8. Spectrum of DNA damage induced by physical and chemical agents (adapted from Casserette and Doull;s “Toxicology: the basic science of poison” Genetic Toxicology, pp 326).

(Chen and Mikecz 2005). The entry of nanoparticles into the nucleus has been demonstrated by earlier studies (Alkilany and Murphy 2010; Shukla et al. 2011). Moreover, even if the nanoparticles are unable to cross the nuclear membrane but are able to accumulate in the cytoplasm, they can still gain access to the nucleus during mitosis when the nuclear membrane breaks down (Singh et al. 2009). The direct interaction of nanoparticles with the DNA and DNA-related protein may lead to physical damage to the genetic material.

Interference with the structure or function of DNA repair enzymes in the nucleus might be another reason for DNA damage. The transport of quantum dots in the cell nucleus via nuclear pore complex with subsequent targeting of histones has been reported earlier.

1.9.2.2. Oxidative DNA damage: The nanomaterials due to their high surface area to volume ratio are known to produce reactive oxidative species (ROS). A previous study showed that the perinuclear distribution of TiO_2 nanoparticles in BEAS-2B cells correlated with the induction of ROS in the same region as visualized by a fluorescence dye. ROS can induce DNA damage in the form of single and double stranded DNA breaks, base modifications and DNA cross-links (Toyokuni 1998). The other way to produce ROS is by interacting with the cellular organelles. It can be by particle-induced disturbance of the mitochondrial electron transport chain function (Li et al. 2003). The ROS can also be generated during particle elicited inflammation. Inflammation from activated phagocytes (macrophages, neutrophils) produces bursts of ROS in order to destroy invading pathogens (Hussain et al. 2007). These ROS can damage the DNA

of the infecting pathogen, the DNA of invaded cells, and also nearby host cells that were not invaded.

1.9.3. Comet assay/ Single cell gel electrophoresis

The Single Cell Gel Electrophoresis, also known as Comet assay is a well established, simple, rapid, visual and a sensitive, extensively used biomarker to assess DNA damage quantitatively as well as qualitatively in individual cell population (Collins 2004). It has gained wide acceptance as a valuable tool in fundamental DNA damage and repair studies (Speit and Hartmann 2006), genotoxicity testing (Moller 2005) and population biomonitoring (Garcia-Leston et al. 2011).

1.9.3.1. Principle

The methods of detection of DNA strand breaks are based on the principle that strand breaking or DNA damaging agents reduce the size of the large duplex DNA molecule. Single and double strand breaks adversely affect the super-coiling and packaging in the nucleus. The lysis step removes cell membranes, bulk of proteins, cytoplasm and nucleoplasm, and disrupts nucleosomes and histones. The nucleoid which is left behind, consist of a nuclear matrix composed of ribonucleic acid (RNA), proteins and negatively supercoiled DNA (Collins 2004). Any breaks present in the DNA cause the super coiling to relax locally and loops of DNA are then free. A high pH facilitates denaturation of DNA (because of the disruption of hydrogen bonds between double-stranded DNA) and expression of alkali labile sites as breaks. The electrophoresis would pull the damaged DNA towards the anode thus making the distinct ‘tail’ of the comet visible after fluorescent staining. Various modifications of the Comet assay protocol to suit the cell

type or experiment have been made during the years (Fairbairn et al. 1995; Speit and Hartmann 2006).

1.9.3.2. Advantages

The Comet assay has various advantages over other DNA damage detecting tests. These include its application in detecting DNA damage at single cell level in proliferating and non-proliferating cell population, and in cells of tissues, which are the first site of contact with mutagenic/ carcinogenic substances (e.g. oral and nasal mucosal cells). The assay requires small number of cells per sample (~ 10,000) and has a higher sensitivity for detecting DNA damage (detects as few as one DNA break per 10^{10} Dalton) as compared with other techniques. It can also be used to detect specific classes of DNA adducts (e.g. thymidine dimers, oxidative damage) by using lesion specific antibodies or specific DNA repair enzymes. The collection of the data at the level of the individual cells allows robust types of statistical analysis. Therefore, it has wide acceptance in fields ranging from molecular epidemiology to genetic toxicology.

The Comet assay has proved to be a versatile, simple and the most useful technique for the detection of a wide range of DNA damage and repair processes in single cells and is the test of choice in preliminary screening of chemical entities for their genotoxic potential.

1.10. Apoptosis

The apoptotsis (programmed cell death) is an active and defined process which plays an important role in the development of multicellular organisms and in the regulation and maintenance of the cell populations in tissues upon pathological conditions. Cells undergoing apoptosis show characteristic

morphological features: the cell shrinks, loses contact with its neighbouring cells, chromatin condenses, the plasma membrane is blebbing or budding, and finally the cell is fragmented into compact membrane-enclosed structures, called 'apoptotic bodies'. The apoptotic bodies are engulfed by macrophages and removed without causing an inflammatory response.

Apoptosis can be triggered by various stimuli from outside or inside the cell, e.g. by ligation of cell surface receptors, by DNA damage, treatment with cytotoxic drugs or irradiation, by a lack of survival signals or oxidative stress.

Molecular mechanism of apoptosis signalling pathways

1.10.1. Intrinsic (mitochondrial) apoptotic pathway: The pro-apoptotic proteins Bax, Bad, Bid, Bik, and Bim contain an alpha-helical BH3 death domain that fits the hydrophobic BH3 binding pocket on the anti-apoptotic proteins Bcl-2 and Bcl-XL, forming heterodimers that block the survival-promoting activity of Bcl-2 and Bcl-XL. Thus, the relative abundance of pro-apoptotic and anti-apoptotic proteins determines the susceptibility of the cell to programmed death (Lee and Wei 2000). The pro-apoptotic proteins act on the surface of the mitochondrial membrane to decrease the mitochondrial trans-membrane potential and promote leakage of cytochrome C. Cytochrome C, a key protein in electron transport, appears to act by forming a multimeric complex with Apaf-1, which in turn activates procaspase 9, and begins a Caspase cascade resulting in apoptosis (Budihardjo et al. 1999) (Figure 1.9).

1.10.2. Extrinsic (death receptor) apoptotic pathway: The extrinsic signaling pathways that initiate apoptosis involve trans-membrane receptor-mediated interactions (Elmore 2007). These involve death receptors that are

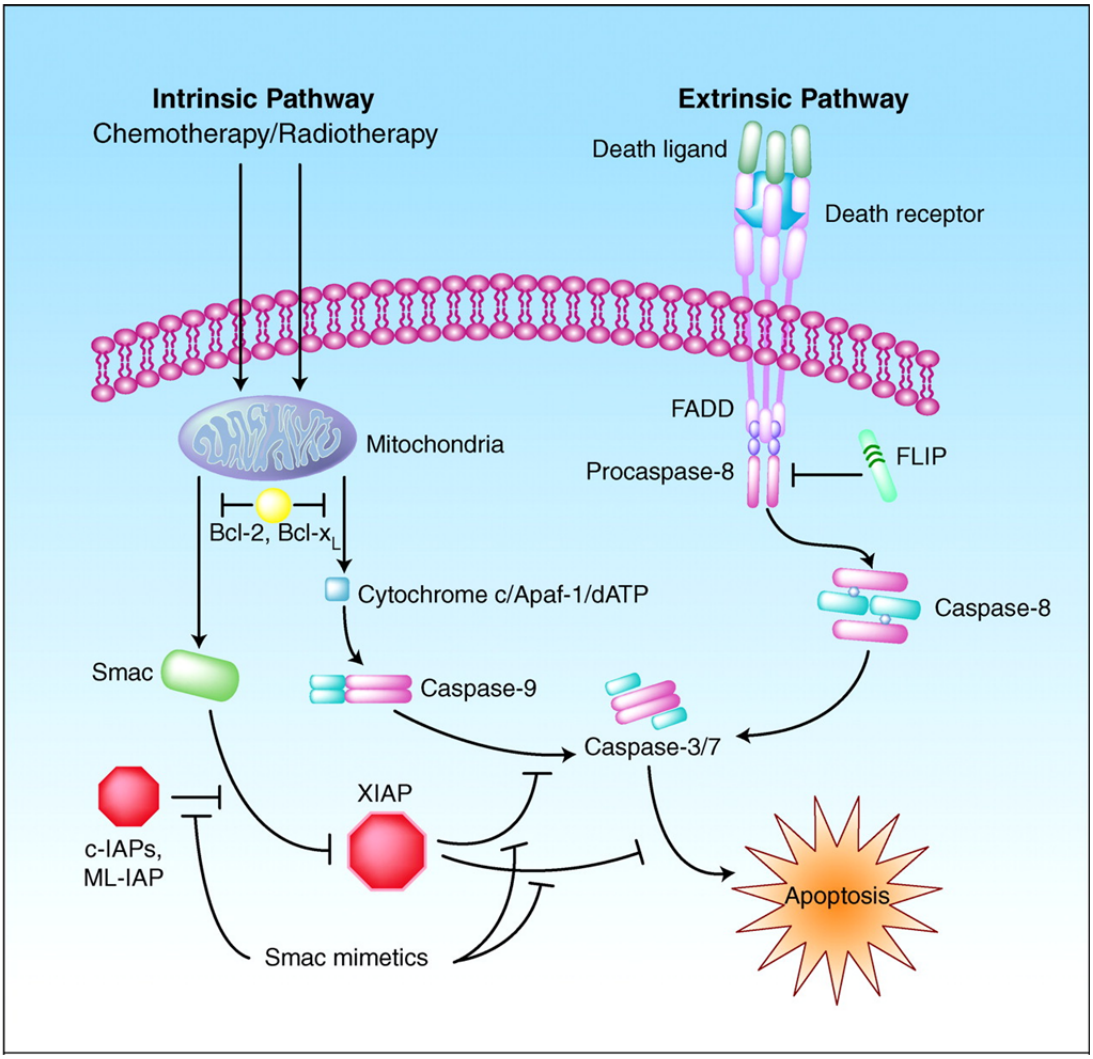

Figure 1.9. The intrinsic and extrinsic apoptotic pathway (Vucic and Fairbrother 2007).

members of the tumour necrosis factor (TNF) receptor gene superfamily. Upon ligation by its cognate ligand, the death receptor recruits adaptor molecules via its cytoplasmic death domains. The binding of Fas ligand to Fas receptor results in the binding of the adapter protein FADD and the binding of TNF ligand to TNF receptor results in the binding of the adapter protein TRADD. FADD then associates with procaspase-8 via dimerization of the death effector domain. At this point, a death-inducing signaling complex (DISC) is formed. When bound to the DISC, several procaspase-8 molecules are in close proximity to each other and therefore are assumed to activate each other by auto-proteolysis (Denault and Salvesen 2002). The initiatior caspase-8 activates effector caspases for the execution of apoptosis (Figure 1.9).

1.11. Mitogen activated protein kinase (MAPK) signalling pathways

Mitogen-activated protein (MAP) kinases are serine/threonine-specific protein kinases that respond to extracellular stimuli and regulate various cellular activities, such as gene expression, mitosis, differentiation, proliferation, and cell survival/apoptosis. MAPK signaling cascades are organized hierarchically into three-tiered modules. MAPKs are phosphorylated and activated by MAPK-kinases (MAPKKs), which in turn are phosphorylated and activated by MAPKK-kinases (MAPKKKs). The MAPKKKs are in turn activated by interaction with the family of small GTPases and/or other protein kinases, connecting the MAPK module to cell surface receptors or external stimuli (Zhang and Dong 2007). In mammals, three major MAPK pathways have been identified (Figure 1.10) which are mentioned below:

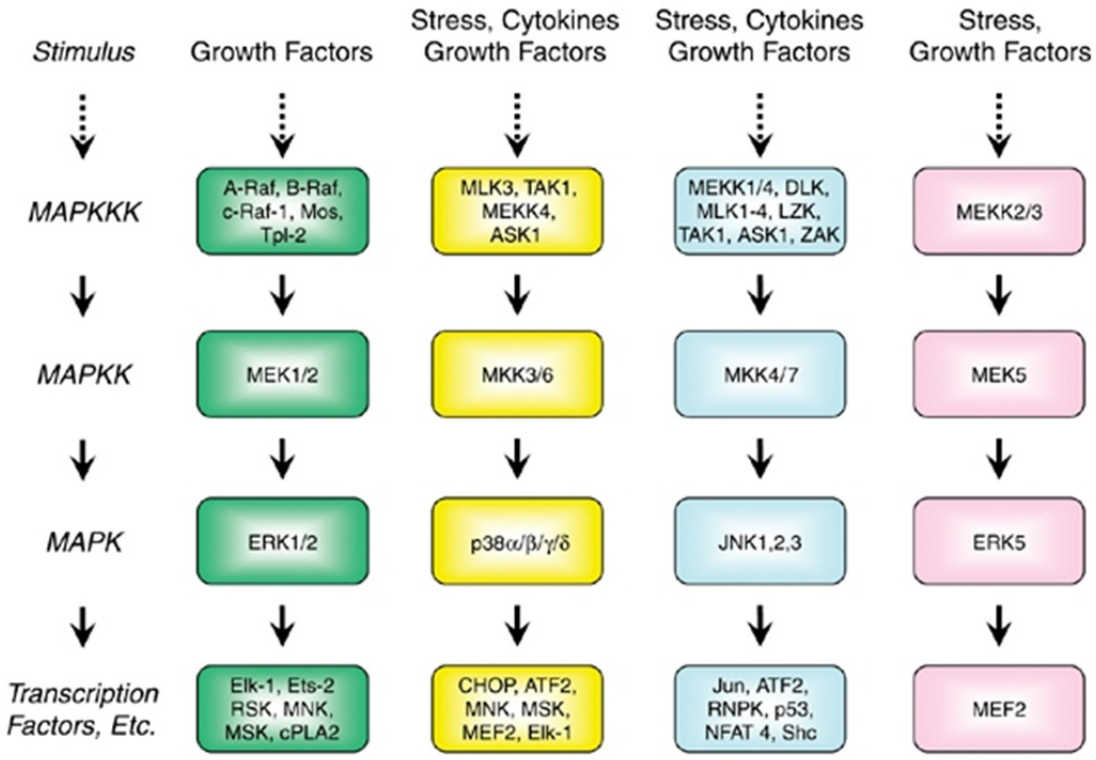

Figure 1.10. Mammalian MAPK cacades. There are four major mammalian MAPKKK–MAPKK–MAPK protein kinase cascades. The ERK pathway is commonly activated by growth factors, the JNK, p38 and ERK5 pathways are activated by environmental stress (Roberts and Der 2007).

1.11.1. Extracellular-signal-regulated kinase (ERK) pathway: These are widely expressed molecules that are involved in functions including the regulation of meiosis and mitosis in differentiated cells. Many different stimuli, including growth factors, cytokines, virus infection and carcinogens activate the ERK pathway (Boulton and Cobb 1991). Phosphorylation of ERKs leads to the activation of their kinase activity.

1.11.2. JNK pathway: c-Jun N-terminal kinase (JNK, also known as stress-activated protein kinase (SAPK)) is one of the leading candidate signal transduction mechanisms that transmits and converts stress signaling into apoptosis signaling in various cell types (Davis et al. 2007). The JNK pathway has been identified as a direct activator of the mitochondrial death machinery providing a molecular linkage from oxidative stress to the mitochondrial apoptosis machinery. It is known to cause the release of cytochrome c and AIF by selective permeabilization of the outer mitochondrial membrane (Aoki et al. 2002). Anti-apoptotic Bcl2 family proteins, namely Bcl2 and $Bclx_L$ were found to be phosphorylated by JNK suppressing their anti-apoptotic function (Maundrell et al. 1997).

1.11.3. p38 pathway: p38 MAPKs (α, β, γ, and δ) are members of the MAPK family that are activated by a variety of environmental stresses and inflammatory cytokines. p38 MAPK is involved in regulation of HSP27 and several transcription factors including ATF-2, Stat1, the Max/Myc complex, MEF-2, Elk-1 and indirectly CREB via activation of MSK1 (Coulthard et al. 2009) Most stimuli that activate p38 also activate JNK.

1.12. Zinc oxide nanoparticles

Zinc oxide is one of the most commonly used nanoparticles with wide ranging applications in various industrial and consumer products. The global production of the nanoparticle for sunscreen products was estimated to be approximately 1000 tons during 2003/2004 (Borm et al. 2006), and principally consisted of TiO2 and ZnO particles.

It forms an essential constituent of sunscreens and other dermatological preparations owing to its transparent appearance in nano form (Schilling et al. 2010). The sunscreens with traditional large sized ZnO particles appear white on skin. This is due to the reason that when light encounters a cluster of atoms or ions suspended in another medium, it gets scattered in multiple directions. The wavelength of light that is reflected/scattered from an object and reaches our eyes gives the object its colour. Scattering depends on cluster size and maximum scattering occurs when the wavelength is twice as large as the cluster size (Figure 1.11). Since traditional inorganic sunscreen ingredients have a diameter > 200nm, they scatter light which is near 400nm which includes light in the visible spectrum. The combination of different colours of visible light is white so the sunscreen appears white. However, the ZnO nanoparticles (<100nm) are too small to scatter visible light. The visible light passes through the sunscreen to the skin, interacts with the pigment melanin and the skin appears ‘skin coloured’ (Figure 1.12).

ZnO nanoparticles are also finding their way into the food industry in the form of additives and in packaging in view of their antimicrobial properties (Gerloff et al. 2009; Jin et al. 2009). They are being used in solar driven self coatings (Cai et al. 2006). They are being explored further by the

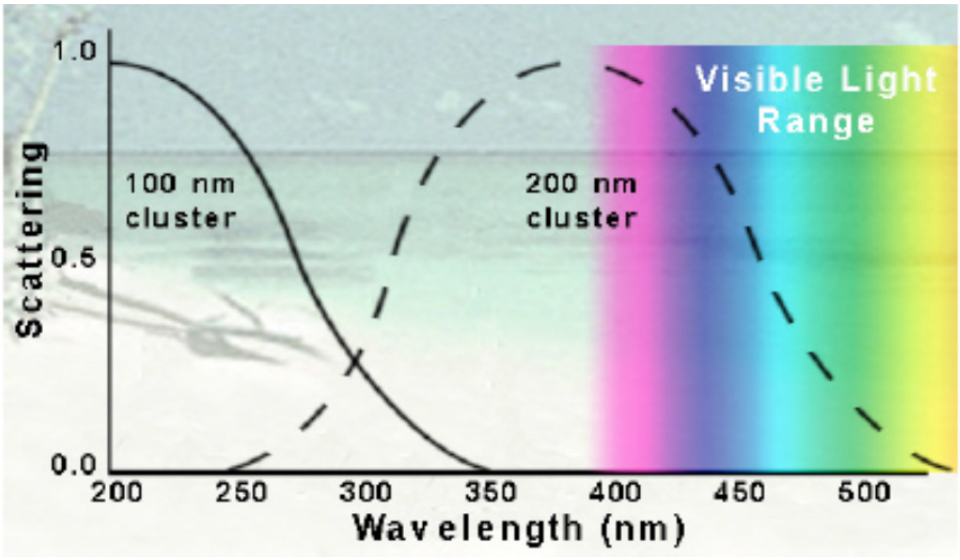

Figure 1.11. Scattering of light for 100nm and 200nm ZnO particles. (Source: www.nanosense.org).

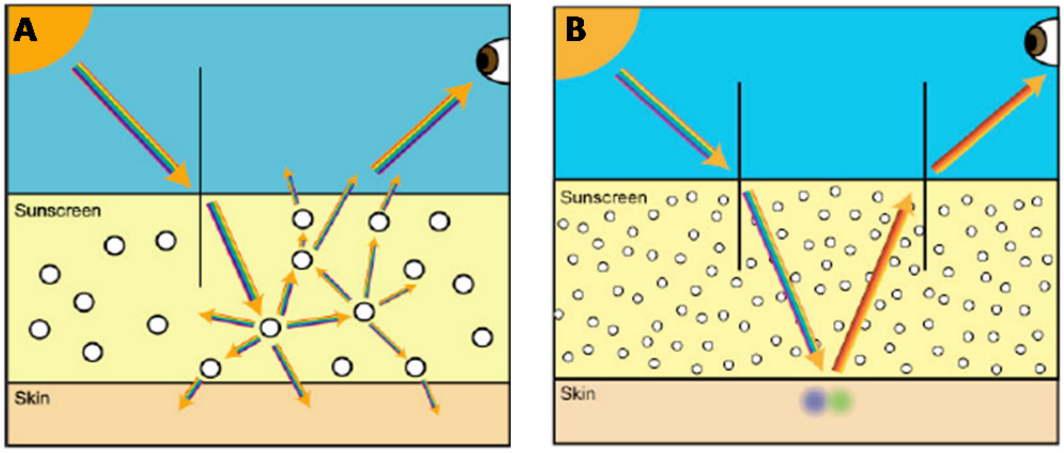

Figure 1.12. Interaction of visible light with different sized particles of ZnO (A) Large particles (>200nm) scatter visible light (B) Nanoparticles (<100nm) do not scatter visible light and let it interact with melanin (Source: www.nanosense.org).

nanotechnology researchers for developing diverse applications such as fungicides in agriculture (He et al. 2010), catalyst (Jung and Choi 2006) for use in fabrics (Yadav et al. 2006; Yuranova et al. 2007) and also in biomedical applications (John et al., 2010; Rasmussen et al. 2010).

ZnO is considered to be a 'GRAS' (generally recognized as safe) substance by the Food and drug administration (FDA), USA. However, the GRAS category refers to materials in the larger size range and even these substances when reduced to the nanoscale can develop new properties and thus may produce toxic effects. Some studies have demonstrated that ZnO nanoparticles were toxic to varying degrees to the bacteria (Reddy et al. 2010; Sinha et al. 2010), the eco-relevant species (Franklin et al. 2007; Zhu et al. 2009) and the mammalian cells (Gojova et al. 2007; Jeng and Swanson 2006; Osman et al. 2010; Yang et al. 2009b). However, the mechanisms of its toxicity are not well understood.

1.13. Aims and objectives of the study

The increased use of ZnO nanoparticles has aroused concerns regarding its unintentional health and environmental impacts. It is therefore prudent to study its toxicological effects on human health. The overall aim of the present study was to assess the *in vitro* and *in vivo* toxicity of ZnO nanoparticles in the mammalian system and to elucidate the possible mechanism of its toxicity. This was achieved by the following objectives:

1. To assess the uptake, cytotoxicity and genotoxicity of ZnO nanoparticles in human epidermal cells (human epidermal cell line and primary human epidermal keratinocytes).
2. To evaluate the cytotoxic and genotoxic potential of ZnO nanoparticles in human liver cells (HepG2) and elucidating the mechanism of its toxicity
3. To investigate the *in vivo* toxicity of ZnO nanoparticles in mice after acute exposure via oral administration.

CHAPTER – 2

Materials and methods

This chapter is a description of the chemicals, methods and instruments used in the present study. A visual display of various techniques used is given in Table 2.1.

Table 2.1. The techniques used in the present study.

Dynamic light scattering	
Transmission electron microscopy	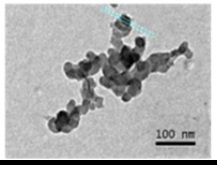
Scanning electron microscopy	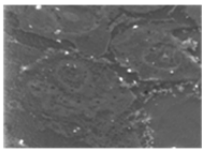
Flow cytometry	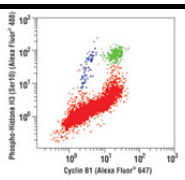
MTT assay	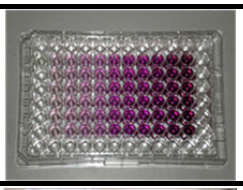
Neutral red uptake assay	
Lactate dehydrogenase release assay	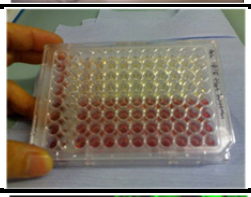
Measurement of reactive oxygen species	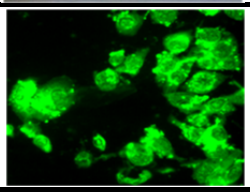
Lipid peroxidation assay	

Oxidative stress enzyme assays	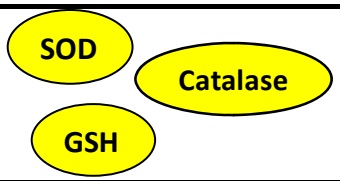
Comet assay	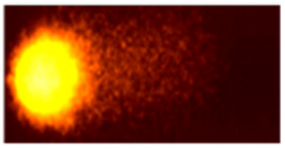
AnnexinV/PI double staining	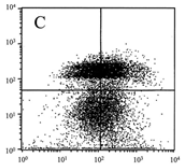
Hoechst staining	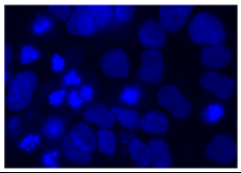
Mitochondrial membrane potential	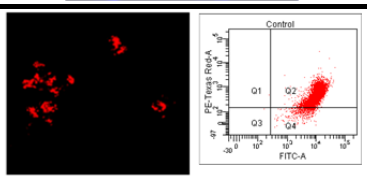
Histopathology	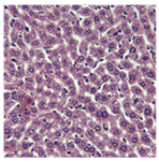
TUNEL assay	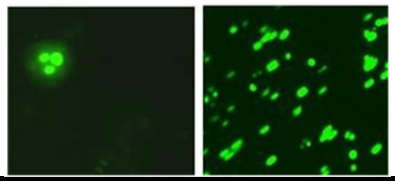
Western blot analysis	

2.1. Chemicals

Zinc oxide nanopowder (CAS No. 1314-13-2; purity >99%), neutral red dye, low melting point agarose (LMA), ethidium bromide (EtBr), Triton X-100, N-acetyl cysteine (NAC), Zinc chloride ($ZnCl_2$), SP600125, SB203580, Na-orthovanadate, Na-fluoride, Ponceau S stain, protease inhibitor cocktail were purchased from Sigma Chemical Co. Ltd. (St. Louis, MO, USA). Normal melting agarose (NMA), ethylenediaminetetraacetic acid (EDTA) disodium salt, and (3-(4, 5-dimethyl- thiazol-2-yl)-2, 5-diphenyl tetrazolium bromide (MTT) dye were purchased from Hi-media Pvt. Ltd. (Mumbai, India). Phosphate buffered saline (Ca2+, Mg2+ free; PBS), minimal essential medium (MEM), Dulbecco's minimal essential medium (DMEM), trypsin–EDTA, fetal bovine serum (FBS), trypan blue, antibiotic and antimycotic solution (10,000 U/ml penicillin,10 mg/ml streptomycin, 25µg/ml amphotericin-B) were purchased from Gibco, USA. Keratinocyte growth medium-2 (KGM-2) was purchased from PromoCell (Heidelberg, Germany). Fungizone (amphotericin-B), RPMI-1640 were purchased from Invitrogen (Loughborough, UK). All other chemicals were obtained locally and were of analytical reagent grade.

2.2. Characterization of nanoparticles

ZnO nanoparticles were suspended in complete culture medium (cell culture medium supplemented with 10% FBS) at a concentration of 80 µg/ml and probe sonicated (Sonics & Material Inc., New Town, CT, USA) at 30 watt for 10 min (2.5 min on and 30 sec off).

2.2.1. Dynamic light scattering

Size and zeta potential were determined using dynamic light scattering and phase analysis light scattering in a Zetasizer Nano- ZS, Model ZEN3600 equipped with 4.0mW, 633nm laser (Malvern instruments Ltd., Malvern, UK).

2.2.2. Transmission electron microscopy

Samples for transmission electron microscopy (TEM) analysis were prepared by drop coating ZnO nanoparticles suspension (8µg/ml in Milli-Q) on carbon-coated copper grids. The films on the TEM grids were allowed to dry prior to measurement. TEM measurements were performed on a JEOL model 1200EX instrument operated at an accelerating voltage at 120 kV.

2.3. Cellular uptake of nanoparticles

2.3.1. Flow cytometry

The uptake of nanoparticles using flow cytometry was carried out according to the method developed by Suzuki et al (2007). 2 x 10^5 cells/ well were seeded in 6-well cell culture plates. After 24 h of seeding, the cells were exposed to ZnO nanoparticles (8, 14, 20µg/ml) for 6 h. After exposure, the culture medium containing nanoparticles was removed and the cells were harvested using 0.05% trypsin. They were then centrifuged at 250g for 5min. The supernatant was discarded and the pellet was re-suspended in 0.5 ml of PBS. The uptake of nanoparticles was determined by a flow cytometer (FACS Canto™ II, BD Biosciences, San Jose, CA, USA) equipped with a 488 nm laser.

2.3.2. Electron microscopy

Transmission electron microscopy (TEM) and back-scattered electron scanning electron microscopy (BSE-SEM) were conducted on ZnO

nanoparticles exposed cells to determine the cellular uptake of nanoparticles according to the modified protocol of Bastian et al (2009). After 6 h exposure, the cells were washed with 1X PBS, harvested with 0.25% trypsin and fixed with 0.5% glutaraldehyde- 2% paraformaldehyde buffered in 0.1M sodium cacodylate at room temperature. The cells were then post-fixed in 1% osmium tetroxide and dehydrated through a series of alcohol (20% to 70%), stained in 0.5% uranyl acetate, followed by dehydration (90% and 100%) and embedded in epoxy resin (British BioCell International, Cardiff, Wales, UK). Ultrathin (60-90 nm) and semithin (200-500nm) sections were cut conventionally using a Reichert-Jung ultramicrotome (Vienna, Austria). The ultrathin sections were mounted on carbon-coated nickel grids (Agar Scientific) and examined on a Jeol-1200 EX transmission electron microscope (Jeol, Tokyo, Japan).

For SEM analysis, the semithin sections were mounted on glass slides and each slide was carbon coated. Specimens were viewed under field emission SEM (FEI, Quanta 400, Oregon, USA) using back scattered electrons at 20 KeV.

2.4. Cytotoxicity assays

2.4.1. MTT assay

This assay was conducted to assess the mitochondrial activity of cells. 3-4, 5-Dimethyl thiazol-2-yl 2,5-diphenyl tetrazolium bromide (MTT), is a yellow dye which is converted into formazan, a violet compound by the activity of the mitochondrial enzyme succinate dehydrogenase. MTT assay was done according to method of Mosmann (1983). Cells (10,000/well in 100µl medium) were seeded in 96 well plate and allowed to adhere overnight.

Medium was aspirated and cells were incubated at 37^{o}C for different time periods with nanoparticles and for 4 h with MTT dye (5mg/ml in PBS). The reaction mixture was carefully aspirated and the resulting formazan crystals were solubilized by adding 200µl dimethylsulphoxide. After 10min, absorbance was read at 530nm in a SYNERGY-HT multiwell plate reader, Bio-Tek (USA) using KC4 software. The untreated sets were also run parallel under identical conditions and served as control.

2.4.2. Neutral red uptake assay

The neutral red uptake assay was done by the method of Borenfreund and Puerner (1985) to determine cell viability. Cells (10,000/well in 100µl medium) were seeded in 96 well plates and allowed to adhere overnight. Medium was aspirated and cells were incubated at 37^{o}C for different time periods with nanoparticles. Thereafter, the medium was discarded and 100µl of neutral red dye (50 µg/ml in serum free medium) was added to each well. After incubation at 37^{o}C for 3 h, cells were washed with a solution of 0.5% formaldehyde and 1% $CaCl_2$. The dye taken up by cells was then dissolved in a medium containing 50% ethanol and 1% acetic acid in Milli-Q water. Absorbance was taken at 540nm in a SYNERGY-HT multiwell plate reader, Bio-Tek (U.S.A.) using KC4 software. The untreated sets were also run parallel under identical conditions and served as control.

2.4.3. Lactate dehydrogenase (LDH) release assay

LDH activity in extracellular medium due to membrane damage was assessed by Tox-7 *in vitro* toxicology assay kit (Sigma–Aldrich Inc., St. Louis, MO, USA) using manufacturer's protocol. The assay is based on the reduction of NAD by the action of LDH. The resulting reduced NAD (NADH)

is utilized in the stoichiometric conversion of a tetrazolium dye. The resulting colored compound is measured spectrophotometrically.

Cells (10,000/well in 100µl medium) were seeded in 96 well plate and allowed to adhere overnight. Medium was aspirated and cells were incubated at 37^{o}C for different time periods with nanoparticles. After completion of exposure period, the culture plates were centrifuged at 250g for 4 min. The supernatant of each well was transferred to a fresh flat bottom 96-well culture plate. LDH assay mixture was prepared by mixing equal amounts of LDH assay substrate, cofactor and dye solutions. This assay mixture was added in an amount equal to 2X the volume of supernatant present in each well. The plate was incubated in dark at room temperature for 20 min and the reaction was terminated by the addition of 1/10 volume of 1N HCl. The untreated cells were also run parallel under identical conditions and served as control. The resulting coloured compound was measured spectrophotometrically at 490nm in SYNERGY-HT multiwell plate reader, Bio-Tek (USA) using KC4 software.

2.5. Assays for oxidative stress markers

2.5.1. Reactive oxygen species (ROS) measurement

The level of intracellular ROS generation was estimated by the method of Wan et al (1993) using 2, 7-dichlorofluorescein diacetate dye (DCFDA; Sigma, St Louis, MO, USA). DCFDA is transported across the cell membrane and deacetylated by esterases to form the non-fluorescent 2',7'-dichlorfluorescein (DCFH). This compound is trapped inside the cells and oxidised to fluorescent product DCF by various ROS.

Cells (10,000/well in 100µl medium) were seeded in 96 well black bottom plate and allowed to adhere overnight. Medium was aspirated and cells were incubated at 37^{o}C for different time periods with nanoparticles. After exposure, the cells were washed twice with PBS and incubated with DCFDA dye (20µM) for 30 min at 37^{o}C. The reaction mixture was then replaced by 200µl of PBS and fluorescence intensity was measured in a SYNERGY-HT multiwell plate reader, Bio-Tek (USA) using KC4 software at excitation and emission wavelengths of 485nm and 528nm respectively. The qualitative analysis of ROS generation was done using a microscope with fluorescence attachment (DMLB, Leica, Germany).

2.5.2. Lipid peroxidation assay

The levels of lipid peroxides were estimated by Lipid Hydroperoxide Assay Kit (Cayman's Chemicals Kit, MI, USA) according to manufacturer's protocol.

A. Background:

The kit measures the hydroperoxides directly utilizing the redox reactions with ferrous ions. Hydroperoxides are highly unstable and react readily with ferrous ions to produce ferric ions. The resulting ferric ions are detected using thiocyanate as the chromogen.

B. Kit contents

(i) Extract R: crystalline solid provided for extraction of samples. A saturated solution of Extract R in methanol was prepared.

(ii) Lipid hydroperoxide standard: 50 µM ethanolic solution of 13-hydroperoxyoctadecadienoic acid (13-HpODE).

(iii) FTS reagent 1: 4.5mM ferrous sulphate in 0.2M hydrochloric acid.

(iv) FTS reagent 2: 3% methanolic solution of ammonium thiocyanate.

C. Procedure:

The cells from 75cm^2 culture flask were scraped and sonicated (10Watt for 5 sec) in chilled de-ionized water (1ml) and 500µl transferred to the glass test tubes. Equal volume (500µl) of Extract R saturated methanol was added to each tube and vortexed. 1ml chloroform was added to this mixture, mixed thoroughly by vortexing, centrifuged at 1500xg/ 0^{o}C for 5min and the bottom chloroform layer was carefully collected. 500µl of this chloroform extract was transferred to fresh glass test tubes and 450µl of chloform-methanol solvent mixture (1:1) was added to each sample tube. Chromogen was prepared by mixing equal amounts of FTS reagent 1 and FTS reagent 2 and 50µl of freshly prepared chromogen was added to each assay tube. After 5min, the absorbance was measured spectrophotometrically at 500nm in SYNERGY-HT multiwell plate reader, Bio-Tek (USA) using KC4 software. In this assay, a range of different concentrations (0-100nmol) of 13-HpODE were used to produce a standard curve.

2.5.3. Catalase assay

The catalase activity was estimated by Catalase Assay kit (Cayman's Chemicals Kit, MI, USA) according to manufacturer's protocol.

A. Background:

The method is based on the peroxidatic activity of catalase enzyme in which low molecular weight alcohols (e.g. methanol) serve as specific substrates for catalase. The product- formaldehyde is measured colorimetrically with 4-amino-3-hydrazino-5-mercapto-1,2,4-trizole (Purpald) as the chromogen.

B. Kit contents

(i) Assay buffer (10X): Diluted to 1X (100 mM potassium phosphate, pH 7.0) with HPLC-grade water before use.

(ii) Sample buffer (10X): Diluted to 1X (25 mM potassium phosphate, pH 7.5 containing 1mM EDTA and 0.1% BSA) with HPLC-grade water before use.

(iii) Formaldehyde standard: 4.25 M formaldehyde.

(iv) Catalase: The lyophilized catalase is reconstituted by adding 2ml of sample buffer to the vial and vortexing. 100µl of reconstituted enzyme is diluted with 1.9ml of sample buffer before use.

(v) Methanol

(vi) Hydrogen peroxide: 8.82 M solution of hydrogen peroxide. 40µl of hydrogen peroxide diluted with 9.96ml of HPLC-grade water before use.

(vii) Purpald: Solution of Purpald in 0.5M hydrochloric acid.

C. Procedure:

The cells from 75cm^2 culture flask were scraped and sonicated (10 Watt for 5 sec) in 1ml of sample buffer. The sonicated cells were centrifuged at 1500xg/ 4^{o}C for 5min and the supernatant was collected. 20µl of each sample along with assay buffer (100µl) and methanol (30µl) was added to the wells of a 96 well plate. At the same time, a range of different concentrations (0-75µM) of formaldehyde were used to produce a standard curve and 20µl of diluted catalase enzyme in two wells was used as the positive control. The reaction in each well was initiated by adding 20µl of hydrogen peroxide to each well for 20 min at room temperature. Purpald (30µl) was added to each well and the plate was incubated for 10min at room temperature. Following incubation, the absorbance was read at 540nm in SYNERGY-HT multiwell plate reader, Bio-Tek (USA) using KC4 software.

2.5.4. Superoxide dismutase (SOD) assay

The SOD activity was estimated by Superoxide Dismutase Assay Kit (Cayman's Chemicals Kit, MI, USA) according to manufacturer's protocol.

A. Background:

This assay utilizes a tetrazolium salt for detection of superoxide radicals generated by xanthine oxidase and hypoxanthine. One unit of SOD is defined as the amount of enzyme needed to exhibit 50% dismutation of the superoxide radical.

B. Kit contents

(i) Assay buffer (10X): Diluted to 1X (50mM tris-HCl, pH 8, containing 0.1mM diethylenetriaminepentaacetic acid (DTPA) and 0.1M hypoxanthine) with HPLC-grade water before use.

(ii) Sample buffer (10X): Diluted to 1X (50mM tris-HCl, pH 8) with HPLC-grade water before use.

(iii) Radical detector: Contains a solution of tetrazolium salt. Prior to use, 50µl of radical detector is diluted with 19.95ml of 1X assay buffer.

(iv) SOD standard: Contains a solution of bovine erythrocyte SOD.

(v) Xanthine oxidase: Prior to use, 50µl of the enzyme is diluted with 1X of 1.95ml of sample buffer.

C. Procedure:

The cells from 75cm^2 culture flask were scraped and sonicated (10Watt for 5 sec) in 1ml of 20mM HEPES buffer, pH 7.2, containing 1 mM EGTA, 210 mM mannitol and 70mM sucrose. The sonicated cells were centrifuged at 1500xg/ 4^{o}C for 5min and the supernatant was collected. 10µl of each sample along with the diluted radical detector (200µl) was added to the wells

of a 96 well plate. The reaction was started by adding 20µl of diluted xanthine oxidase to each well. The plate was incubated on a shaker for 20 min at room temperature. The absorbance was read at 450 nm in SYNERGY-HT multiwell plate reader, Bio-Tek (USA) using KC4 software. In this assay, a range of different concentrations (0-200µl) of SOD were used to produce a standard curve.

2.5.5. Glutathione (GSH) estimation

Glutathione content was measured according to the method of Ellman (1959).

Reagents:

(a) 0.2 M Phosphate PO_4 buffer, pH 8

(b) 0.01 % DTNB in PO_4 buffer (freshly prepared)

(c) 0.02 % Glutathione (freshly prepared)

(d) 5 % Trichloroacetic acid (TCA)

The cells from 75cm^2 culture flask were scraped and sonicated (15Watt for 10 sec) in 3ml of 1X PBS. 1ml of this cell homogenate was deproteinized by addition of an equal volume of 10% TCA and incubated at room temperature for 0.5h. It was then centrifuged at 2,500 rpm for 15min. To 0.5ml of supernatant, 2.5ml of DTNB reagent was added and kept for incubation for 15min. It was then read at 412nm. Different concentrations of glutathione were taken as standard. From the standard curve, glutathione content was calculated and expressed as µmole/mg of protein.

2.6. Cell viability assay using Trypan blue

Assessment of cell viability was made for all experiments of the Comet assay as per the guidelines of Tice et al (2000). Cell viability was assessed

by the trypan blue dye exclusion method (Phillips 1973). The principle of the assay is based on the fact that the live (viable) cells have an intact cell membrane that excludes dyes such as trypan blue, while the dead (non viable) cells have a compromised (permeable) cell membrane and hence take up the dye. Live cells appear shiny yellow and dead cells appear blue when observed under a bright field microscope.

10µl of cell suspension (~10^6 cells/ml) was added to 10µl trypan blue dye (0.4%) and mixed well. After 1-2min, 20µl of the mixture was loaded on to a clean haemocytometer and observed under bright field microscope under a 10X objective with a total magnification of 100X.

The viability (%) was calculated as follows:

$$\text{Viability (\%)} = \frac{\text{Total number of cells – stained (blue) cells}}{\text{Total number of cells}} \times 100$$

2.7. Single cell gel electrophoresis (SCGE) assay/ Comet assay

DNA damage was assessed using the Comet assay for *in vitro* studies employing cell line and for *in vivo* studies in different organs and tissues of mouse.

2.7.1. Standard alkaline Comet assay

Slides were prepared by the method as described (Singh et al. 1988) and modified (Bajpayee et al. 2005) in previous studies. Single cell suspension containing ~20,000 cells of interest in 100µl medium 1XPBS was mixed (1:1) with 1% low melting point agarose (LMPA). 80µl of the suspension was layered on to a microscopic slide pre-coated with 1% normal melting agarose. A coverslip was placed on the slide to ensure that the gel was evenly spread, and the slide was kept on ice to allow the gel to solidify. A

third layer of LMPA was added and again allowed to solidify on ice. Duplicate slides were prepared for each sample. The cover slips were removed and the slides immersed in freshly prepared and chilled lysis solution (2.5M NaCl, 100mM EDTA, 10mM Tris, pH10) with 1% Triton X-100 being added just before use (10% DMSO was also added when preparing slides from whole blood). The slides were kept in lysis solution overnight at 4^{o}C. The slides were subjected to DNA unwinding for 20min and subsequently electrophoresis was performed at 0.7V/cm and 300mA at 4^{o}C for 25min in freshly prepared electrophoresis buffer (1mM EDTA sodium salt and 300mM NaOH). All the steps were performed under dim light. After electrophoresis, the excess alkali was neutralized with Tris buffer (0.4M, pH7.5), and slides were stained with 75µl ethidium bromide (20µg/ml).

Slides were scored at a final magnification of 400X using an image analysis system (Kinetic Imaging, Liverpool, U.K.) attached to a microscope (Leica, Germany) equipped with fluorescence attachment and appropriate filter (N2.1). The Comet parameters used to measure DNA damage in the cells were % tail DNA (fraction of DNA in the tail) and Olive tail moment (OTM; arbitrary units, the product of the distance of DNA migration from the body of nuclear core and the total fraction of DNA in the tail; figure 2.1). As per the Comet assay guidelines (Hartmann et al. 2003; Tice et al. 2000) images from 50 cells (25 cells /replicate slide) were scored for *in vitro* studies while 100 cells (50 cells/ replicate slide) were scored for *in vivo* studies.

2.7.2. Fpg-modified Comet assay

To determine the oxidative DNA damage, the slides were immersed in two changes of enzyme buffer (40mM HEPES, 0.1M KCl, 0.5mM EDTA and 0.2

mg/ml bovine serum albumin (pH 8.0)) after lysis. Gels were then covered with 30µl Fpg enzyme (1:3000 dilution in enzyme buffer) and a cover slip and incubated in a humidified chamber for 30min at 37^{o}C (Smith et al. 2006). The slides were processed as in the standard alkaline Comet assay.

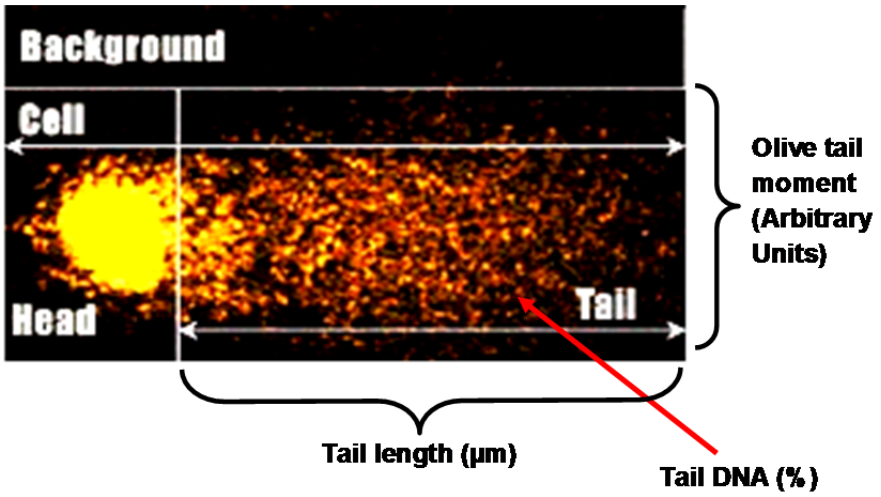

Figure 2.1. Cell marked with comet parameters.

2.8. Detection of apoptosis

2.8.1. AnnexinV/PI staining

Annexin V-FITC/PI staining was carried out by Annexin V-FITC apoptosis detection kit (Sigma, St Louis, MO, USA) as per the manufacturer's protocol using flow cytometry.

A. Kit contents

(i) Annexin V-FITC conjugate: 50 µg/ml in 50 mM Tris-HCl, pH 7.5 containing 100 mM NaCl.

(ii) Propidium Iodide (PI) solution: 100 µg/ml in 10 mM potassium phosphate buffer, pH 7.4, containing 150 mM NaCl

(iii) 10X binding buffer: 100 mM HEPES/NaOH, pH 7.5 containing 1.4 M NaCl. A working solution of 1X was prepared by diluting 1 part of stock with 9 parts of distilled H_2O.

B. Harvesting and staining

Cells were harvested with 0.05% trypsin and placed into a round bottom tube. They were centrifuged at 300xg for 5min at room temperature (20-25°C). Supernatant was discarded, pellet resuspended in cold PBS and centrifuged again at 300xg for 5min. The pellet was resuspended in binding buffer at a concentration of 1.0 x 10^6 cells/ml. 500µl of the cell suspension was transferred to 12 x 75 mm test tube. 5µl of Annexin V-FITC and 10µl of PI, was added to the tube and incubated for 15min in dark at room temperature. Analysis was done immediately using flow cytometer.

C. Flow cytometric analysis

Cells were analyzed using FACS Canto^{TM} II (BD Biosciences, San Jose, CA, USA). The events were recorded at wavelengths of 488nm (excitation) and 600nm (emission) as red fluorescence and 520nm (emission) for green fluorescence. Data was acquired using FACSDiva software (V6.1.2, BD Biosciences). A minimum of 10,000 events per sample was analyzed. Quadrant analysis of dot plot was done using FACSDiva software (V6.1.2, BD Biosciences) so as to estimate percentage of cells undergoing early and late apoptosis.

2.8.2. Hoechst staining

Apoptotic nuclear morphology was also assessed using Hoechst 33342 (Sigma, St Louis, MO, USA). Cells were fixed with 4% paraformaldelyde at room temperature for 30min, washed with PBS and stained with 2µg/ml

Hoechst 33342 at 37°C for 10min. The cells were washed and the morphology was observed by fluorescence microscopy (DMLB, Leica, Germany) at 200X.

2.9. Assessment of mitochondrial membrane potential

Mitochondrial membrane potential ($\Delta\Psi_m$) was detected with fluorescent probe 5,5′,6,6′-tetrachloro-1,1′,3,3′-tetraethylbenzimidazolcarbocyanine iodide (JC-1; Molecular probes, USA), which exists predominantly in green fluorescent monomeric form in cells with depolarized mitochondria and in aggregate form (reddish orange) in cells with polarized mitochondria. Cells exposed to ZnO nanoparticles were harvested with 0.05% trypsin and placed into a round bottom tube. They were centrifuged at 300xg for 5min at room temperature (20-25°C). Supernatant was discarded, pellet resuspended in cold PBS and centrifuged again at 300 x g for 5min. The cells were incubated with 10 µM JC-1 dye for 15min at 37^{o}C, washed with PBS and re-suspended in PBS at a concentration of 1.0 x 10^6 cells/ml. Cells were analyzed using FACS Canto^{TM} II (BD Biosciences, San Jose, CA, USA) and the events were recorded at wavelengths of 488 nm (excitation) and 600nm (emission) as red fluorescence and 520nm (emission) for green fluorescence. Data was acquired was using FACSDiva software (V6.1.2, BD Biosciences). A minimum of 10,000 events per sample was analyzed. Quadrant analysis of dot plot was done using FACSDiva software (V6.1.2, BD Biosciences).

For qualitative analysis, the cells were imaged for green and red fluorescence using a microscope with fluorescence attachment (DMLB, Leica, Germany) at 200X.

2.10. Western blot analysis

Western blotting was done to assess the expression levels of proteins of interest.

Protein extraction

For *in vitro* experiments, cells treated with ZnO nanoparticles were collected in chilled PBS by scraping and pelleted by centrifugation at 500xg for 10min. The cell pellet was then washed with PBS and 150µl of CelLytic^{TM} M Cell Lysis Reagent (Sigma, St. Louis, MO, USA) supplemented with Na-orthovanadate, Na-fluoride, protease inhibitor cocktail was added to it. The cell pellet was vortexed gently and kept for 10min in ice. Finally, the lysed cells were centrifuged at 10,000xg for 5 min and the supernatant containing the solublised protein collected and stored at 80^{o}C.

For *in vivo* samples, the tissue was homogenized with Polytron PT 1600 E (KINEMATICA, Switzerland) in CelLytic^{TM} M Cell Lysis Reagent (25µl/mg of tissue; Sigma, St. Louis, MO, USA) supplemented with Na-orthovanadate, Na-fluoride, protease inhibitor cocktail and subsequently processed as described above.

Protein estimation

The total protein concentration was measured by the method of Bradford (1976). The assay is based on an absorbance shift in the dye coomassie (red colour) which changes and stabilizes into coomassie blue by the binding of protein. The characteristic blue colour has a maximum absorbance at 595nm which is proportional to the amount of bound dye, and thus to the concentration of protein present in the sample. In this assay a range of different concentrations (0-100µg/ml) of bovine serum albumin were used to

produce a standard curve. The optical densities of BSA standards and unknown samples were read at 595nm on a SYNERGY-HT multiwell plate reader, Bio-Tek (U.S.A.) using KC4 software.

Sodium dodecyl sulphate-polyacrylamide gel electrophoresis (SDS-PAGE)

The 10% resolving gel solution (30% acrylamide, 1.5M Tris-Cl (pH 8.8), 10% SDS, 10% ammonium persulphate and 20µl TEMED) was mixed thoroughly and poured into the preset casting assembly (Bio-Rad Laboratories, California, USA) followed by the 5% stacking gel solution (30% Acrylamide, 1.5M Tris-Cl (pH 6.8), 10% SDS, 10% ammonium persulphate and 20 µl TEMED). Gel was placed in the electrophoresis tank as instructed by the manufacturer and bathed in gel running buffer (0.125M Tris base, 1M Glycine, 0.5% SDS). 2X Laemmeli buffer (4% SDS, 20% glycerol, 10% 2-mercaptoethanol, 0.004% bromphenol blue, 0.125 M Tris HCl, pH6.8) was added to the whole cell lysate proteins in equal amount and the samples were heated at 95^{o}C for 5 min. 4 µl of the pre-stained protein ladder (PageRuler^{TM} Plus; Fermentas Life Sciences, USA) and denatured protein samples (40µg) were loaded into the appropriate well. The gel was run at a constant voltage of 100V until the dye from Laemmeli buffer reached the lower window on the cassette.

Electro-transfer of protein on nitrocellulose membrane

After separation of proteins on the SDS-PAGE gel, proteins were electro transferred to a nitocellulose membrane (Pall Corporation, Florida, USA). The nitrocellulose membrane was equilibrated in transfer buffer (192 mM glycine, 25 mM Tris base and 20%methanol). The membrane was placed

next to the gel and sandwiched between sponges. All were clamped tightly together after ensuring no air bubbles have formed between the gel and membrane. The sandwich was submerged in transfer buffer in an electrotransfer apparatus (Bio-Rad Laboratories, California, USA). The power supply was connected at a constant voltage of 100V for 1h. The negatively-charged proteins travel towards the positively-charged electrode, but the membrane stops them and binds them. The membrane was then blocked with blocking buffer.

Incubation with antibodies and detection of protein bands

TBST buffer was prepared by adding 0.05% Tween-20 in Tris buffer saline (10mM Tris base, 150mM Sodium chloride; pH7.2). The non-specific binding sites were blocked with blocking buffer - 5% non fat milk in TBST buffer. After 1.5h of blocking at room temperature on a rocking platform, the membrane was probed with anti-human primary antibodies (1:1000 diluted in TBST) against β-actin, JNK, phospho-JNK, ERK1/2, phospho-ERK1/2, p38, phospho-p38, caspase-9, p53, phospho-p53 (Ser15), Bcl2, Bax, nuclear factor kappa β (NF-kβ), (Cell Signaling Technology, Danvers, MA, USA) for 1h at room temperature followed by overnight incubation at 4^{o}C. The membranes were then washed with TBST thrice (4min each time). After washing, the membrane was incubated with secondary anti-primary antibody conjugated to horseradish peroxidase (Calbiochem,USA) for 1h at room temperature. The membrane was again washed thoroughly with TBST buffer and antigen antibody complex signals were detected using an enhanced chemiluminescence detection system according to the manufacturer's protocol (Super Signal West Pico Chemiluminescent Reagent, Pierce,

Rockford, IL, USA). Relative expression of each protein was determined by densitometric analysis using Scion Image program (Scion Corporation, Fredrick, MD, USA). β-actin served as protein loading control.

2.11. *In vivo* studies

2.11.1. Animals and treatment

All animal-handling procedures were carried out following the regulations of Institutional Animal Ethics Committee and with their prior approval for using the animals. Male Swiss albino mice (~6-week-old, 20 ± 2g) were obtained from the Indian Institute of Toxicology Research (Lucknow, India) animal breeding colony and were housed in a 12-h day and light cycle environment with *ad libitum* availability of diet and water, at the controlled temperature of 23 ± ^{o}C, humidity of 55 ± 5%. The animals were maintained. The animals were divided into 3 groups containing 25 mice each: Group 1- vehicle control (water); Group 2- ZnO nanoparticles (300mg/Kg body weight); Group 3- ZnO nanoparticles (50mg/Kg). The animals were treated daily through gavage for 14 consecutive days according to the fixed dose procedure OECD Guideline 420 (OECD 2001).

All animals were weighed at the beginning and end of each treatment. After the treatments, the animals were sacrificed by cervical dislocation. Organs were taken out immediately for isolation of single cells.

2.11.2. Zn content analysis in tissues

Approximately 1g of the tissue from liver, kidney and brain were taken in a 100ml conical glass flask. Each sample was solubilised by the addition of 2 ml concentrated nitric acid and left overnight. After 24h, 5ml of concentrated nitric acid and perchloric acid mixture (6:1) was added to each sample and

heated at 80-90^{o}C until the solutions were colourless and clear.The concentrated solutions were diluted to 5ml with 1% nitric acid. The Zn content was analyzed by an atomic absorption spectrophotometer (ZEEnit 700 P, Analytikjena, Germany). Before analysis, the atomic absorption spectrophotometer (AAS) was calibrated every time by running at least three standard concentrations (0.25, 0.5 and 1 mg/L) of zinc.

2.11.3. Biochemical assays in serum

The serum was obtained by centrifugation of the whole blood at 3000 rpm for 15min. The serum biochemical levels including alanine aminotransferase (ALT), alkaline phosphatase (ALP), bilirubin, creatinine, blood urea nitrogen were assayed by an automated haematology analyzer (Bayer, USA). Standard controls were run before each determination.

2.11.4. Lipid peroxidation (LPO) assay

A 10% homogenate was made in ice cold buffer comprising 0.1M Na_2HPO_4, 0.1M NaH_2PO_4 and 0.1M KCl, using a Polytron PT 1600 E (KINEMATICA, Switzerland). The homogenate was then centrifuged at 9000xg for 10min and the supernatant was used for the enzymatic assay.

LPO was measured using the method of Utley et al (1976) by estimating malondialdehyde (MDA) formed with 2-thiobarbituric acid (TBA). An aliquot of homogenate (10% w/v) was taken in a test-tube and incubated for 1h at 37^{o}C in water bath with constant shaking. The reaction was terminated by the addition of 1ml of chilled 10% Trichloroacetic acid (TCA) (w/v). The control tubes received TCA prior to the start of incubation. The contents were then centrifuged at 2000g for 10min and 1ml of clear supernatant was withdrawn and mixed with 1ml of TBA (0.67% w/v) and kept in a boiling

water bath for 10min. The intensity of developed colour was measured at 535nm after dilution with 1ml of water. The results were expressed as nanomoles of MDA formed per hour per g tissue.

2.11.5. Histopathology

The organs (liver, kidney) from control and treated mice were fixed in 10% formalin for 24-48h at room temperature (RT). The tissue slices from these organs were dehydrated through 50%, 70%, 80%, 90% alcohol, followed by 3 changes of 100% alcohol, 1 h each. The tissue slices were kept in chloroform, 2 changes of 1 h each and then for 1.5 h at last. They were then dipped in molten paraffin wax, 2 changes for 1.5 hr each and then embedded in paraffin wax in a steel mould. The prepared paraffin tissue blocks were stored at RT until used for cutting sections.

From the paraffin-embedded tissue blocks 5-8µm thick sections were cut using microtome and floated in 40°C water bath containing distilled water. The sections were mounted onto glass slides. The slides were allowed to dry overnight and stored at RT until used for staining.

The paraffin embedded sections were dewaxed in xylene and rehydrated by passage through gradient alcohol series. They were stained with Harris's haematoxylin for 5 min and washed in running tap water followed by acid alcohol wash for 5-10 sec. After washing with tap water, sections were rinsed with ammonia water. Sections were then stained with 1% eosin for 30 sec and washed in tap water for 15-30 sec. The sections were then dehydrated through alcohol, cleared in xylene and mounted in DPX. The stained sections were then examined by light microscopy for the histopathological changes.

2.11.6. TUNEL assay

Principle:

In situ detection of apoptosis was performed by terminal deoxynucleotide-transferase (TdT)-mediated dUTP nick end labeling (TUNEL) using a "*In Situ* Cell Death Detection Kit, Fluorescein" (Roche, UT, USA). Cleavage of genomic DNA during apoptosis may yield double-stranded, low molecular weight DNA fragments (mono- and oligonucleosomes) as well as single strand breaks ("nicks") in high molecular weight DNA. Those DNA strand breaks can be identified by labeling free 3'-OH termini with modified nucleotides in an enzymatic reaction. DNA strand breaks are labelled by Terminal deoxynucleotidyl transferase (TdT), which catalyzes polymerization of labelled nucleotides to free 3'-OH DNA ends in a template-independent manner (TUNEL-reaction). Fluorescein labels incorporated in nucleotide polymers are detected and quantified by fluorescence microscopy.

Procedure:

After de-paraffinization and rehydration, paraffin embedded sections were incubated in permeabilization solution (0.1% Triton X-100, 0.1% sodium citrate, freshly prepared) for 2min on ice. After washing with PBS, the area around the section was dried and 50µl of TUNEL reaction mixture (5µl deoxynucleotide-transferase enzyme in 45µl labeled thymidine solution) was added on each section. The slides were incubated in a humidified atmosphere for 60min at 37°C in the dark. The slides were rinsed 3 times with PBS and counterstained with Hoechst 33258 (Molecular probes)

nuclear stain and mounted in antifade mountant. The coverslips were sealed and observed under fluorescent microscope. Then, stained cells were visualized using a microscope with fluorescence attachment (DMLB, Leica, Germany).

2.12. Statistical analysis

Appropriate statistical methods [Student's t-test, one way analysis of variance (ANOVA)] were employed for data analysis and have been described in the relevant chapters. Prior to analysis, homogeneity of variance between treatment and normality assumption of data were tested. $p<0.05$ was considered significant.

CHAPTER – 3

Toxic responses to ZnO nanoparticles in human epidermal cells

3.1. Introduction

Increased consumer demands in conjunction with rapid technological advances have resulted in an intensive expansion of nanotechnology applications all over the world. However, it has raised concerns with the public as well as in the scientific community regarding the unanticipated and adverse affects of nanoparticles on human health and the environment.

This widespread use of nanotechnology may expose humans to nanoparticles through different routes such as- oral, dermal and inhalation (Nel et al. 2006). Out of all these possible routes, the skin may serve as the first portal of entry for these nanoparticles either directly or indirectly through intercellular, trans-cellular or trans-appendageal routes (Baroli 2009; Crosera et al. 2009). This high probability of nanoparticle-skin contact has raised the debate on nanoparticle-skin penetration and subsequent interaction with skin cells yielding a few studies on the topic (Cross et al. 2007; Wu et al. 2009). However, the outcomes of these studies are contradictory and inconclusive. Some of these studies report the inability of nanoparticles to pass through the protective skin barrier (Cross et al. 2007; Gamer et al. 2006; Schulz et al. 2002) while others have shown the possible absorption of nanoparticles with diverse physicochemical properties through cutaneous barrier (Baroli et al. 2007; Ryman-Rasmussen et al. 2006; Sonavane et al. 2008; Wu et al. 2009; Zhang et al. 2008).

Furthermore, it cannot be ruled out that the stratum corneum barrier may be compromised in many conditions like abrasions, wounds, burns, pathological alterations (psoriasis; atopic dermatitis), prolonged exposure to chemicals, detergents, skin flexures etc (Baroli 2009). There is evidence that

nanoparticle penetration/permeation is facilitated by these breaches in skin integrity (Kuo et al. 2009; Mortensen et al. 2008; Nielsen et al. 2007; Oberdorster et al. 2005; Zhang and Monteiro-Riviere 2008). Larese et al. (2009) suggested an increased dermal penetration of silver nanoparticles associated with damaged skin *in vitro* in Franz diffusion cells with full thickness human skin. Similar observations were made by Trop et al. (2006) following the use of nanosilver coated dressings in case of extensive burns. Skin flexions facilitating nanoparticles uptake has also been reported (Rouse et al. 2008; Tinkle et al. 2003).

ZnO nanoparticles are one of the widely used nanoparticles in cosmetics and sunscreens as they do not scatter visible light. This makes them transparent and more aesthetically acceptable compared to their larger opaque counterparts (Cross et al. 2007). Due to high possibilities of nanoparticle-skin penetration and subsequent interactions make it necessary to evaluate the potential adverse effects of nanoparticles on human skin cells.

Therefore, the aim of the present study was to assess the effects of ZnO nanoparticles in human skin cells (primary human epidermal keratinocytes and A431 cell line). This was done to evaluate the toxicity of ZnO nanoparticles on human skin cells as well as to understand if the responses observed in the primary human skin cells are similar to that observed in the human skin cell line.

3.2. Materials and methods

3.2.1. Cell culture

3.2.1.1. A431 cell culture

Human epidermal cell line (A431) obtained from National Centre for Cell Sciences, Pune, India was cultured in DMEM supplemented with 10% fetal bovine serum, 10ml/l of antibiotic and antimycotic solution at 37^{o}C under a humidified atmosphere of 5%CO_2/ 95% air.

3.2.1.2. Isolation and culture of human epidermal keratinocytes

The study with primary human epidermal keratinocytes was done in collaboration with Centre for Skin Sciences, University of Bradford, Bradford. Human scalp tissue was obtained with informed consent and local research ethics committee approval (Reference number: E01) from a normal healthy Caucasian donor (female 66y) after elective plastic surgery. Skin samples were collected in RPMI 1640 medium and were processed within 5 h of surgery. Epidermal keratinocyte cultures were established as previously described by Kauser et al. (2003). Briefly, tissue specimens were washed with 0.1 M phosphate-buffered saline (PBS) pH 7.4 containing fungizone (12.5 µg/ml), penicillin (500 U/ml) and streptomycin (12.5 µg/ml). Epidermal sheets were separated from the underlying dermis after 18 h incubation in 0.25% trypsin solution at 4°C and dispersed into individual cells. The cells were then grown in KGM-2 containing 0.004ml/ml bovine pituitary extract, 0.125 ng/ml recombinant epidermal growth factor, penicillin (100 U/ml) /streptomycin (100 µg/ml) and 2 mM L-glutamine. The cells were incubated at 37°C under a humidified atmosphere of 5%CO_2/ 95% air and the culture medium was changed every second day.

3.2.2. Characterization of ZnO nanoparticles

The particles were characterized by dynamic light scattering and transmission electron microscopy (TEM) as described in Chapter 2 (2.2).

3.2.3. Exposure of cells to nanoparticles

The cells were plated at a density of 10^5 cells/ml in a 96 well plate and 12 well plate for the cytotoxicity assays and Comet assay respectively. They were then allowed to attach for 24h before the addition of nanoparticles suspension. Stock suspension of ZnO nanoparticles (80 µg/ml) in DMEM (for A431cells) and KGM-2 (for primary human epidermal keratinocytes) was diluted to different working concentrations. Cells were then exposed to different concentrations of ZnO nanoparticles for diverse time periods as per the experimental design.

To determine the cellular uptake of nanoparticles, the cells were seeded in cell culture flasks ($25cm^2$) and grown to 70% confluency at 37^oC in a humidified 5% CO_2 environment. The cells were then treated with ZnO nanoparticles for 6h.

For evaluating oxidative stress markers, the cells were cultured in $75cm^2$ culture flask and exposed to ZnO nanoparticles for 24h.

3.2.4. Cellular uptake

The cellular uptake of nanoparticle in the cells was determined by electron microscopy as described in Chapter 2 (2.3.2).

3.2.5. Cytotoxicity assays

The cytotoxicity assays viz. MTT, neutral red uptake and LDH release were performed as described in Chapter 2 (2.4).

3.2.6. Cell morphology

Cell morphology was assessed following exposure to nanoparticles using a Leica DMIL phase contrast microscope (magnification X100).

3.2.7. Cell viability

Cells were incubated with ZnO nanoparticles for 6h at different concentrations and assayed for viability using Trypan blue dye exclusion (Philips 1973) as described in Chapter 2 (2.6).

3.2.8. Single cell gel electrophoresis/ Comet assay

The Comet assay was performed as described previously in Chapter 2 (2.7.1).

3.2.9. Oxidative stress markers

The levels of oxidative stress in ZnO nanoparticles exposed cells were analysed by measuring lipid peroxidation, glutathione, superoxide dismutase and catalase levels as described in Chapter 2 (2.5).

3.2.10. Statistical analysis

Results were expressed as mean ± standard error of mean (S.E.M.) and the data were analyzed by one way analysis of variance (ANOVA) with Dunnett post hoc test to determine significance compared to unexposed control, using SPSS v. 16.0 software (SPSS Inc., Chicago, IL, USA). In all cases, $p < 0.05$ was considered significant.

3.3. Results

3.3.1. Characterization of ZnO nanoparticles

The mean hydrodynamic diameter and zeta potential of the ZnO nanoparticles (80µg/ml) suspension in DMEM (supplemented with 10% FBS)

was 273nm and -12.7mV respectively (Figure 3.1A-B), while in KGM-2, it was 245nm and −15.8mV (Figure 3.1C-D).

The average size reported by TEM was 30nm. Figure 3.1E shows a representative TEM image recorded from a drop-coated film of ZnO nanoparticles.

3.3.2. Studies with human epidermal skin cells (A431)

3.3.2.1. Cellular uptake of ZnO nanoparticles

A431 cells exposed to ZnO nanoparticles (8µg/ml) for 6h showed a significant cellular uptake of the nanoparticles and their accumulation in the vesicles and nucleus as evident from the TEM microphotographs (Figure 3.2).

3.3.2.2. Cytotoxicity of ZnO nanoparticles

A431 cells were exposed to ZnO nanoparticles (0.008–20µg/ml) for 3, 6, 24 and 48h and cytotoxicity was determined with MTT assay, LDH release assay, and NRU assay. The MTT results demonstrated a concentration and time dependent cytotoxicity after exposure to nanoparticles (Figure 3.3A). The cytotoxicity was evident even after 3h at the highest concentration (20µg/ml). The percentage (%) MTT reduction (relative to control) observed after 24h exposure at concentrations 0.8, 5 and 8µg/ml was 91%, 52% and 25% respectively with a further decrease to 86%, 42% and 9% after 48h exposure. The results of NRU assay showed a similar concentration and time dependent response with a loss in cell viability at 8-20µg/ml after 24 and 48h exposure (Figure 3.3B). A significant ($p < 0.05$) LDH leakage was observed at 24h and 48h on exposure to 5, 8 and 20µg/ml ZnO nanoparticle concentrations (Figure 3.3C).

3.3.2.3. Cell morphology

A comparative morphology of unexposed cells and ZnO nanoparticles exposed cells is shown in figure 3.4. Cells treated with ZnO nanoparticles (8µg/ml) for 24h retracted into spherical shape and detached from the surface of culture flask forming clusters (Figure 3.4A–D). The changes in morphology started becoming visible even after 6h exposure with a few cells becoming spherical.

3.3.2.4. Cell viability

The cell viability in the Comet assay exceeded 90% for all experimental groups (data not shown) before and after the treatment as assessed by Trypan blue dye exclusion assay.

3.3.2.5. Genotoxic potential of ZnO nanoparticles

A significant induction ($p < 0.05$) in the DNA damage was observed in cells exposed to ZnO nanoparticles for 6h compared to control as evident by the Comet assay parameters i.e. Olive tail moment (arbitrary unit) and tail DNA (%) (Table 3.1).

3.3.2.6. Oxidative stress parameters

Effect of ZnO nanoparticles on lipid peroxidation

Lipid peroxidation was examined by measuring hyderoperoxide concentration. A significant increase ($p<0.05$) in hydroperoxide formation was observed at all concentrations above 0.008µg/ml of ZnO nanoparticles as evident from Figure 3.5A.

Effect of ZnO nanoparticles on glutathione level

Cells exposed to ZnO nanoparticles showed statistically significant ($p<0.05$) depletion of GSH levels at 0.8 and 0.08µg/ml respectively after 24h (Figure 3.5B).

Effect of ZnO nanoparticles on catalase activity

ZnO nanoparticles exposed cells at the highest concentration (0.8µg/ml) showed 64% decrease ($p < 0.05$) when compared to control. Cells exposed to 0.08 and 0.008µg/ml of concentrations also exhibited decrease ($p < 0.05$) of 55% and 36% respectively (Figure 3.5C).

Effect of ZnO nanoparticles on SOD activity

SOD activity in cells treated with 0.008, 0.08 and 0.8µg/ml ZnO nanoparticles was significantly ($p<0.05$) reduced after 24h of exposure when compared to unexposed cells as evident from Figure 3.5D.

3.3.3. Studies with primary human epidermal keratinocytes

3.3.3.1. Cellular uptake of ZnO nanoparticles

The primary human epidermal keratinocytes were treated with ZnO nanoparticles (14 µg/ml) for 6h and the cellular uptake of nanoparticles was investigated by scanning electron microscope using back scattered electrons imaging. Nanoparticle agglomerates with strong BSE signals were visible in cells treated with ZnO nanoparticles (Figure 3.6A-B).

Further confirmation of ZnO nanoparticles internalization into the cells was obtained by transmission electron microscopy which revealed nanoparticles in the cytoplasm (Figure 3.7A-B) and in the filopodia extending from the cell body (Figure 3.7C, High power view).

3.3.3.2. Cytotoxicity of ZnO nanoparticles

The primary human epidermal keratinocytes were exposed to ZnO nanoparticles (4-20µg/ml) for 6, 12 and 24h and cytotoxicity was determined with the MTT assay which demonstrated a concentration and time dependent decrease in the mitochondrial activity (Figure 3.8). The cytotoxicity was evident after 6h at the highest concentration (20µg/ml). The percentage (%) MTT reduction (relative to control) observed after 12h exposure at concentrations 8, 14 and 20 µg/ml was 80%, 72% and 69% respectively with a further decrease to 59%, 51% and 31% after 24h exposure.

3.3.3.3. Cell morphology

The changes in cell morphology on exposure to ZnO nanoparticles (20µg/ml for 6h) also corroborated our cytotoxicity results (Figure 3.9). The cells started retracting from their normal morphology giving rise to blank spaces in a uniformly spread cell monolayer. With increasing concentration and time they tended to become round detaching from the culture surface and coming into the medium.

3.3.3.4. Cell viability

The cell viability in the Comet assay exceeded 90% for all experimental groups (data not shown) before and after the treatment as assessed by Trypan blue dye exclusion assay.

3.3.3.5. Genotoxic potential of ZnO nanoparticles

A significant induction ($p<0.05$) in DNA damage was observed in cells exposed to ZnO nanoparticles for 6h at 8 and 14µg/ml concentrations

compared to control as evident by the Comet assay parameters i.e. Olive tail moment (arbitrary unit) and tail DNA (%) (Table 3.1).

3.4. Discussion

The human epidermal cells may be the first portal of entry for nanoparticles through consumer products and to some extent the environment. Moreover, any perturbation in the integrity of skin barrier may provide easy access to these nanoparticles into the skin. This necessitated the study to understand the biological consequences of interactions of ZnO nanoparticles with human skin cells. The present study demonstrates that ZnO nanoparticles are internalized in the human epidermal cells and elicit a cytotoxic response. We have also observed DNA damaging effects of ZnO nanoparticles on human epidermal cells for which lipid peroxidation and oxidative stress may be attributed as one of the probable reason.

The characterization of ZnO nanoparticles was done by DLS and the mean hydrodynamic diameter was in the range of 245-273 nm. However, the size reported by its commercial supplier (Sigma–Aldrich, USA) using Brunauer–Emmett–Teller (BET) method was 50-70nm, while that assessed by transmission electron microscopy (TEM) was 30nm. This difference in sizes is due to the fact that the methods employed (e.g. BET, TEM and DLS) are based on difference principles. The size obtained from DLS was more than the size measured by TEM (30 nm) or BET (50–70 nm). This can be attributed to the facts that (1) DLS measures Brownian motion and subsequent size distribution of an ensemble collection of particles in solution and gives mean hydrodynamic diameter which is usually larger than BET or TEM diameter as it includes a few solvent layers (Hradil et al., 2007); (2)

during DLS measurement there is a tendency of particles to aggregate in aqueous state thereby giving the size of clustered particles rather than individual particles; (3) it reports an intensity weighted average hydrodynamic diameter of a collection of particles so any polydispersity of the sample will skew the average diameter towards larger particle sizes.

The internalization of ZnO nanoparticles was observed in primary human epidermal keratinocytes as revealed by the back scattered electron (BSE) imaging and transmission electron microscopy after 6h exposure at 14 µg/ml. Analyzing sections of biological samples by back scattered electron imaging using a scanning electron microscope (SEM) enables brightly shining nanoparticles to be observed against the cellular dark background (Bastian et al. 2009). The nanoparticle agglomerates with strong BSE signals were visible in the cells when viewed by the BSE-SEM. In addition, the transmission electron microscopy also confirmed that ZnO nanoparticles were internalized in the cells. Although, the mechanism of ZnO nanoparticles uptake in keratinocytes remains to be elucidated, endocytosis has been suggested as the main mode of nanoparticle uptake by several authors. Xia et al. (2008) showed the uptake of ZnO nanoparticles in human lung epithelial cells (BEAS-2B) cells by endocytosis involving caveolae. This was also observed in A431 cells in our study where the ZnO nanoparticles were found to be present in the vesicles inside the cells.

While evaluating the cytotoxic potential of ZnO nanoparticles in A431 cells, more than one assay of cytotoxicity was used to get more reliability. The cytotoxicity assays revealed a time and concentration dependent cytotoxicity in A431 cells on exposure to ZnO nanoparticles.

ZnO nanoparticles exposure in primary human epidermal cells also exhibited a time (6 -24 h) as well as concentration (8-20 µg/ml) dependent inhibition of mitochondrial activity. A previous investigation revealed the cytotoxic nature of ZnO nanoparticles on human mesothelioma MSTO-211H and rodent 3T3 fibroblast cells at concentrations of 3.75, 7.5 and 15µg/ml after 3-day exposure (Brunner et al. 2006). The cytotoxic doses of ZnO nanoparticles in this study were found to be in a very narrow range viz 8µg/ml to 20µg/ml. This is supported by a similar observation made previously for ZnO nanoparticles although in human lung carcinoma cells (A549; (Lin et al. 2009b). Some earlier investigations have also observed the cytotoxic nature of these nanoparticles using diverse end- points in different mammalian cell types (Gojova et al. 2007; Jeng and Swanson 2006; Lai et al. 2008; Reddy et al. 2007; Sayes et al. 2007). The changes in cell morphology on exposure to ZnO nanoparticles also corroborated our cytotoxicity results (Figure 5). These morphological changes could be attributed to the cytotoxic potential of the ZnO nanoparticles evident by a decrease in the mitochondrial activity.

The DNA damaging potential of the ZnO nanoparticles was assessed by the Comet assay which detects single as well as double strand breaks and alkali labile sites. Our results demonstrate that ZnO nanoparticles cause statistically significant DNA damage in A431 cells at concentrations of 5 and 0.8µg/ml after an exposure period of 6h. A significant DNA damage was also observed at 14 µg/ml in primary human epidermal keratinocytes after 6 h exposure. Dufour et al. (2006) have shown a concentration related increase in chromosome aberrations after exposure to ZnO nanoparticles (<100 nm)

in CHO cells (Chinese hamster ovary), although at a very high concentration (≥105µg/ml).

The production of free radicals is one of the primary mechanisms of nanoparticles toxicity (Nel et al. 2006). It may result in oxidative stress, inflammation and consequent damage to proteins, membranes and DNA (Donaldson and Stone, 2003). Therefore, the levels of GSH and the other antioxidant marker enzyme levels were assessed in the A431 cells. A significant depletion in the GSH, SOD and catalase levels were observed at 0.8 and 0.08µg/ml on 24h exposure. This indicates a condition of oxidative stress in cells which may arise due to imbalance in the ROS formation and antioxidant defence system of cells. An increase in the lipid peroxidation which represents another marker of oxidative stress was also observed. This increase in lipid peroxidation may lead to membrane damage indicated by enhanced LDH release on ZnO nanoparticles exposure. As there is a well documented link between nanoparticles and oxidative stress, one of the possible modes that can be suggested for ZnO nanoparticles induced DNA damage and cell death is oxidative stress (Figure 3.10) (Xia et al. 2006). These results stress upon the need for a thorough safety/ toxicity assessment of new engineered nanoparticles that are used in consumer products.

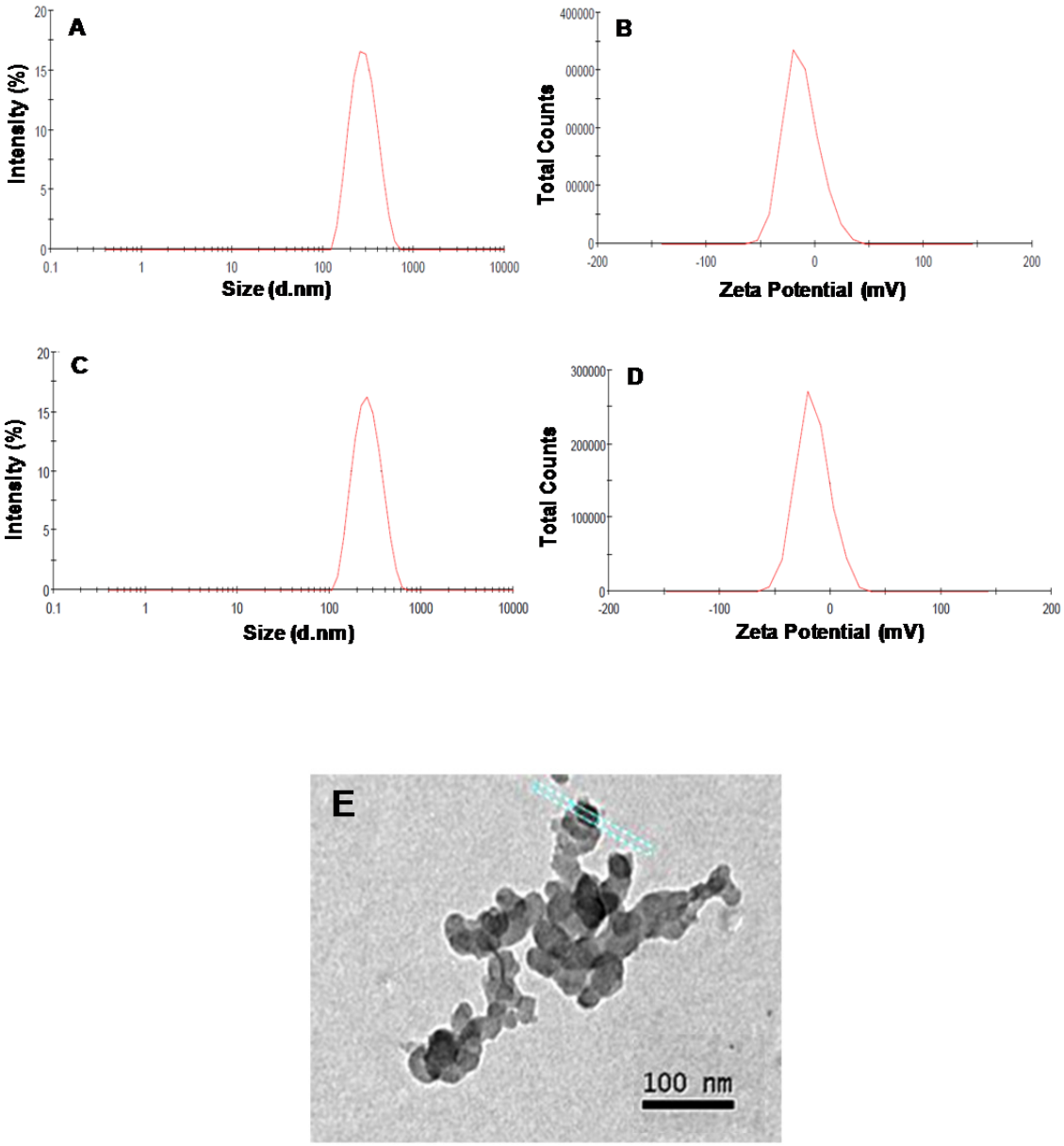

Figure 3.1. Characterization of ZnO NPs (A-B) Hydrodynamic diameter and zeta potential in DMEM medium (C-D) Hydrodynamic diameter and zeta potential in KGM-2 medium (E) TEM microphotograph of ZnO NPs.

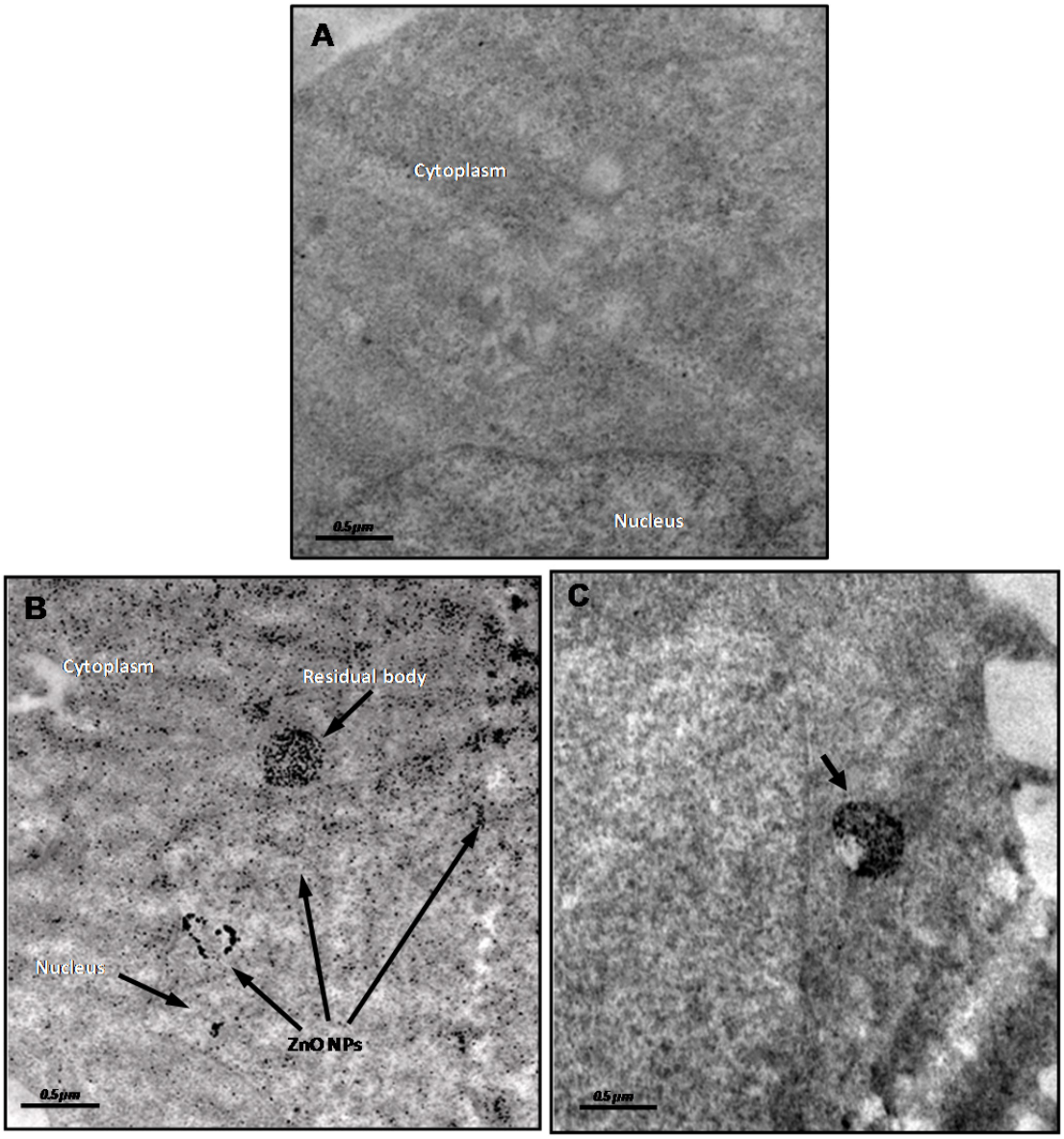

Figure 3.2. TEM microphotographs of human epidermal cells (A431) (A) Control cells (B-C) Cells treated with ZnO NPs depicting intracellular localization of ZnO NPs *(black arrow).*

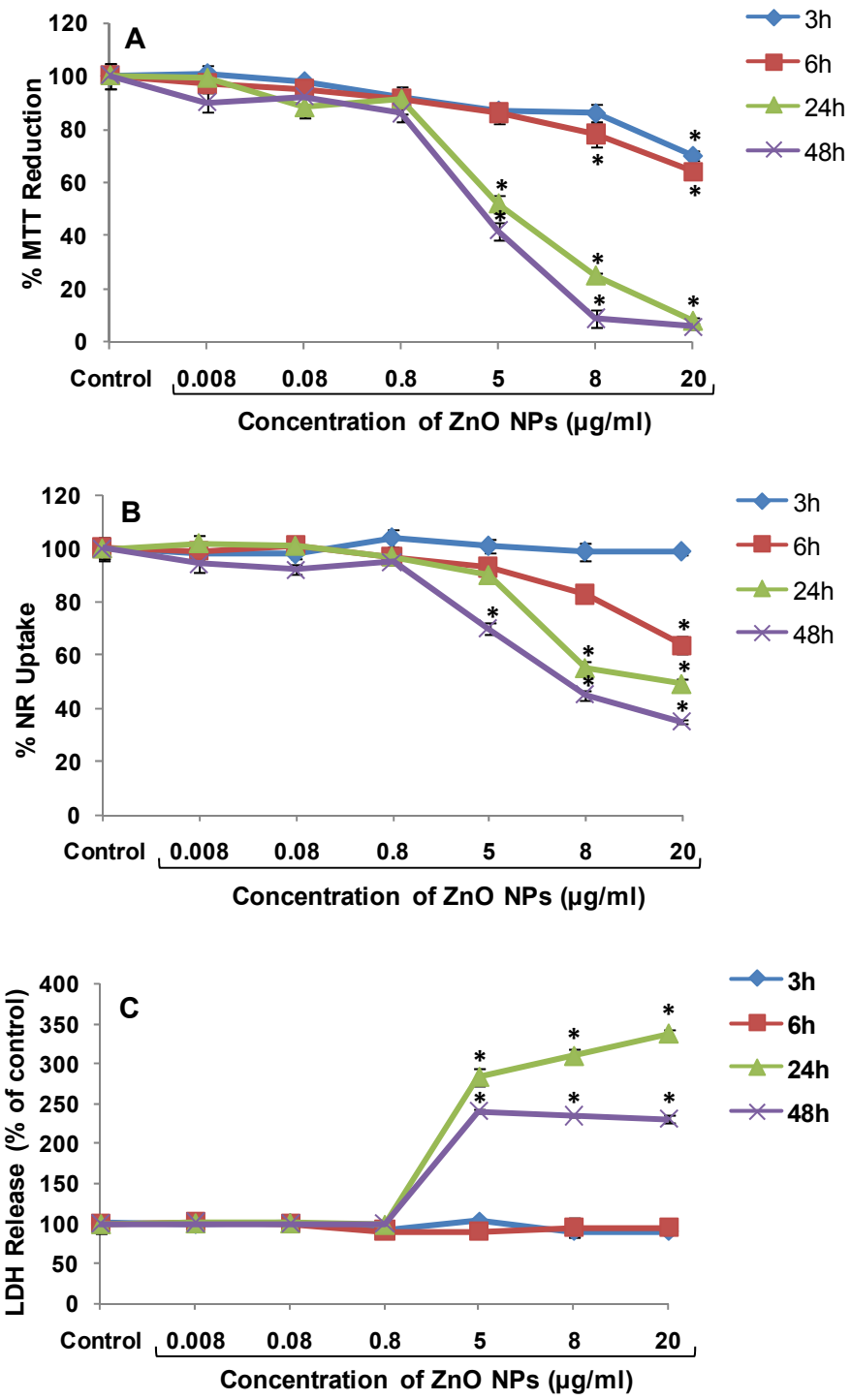

Figure 3.3. Cytotoxic effect of ZnO NPs in human epidermal cells (A431) as assessed by (a) MTT assay; (b) Neutral red uptake assay; (c) Lactate dehydrogenase release assay. Data are expressed as the percentage viability of cells exposed to ZnO NPs relative to control cells and are mean ± S.E.M. of triplicates.*$p < 0.05$, compared to control.

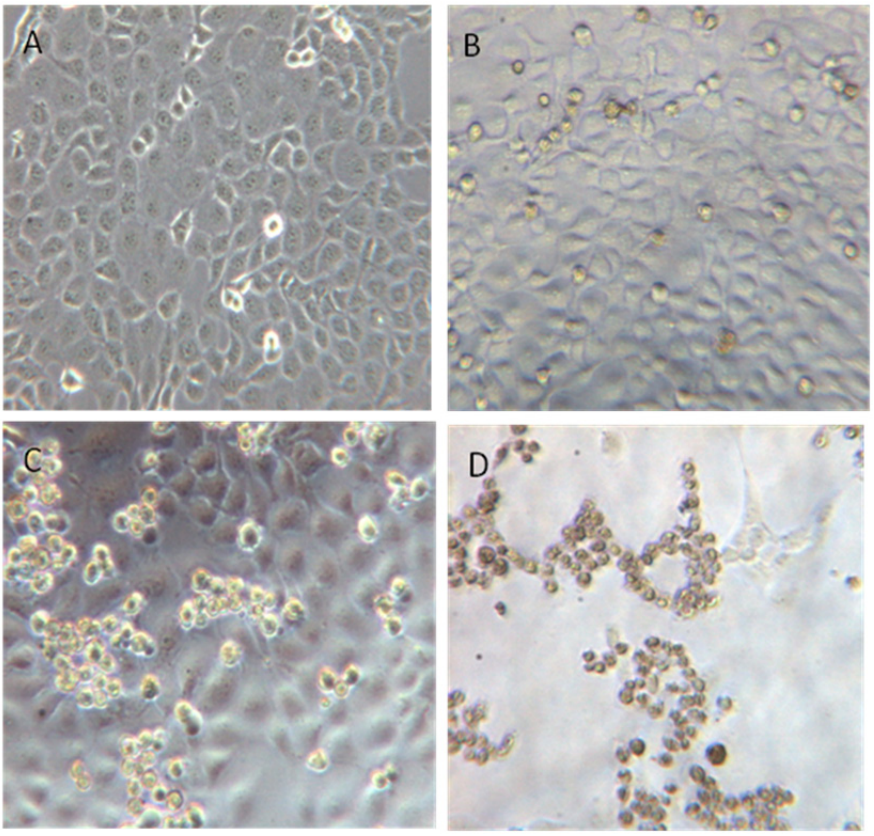

Figure 3.4. Morphology of human epidermal cells (A431) (A) normal, and ZnO NP treated (B) 8µg/ml for 6h, (C) 8µg/ml for 24h, (D) 8µg/ml for 48h. Magnification X100.

Table 3.1. DNA damage by ZnO NPs after 6h exposure to human epidermal cells (A431) as evident by the comet parameters.

Concentration	Olive Tail Moment (OTM; arbitrary Units)	% Tail DNA
Control	1.37 ± 0.12	8 ± 0.71
1mM EMS	20.83 ± 0.53**	53.3 ± 1.2**
ZnO NPs (0.001µg/ml)	1.43 ± 0.17	9 ± 0.69
ZnO NPs (0.008µg/ml)	1.5 ± 0.1	9.2 ± 0.23
ZnO NPs (0.08µg/ml)	1.83 ± 0.18	11 ± 0.91
ZnO NPs (0.8µg/ml)	2.13 ± 0.12*	10.6 ± 0.76*
ZnO NPs (5µg/ml)	2.33 ± 0.32*	13 ± 1.50*

Values represent mean ± S.E.M of three experiments.
[a]EMS- ethyl methanesulfonate – positive control.
* $p < 0.05$; ** $p < 0.01$; *** $p < 0.001$ when compared to control

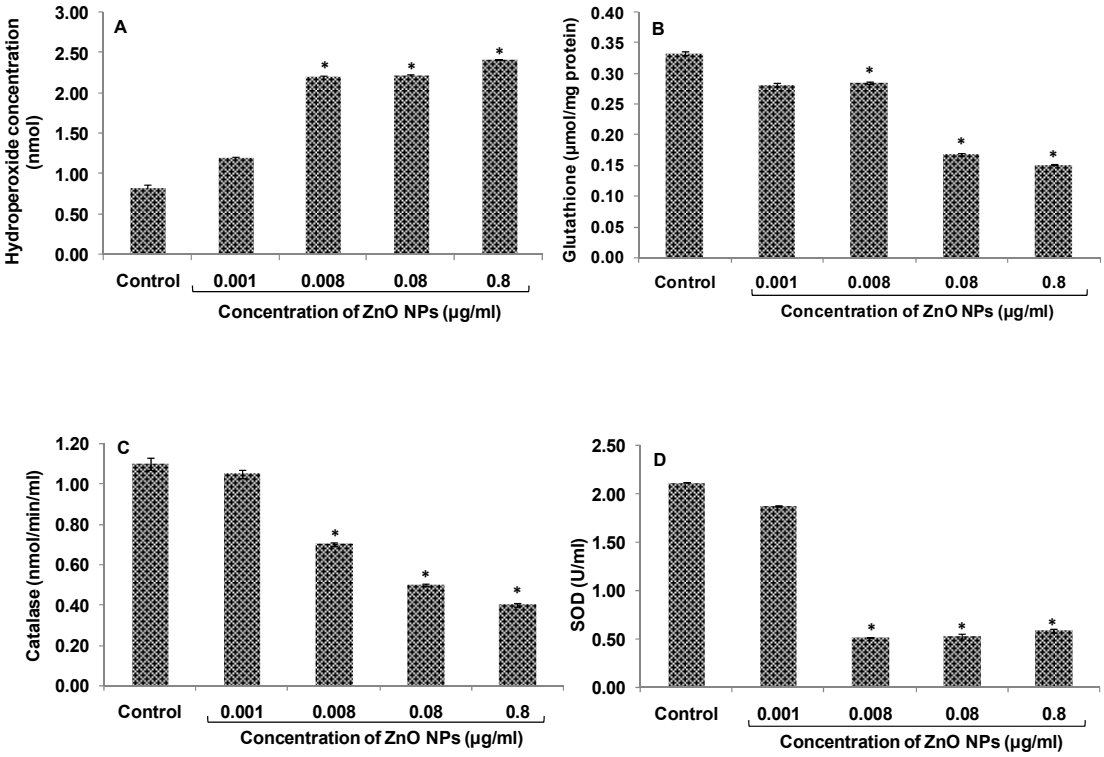

Figure 3.5. Effect of ZnO NPs on the oxidative stress markers in human epidermal cells (A431) (A) lipid peroxidation, (B) glutathione content, (C) catalase activity and (D) superoxide dismutase activity. Data represent mean± S.E.M. of three experiments. *$p < 0.05$, compared to control.

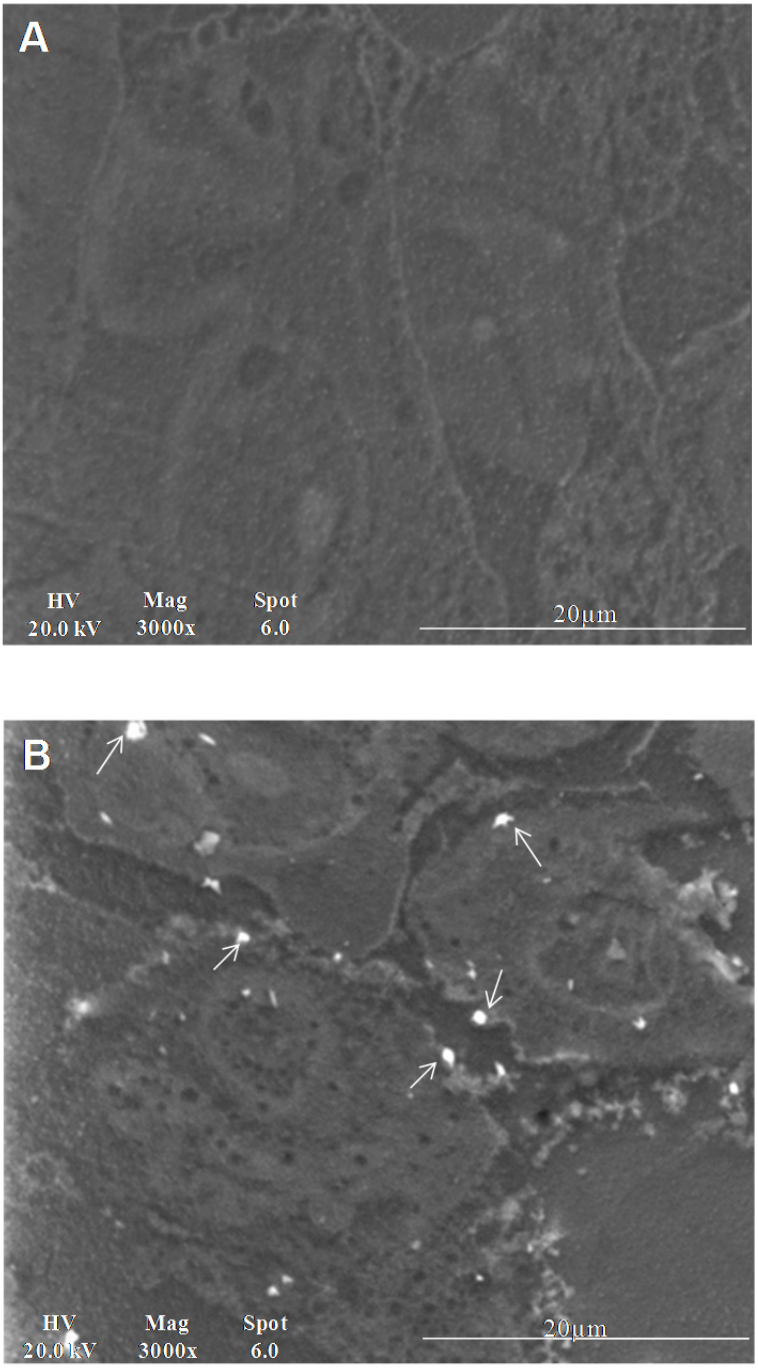

Figure 3.6. Scanning electron microscopy (back scattered electron imaging) microphotographs of primary human epidermal keratinocytes. (A) Control cells (B) Cells treated with ZnO NPs (14 µg/ml) for 6 h showing ZnO NP agglomerates *(white arrow)* inside cells.

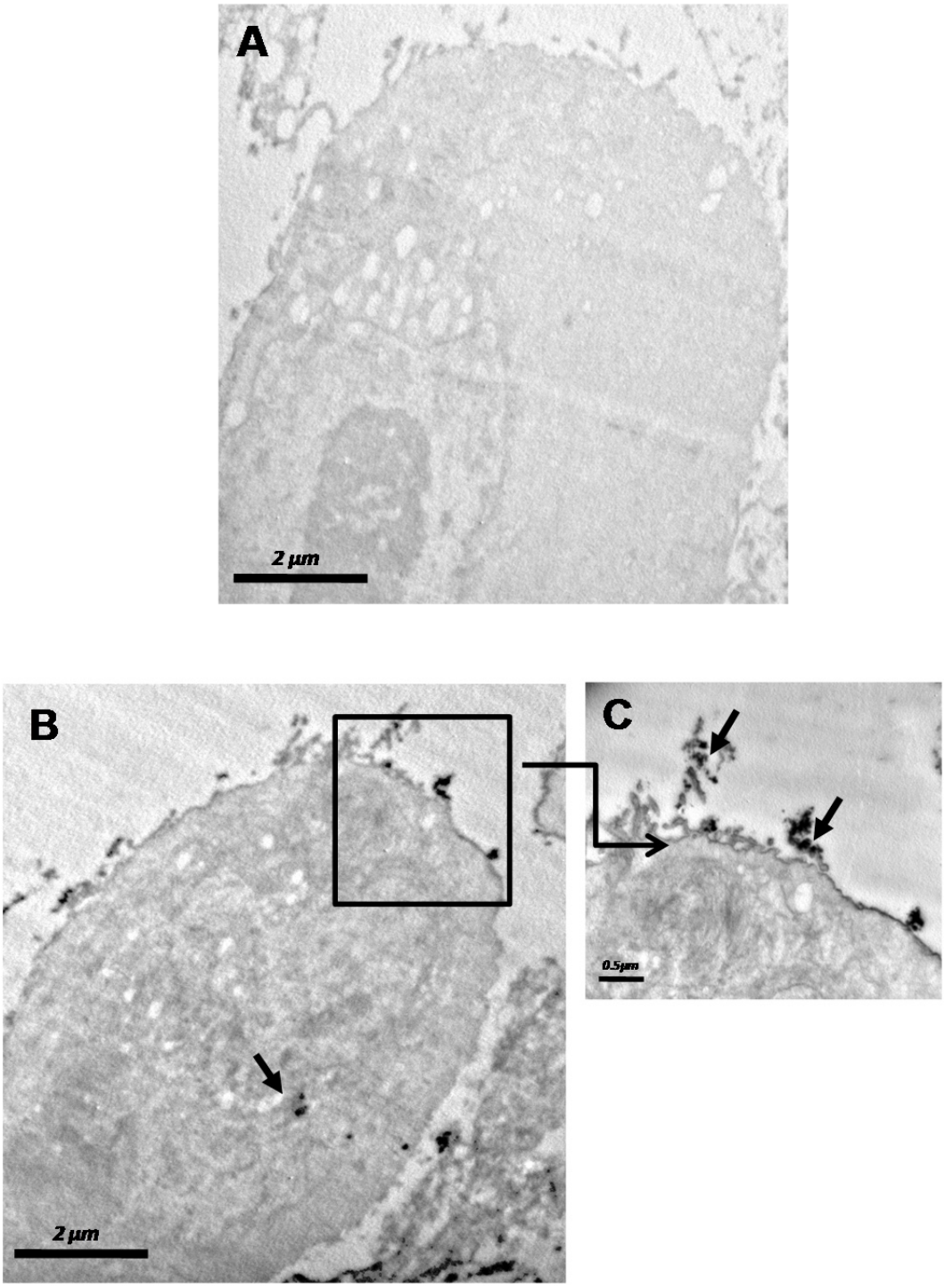

Figure 3.7. Transmission electron microscopy microphotographs of primary human epidermal keratinocytes. (A) Control cells (B) Cells treated with ZnO NPs (14µg/ml) for 6h depicting intracellular localization ZnO NPs *(black arrow)* (C) High power view shows localization of these nanoparticles in the filopodia.

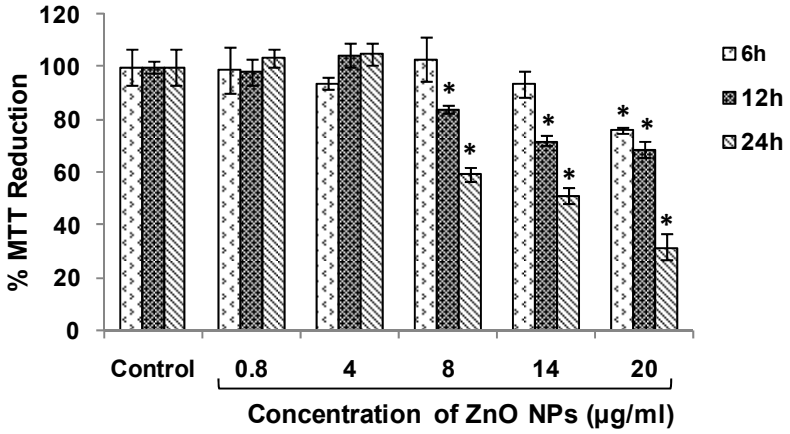

Figure 3.8. Concentration and time dependent cytotoxicity of ZnO NPs in primary human epidermal keratinocytes. Data are expressed as the percentage viability of cells exposed to ZnO NPs relative to control cells and are mean ± S.E.M. of triplicates.*$p < 0.05$, compared to control.

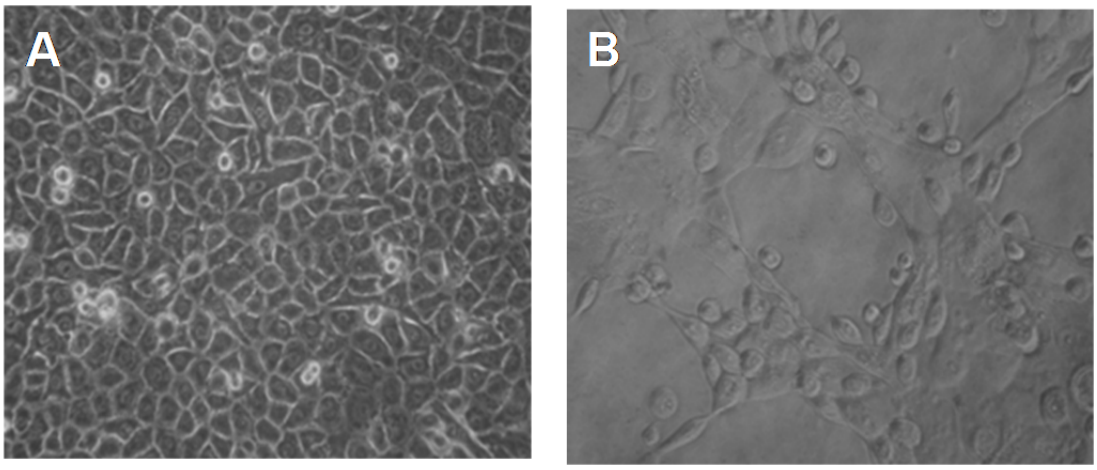

Figure 3.9. Morphology of primary human epidermal keratinocytes (A) Control cells and (B) Cells treated with ZnO NPs (20µg/ml) for 6 h. Magnification X100.

Table 3.2. DNA damage by ZnO NPs after 6 h exposure to primary human epidermal keratinocytes as evident by the comet parameters

Concentration	Olive Tail Moment (OTM; arbitrary Units)	% Tail DNA
Control	0.77±0.08	5.80±0.66
H_2O_2†	10.85±1.58***	31.19±2.09***
ZnO NPs (4µg/ml)	0.92±0.02	6.42±0.19
ZnO NPs (8µg/ml)	2.84±0.64*	14.62±2.44**
ZnO NPs (14µg/ml)	5.32±0.79**	19.90±1.79***

Values represent mean ± S.E.M of three experiments.
†H_2O_2 ,Hydrogen peroxide-positive control (25µM for 15min).
* $p < 0.05$; ** $p < 0.01$; *** $p < 0.001$ when compared to control.

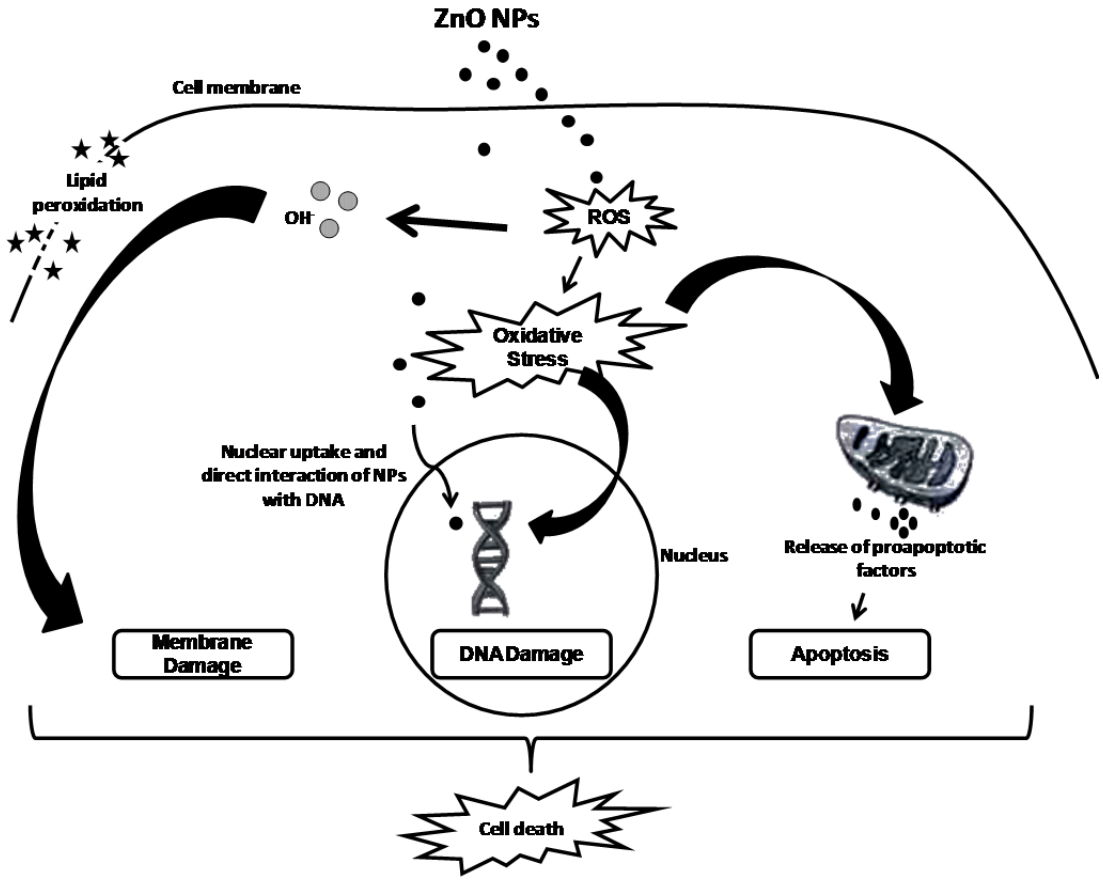

Figure 3.10. A representation of results from this study depicting the ZnO NPs induced cellular toxicity.

CHAPTER – 4

Mechanism of toxicity of ZnO nanoparticles

4.1. Introduction

The field of nanotechnology is rapidly expanding with continuous development of nanomaterials based consumer products and industrial applications. Nano forms of carbon based materials, metals, metal oxides and biopolymers are being used in several industries including diagnosis, drug delivery, cosmetics, sunscreens, food, paints, electronics, sports, imaging etc. Zinc oxide nanoparticles are one of the most abundantly used nanomaterials in cosmetics and sunscreens as they efficiently absorb UV light and also do not scatter visible light. This makes them transparent and more aesthetically acceptable compared to their bulk counterpart (Schilling et al. 2010). ZnO nanoparticles are being used in food industry as additives and in packaging due to their antimicrobial properties (Gerloff et al. 2009; Jin et al. 2009). They are also being explored for their potential use as fungicides in agriculture (Chen et al. 2005), antimicrobial agents in fabrics (Yadav et al. 2006) and as anticancer drugs and imaging in biomedical applications (John et al. 2010; Rasmussen et al. 2010).

The increased production and use of ZnO nanoparticles enhances the probability of their exposure in occupational and environmental settings. This has raised concerns in the public and scientific community regarding their unanticipated and adverse health effects. Toxicity of ZnO nanoparticles has been evaluated in different biological systems, such as, bacteria (Miller et al. 2003; Sinha et al. 2010), mammalian cells (Jeng and Swanson 2006; Wang et al. 2010a) and *in vivo* models (Wang et al. 2008a). In mammalian cells, the toxic effects of ZnO nanoparticles such as membrane injury, inflammatory response, DNA damage and apoptosis have been

demonstrated (Gojova et al. 2007; Jeng and Swanson 2006; Osman et al. 2010; Yang et al. 2009a). In some studies, the toxicity of ZnO NPs has been ascribed to Zn^{2+} ions release (Franklin et al. 2007; George et al. 2009). However, studies have also shown that the toxicity of ZnO nanoparticles is due to their particulate nature which may give rise to reactive oxygen species (ROS) (Moos et al. 2010; Yang et al. 2009a). ROS generation is linked to DNA damage and cellular apoptosis (Cadet et al. 2010; Neuzil et al. 2006) and is also known to activate the mitogen activated protein kinase (MAPK) pathways which are important mediators of signal transduction and play a key role in regulating many cellular processes (Navarro et al. 2006). Despite the existing studies on ZnO nanoparticle toxicity, the underlying molecular mechanism leading to toxicity remains largely unclear. Moreover, none of the studies, so far, have explored the adverse effects of ZnO nanoparticles in human liver which is the primary organ of metabolism. Given that humans are being directly exposed to ZnO nanoparticles, it seems logical that liver might act as a major target organ for ZnO nanoparticles after they have gained entry into the body through any of the possible routes. Therefore, the aim of the present study was to assess the cytotoxic and genotoxic potential of ZnO nanoparticles in human liver cells (HepG2) and to understand the mechanism involved.

Cell lines of different origins have widely been used as a model for general toxicity studies because they are well characterized and more homogenous than primary cultures. They have been used to predict potential toxic effects as well as the mechanism of new toxicants on human body. Even the

regulatory authorities like OECD approve the use of cell lines in toxicity testing (OECD-473 1997).

The HepG2 cell line is a well established *in vitro* toxicity model being used for toxicological assessment of a variety of compounds and xenobiotics (Chavan et al. 2011 ; Rouas et al. 2010; Slamenova et al. 2010; Wu et al. 2010; Zhang et al. 2011). Dehn et al (2004) have shown that the HepG2 cell line is a useful *in vitro* model for cadmium toxicity studies and mimic *in vitro* and *in vivo* responses of mammalian systems. HepG2 cells display robust morphological and functional differentiation and have biosynthetic capabilities similar to those of normal hepatocytes. They produce most of the plasma proteins, retains cell surface receptors, can induce metallothionein in response to metals, can synthesize, assemble and secrete both very low and high density lipoproteins. HepG2 cells have been shown to retain P450-dependent monooxygenase enzymes. They also have the ability to carry out normal biotransformation reactions essential to detoxification process. All these features have made this cell line a potentially useful model in investigating toxicity mechanisms (Chaudhary et al. 2010; Mantzaris et al. 2011; Munro et al. 2008; Zhou et al. 2010); gene delivery studies (Le et al. 2010), mitochondrial toxicity (Jasionek et al. 2010).

Several recent studies involving toxicity assessment of engineered nanomaterials have used HepG2 as a model cell line (Jan et al. 2008; Kawata et al. 2009; Leonov et al. 2008; Liu et al. 2010; Nemmar et al. 2011; Romero et al. 2010; Thakor et al. 2011). Therefore in the present study it was found prudent to take HepG2 cells to understand the mechanism of toxicity of ZnO nanoparticles.

To achieve the aim of present study, a systematic study (Figure 4.1) which involved the assessment of cytotoxicity, ROS generation, lipid peroxidation, oxidative DNA damage and apoptosis was undertaken. Levels of key signalling and apoptotic proteins along with the involvement of MAPK signalling pathways were analyzed. We also investigated if the toxicity is being mediated by the Zn^{2+} ions liberated from nanoparticles.

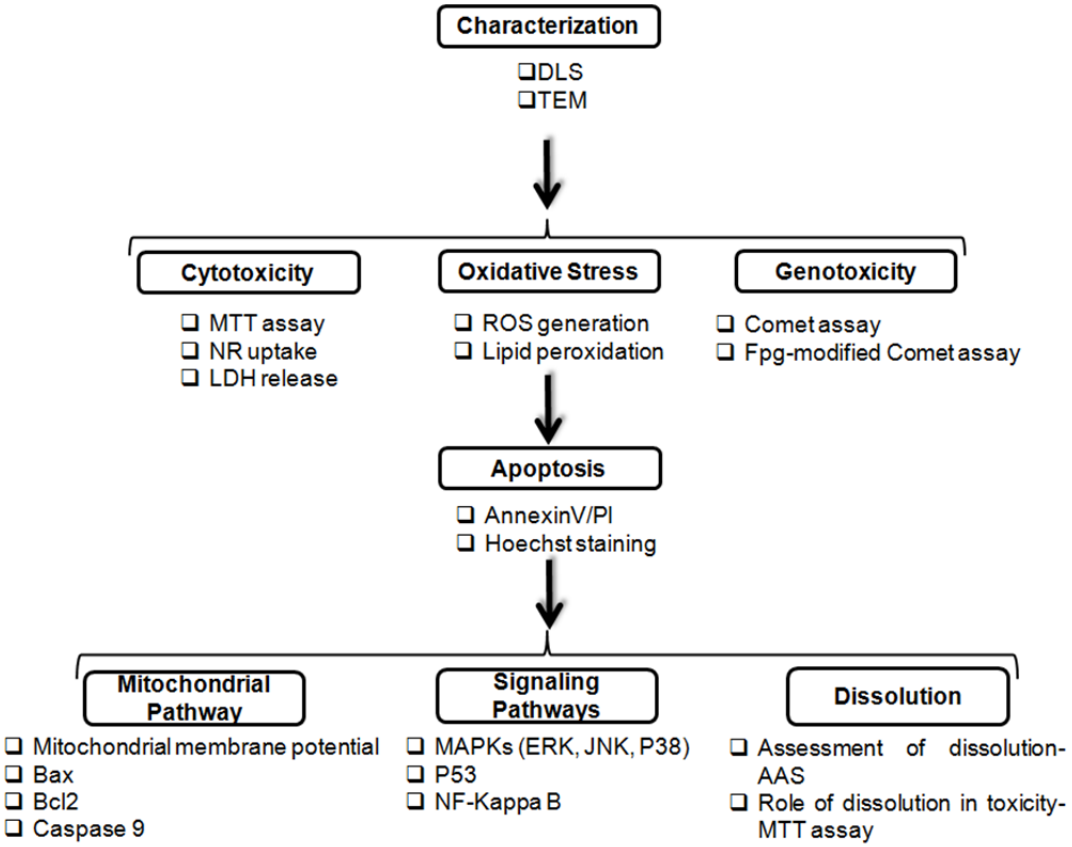

Figure 4.1. Schematic diagram of the study design.

4.2. Material and methods

4.2.1. Dynamic light scattering

ZnO NPs were suspended in complete minimal essential medium (CMEM; MEM supplemented with 10% FBS) at a concentration of 80 µg/ml and characterized by dynamic light scattering as described in Chapter 2 (2.2).

4.2.2. Cell culture and exposure to nanoparticles

The human hepatocarcinoma cell line (HepG2; procured from the National Centre for Cell Sciences, Pune, India) was cultured in CMEM containing 10 ml/L of antibiotic and antimycotic solution at 37^{o}C under a humidified atmosphere of 5%CO_2/ 95% air.

HepG2 cells were plated at a density of 10^5 cells/ml in a 96 well plate and 12 well plate for the cytotoxicity assays (MTT, neutral red uptake and lactate dehydrogenase) and other parameters (Comet assay, apoptosis, mitochondrial membrane potential) respectively and allowed to attach for 24h before the addition of NPs suspension. A stock suspension of ZnO NPs (80µg/ml) was prepared as described before and diluted to different concentrations (0.8, 2, 8, 14 to 20 µg/ml). Cells were then exposed to the above concentrations for varied lengths of time as per the experimental design.

To investigate the role of oxidative stress in ZnO nanoparticles elicited toxic responses, cells co-treated with ZnO nanoparticles and 1mM NAC were also included in the MTT assay, Comet assay and apoptosis experiment. Similarly, for analyzing the role of different signalling pathways the cells were pre-treated with SB203580 (20µM) and SP600125 (20µM) for 2 h followed by simultaneous treatment of ZnO nanoparticles with the respective inhibitor.

After 24h exposure, the cells were checked for cell viability by the MTT assay.

4.2.3. Cellular uptake of nanoparticles

The cellular uptake of nanoparticles was analysed by flow cytometry (Suzuki et al. 2007) as described in Chapter 2 (2.3.1).

4.2.4. Cytotoxicity assays

4.2.4.1. MTT assay

The cells were exposed to different concentrations of ZnO nanoparticles (0.8, 2, 8, 14 and 20 µg/ml) for 6, 12 and 24h. The mitochondrial activity was assessed using the MTT assay according to the method of Mosmann (Mosmann 1983) as described in Chapter 2 (2.4.1.)

4.2.4.2. Neutral red uptake assay

The neutral red uptake assay was done according to the method of Borenfreund and Puerner (1985) after exposing the cells to ZnO nanoparticles (0.8, 2, 8, 14 and 20 µg/ml) for 6, 12 and 24h. The method for neutral red uptake assay has been described in detail in the Chapter 2 (2.4.2.).

4.2.4.3. Lactate dehydrogenase release assay

The cells were exposed to different concentrations of ZnO nanoparticles (0.8, 2, 8, 14 and 20 µg/ml) for 6, 12 and 24h. LDH activity in extracellular medium due to membrane damage was assessed by Tox-7 *in vitro* toxicology assay kit (Sigma–Aldrich Inc., St. Louis, MO, USA) using manufacturer's protocol as described in Chapter 2 (2.4.3.).

4.2.5. Measurement of intracellular reactive oxygen species (ROS)

The level of intracellular ROS generation was estimated by the method of (Wan et al. 1993) using 2,7-dichlorofluorescein diacetate (DCFDA; Sigma, St Louis, MO, USA) dye. Cells ($1X10^4$cells/well) were seeded in a 96-well black bottom plate. After 24h, the cells were exposed to ZnO NPs (8, 14, 20µg/ml) for 6h and the intracellular generation of ROS was measured as described in the Chapter 2 (2.5.1.).

4.2.6. Lipid peroxidation

The cells were cultured in 75-cm^2 culture flask and exposed to ZnO nanoparticles (8, 14 and 20 µg/ml) for 24h. Subsequently, the levels of lipid peroxides were estimated by Cayman's Chemicals Kit (USA) according to manufacturer's protocol as described in Chapter 2 (2.5.2).

4.2.7. Genotoxicity assessment

4.2.7.1. Single cell gel electrophoresis/Comet assay

The cells were exposed to ZnO nanoparticles (8, 14 and 20 µg/ml) for 6h and the DNA damage was assessed by the standard Comet assay which has been described in Chapter 2 (2.7.1.)

4.2.7.2. Fpg-modified Comet assay

The cells were exposed to ZnO nanoparticles (8, 14 and 20 µg/ml) for 6h and the oxidative DNA damage was assessed by the Fpg-mdified Comet which has been described in Chapter 2 (2.7.2.)

4.2.8. Annexin V-FITC/PI staining

Annexin V-FITC/PI staining was carried out by Annexin V-FITC apoptosis detection kit (Sigma, St Louis, MO, USA) as per the manufacturer's protocol described in Chapter 2 (2.8.1).

4.2.9. Hoechst staining

Apoptotic nuclear morphology was assessed using Hoechst 33342 (Sigma, St Louis, MO, USA) as described in Chapter 2 (2.8.2).

4.2.10. Mitochondrial membrane potential

Mitochondrial membrane potential (MMP) was detected with fluorescent probe 5,5′,6,6′-tetrachloro-1,1′,3,3′-tetraethylbenzimidazolcarbocyanine iodide (JC-1; Molecular probes, USA). Cells exposed to ZnO NPs were harvested by trypsinization and processed for MMP analyses as described in Chapter 2 (2.9).

4.2.11. Western blot analysis

Levels of key signalling and apoptotic proteins along with the involvement of MAPK signalling pathways were analyzed in cells exposed to ZnO nanoparticles using western blotting. The methodology for western blot analysis has been described before in Chapter 2 (2.10).

4.2.12. Effect of dissolution on ZnO NPs induced cytotoxicity

Zinc ions released from ZnO NPs were evaluated for their cytotoxicity. Cell culture medium containing ZnO NPs at a concentration of 20µg/ml was incubated at 37^{o}C for 6, 12 and 24h. The NPs suspension was then centrifuged at 20,000 g (4^{o}C) for 30 min to remove the NPs and the resulting supernatant was collected. Cell culture medium without nanoparticles, subjected to the same conditions was used as the blank control. The cells were incubated with the supernatant for 6, 12 and 24h and the cell viability was assessed by the MTT assay as described earlier.

The Zn content in the supernatant was measured by an atomic absorption spectrophotometer (ZEEnit 700 P, Analytikjena, Germany). Before analysis,

the atomic absorption spectrophotometer (AAS) was calibrated every time by running at least three standard concentrations (0.25, 0.5 and 1 mg/L) of zinc.

The cells were then treated with $ZnCl_2$, equimolar in amount to the Zn content, found in the supernatant to evaluate the contribution of Zn^{2+} towards ZnO NP toxicity. The cytotoxicity was assessed after 6, 12 and 24h exposure by the MTT assay.

4.2.13. Statistical analyses

Results were expressed as the mean ± S.E.M. and data were analyzed by means of one way analysis of variance (ANOVA) with the Dunnett post hoc test to determine significance relative to the unexposed control using SPSS v. 16.0 software (SPSS Inc., Chicago, IL, USA). In all cases, $p < 0.05$ was considered significant.

4.3. Results

4.3.1. Dynamic light scattering

The mean hydrodynamic diameter and zeta potential of the nanoparticle suspension in CMEM as determined by DLS measurement was 267nm and −12mV respectively (Figure 4.2A-B).

4.3.2. Cellular uptake of ZnO nanoparticles

The internalization of ZnO nanoparticles in human liver cells (HepG2) was assessed using flow cytometry. We observed a significant ($p<0.05$) increase in the SSC-A Mean of cells treated with ZnO nanoparticles (14 and 20µg/ml) for 3h as compared to the control cells (Figure 4.3).

4.3.3. Cytotoxicity of ZnO nanoparticles

The cytotoxicity of ZnO nanoparticles in HepG2 cells was evaluated by the MTT, NRU and LDH assays. HepG2 cells were exposed to ZnO nanoparticles (0.8 to 20µg/ml) for 6, 12 and 24h. The MTT and NRU results demonstrated a concentration and time dependent cytotoxicity after exposure to nanoparticles (Figure 4.4A). The percentage mitochondrial activity (relative to control) observed after 12 h exposure at concentrations 14 and 20µg/ml was 80 and 74% respectively with a further decrease to 53% and 43% after 24 h exposure.

The results of the NRU assay showed a similar concentration and time dependent response with a loss in cell viability at 14 and 20µg/ml on 12 and 24 h exposure (Figure 4.4B).

A significant ($p < 0.05$) LDH leakage was observed at 14µg/ml and 20µg/ml after 24h and 12h exposure respectively (Figure 4.4C).

4.3.4. Measurement of intracellular ROS

A significant ($p<0.05$) qualitative and quantitative dose dependent increase in % ROS generation was observed in the form of fluorescence on treatment with ZnO nanoparticles for 6h at 14 and 20 µg/ml (Table 4.1, Figure 4.5).

4.3.5. Effect of ZnO nanoparticles on lipid peroxidation

Lipid peroxidation was examined by measuring hydroperoxide concentration. A statistically significant ($p< 0.05$) increase in hydroperoxide formation was observed only at the higher concentration (20 µg/ml; 20µM) after 6h exposure to ZnO nanoparticles (Table 4.1).

4.3.6. DNA damage

The cell viability in the Comet assay exceeded 90% for all experimental groups before and after the treatment as assessed by the Trypan blue dye exclusion assay (data not shown).

A significant induction ($p < 0.05$) in DNA damage was observed in cells exposed to ZnO nanoparticles for 6h at 14 and 20µg/ml concentrations compared to control cells in standard alkaline Comet assay as evident by the Comet assay parameters i.e. Olive tail moment (arbitrary unit) and % tail DNA (Table 4.2; Figure 4.7). Moreover, in Fpg modified Comet assay, the OTM values of cells treated with 14 and 20 µg/ml ZnO nanoparticles were significantly higher than the respective OTM values observed in standard alkaline Comet assay suggesting the oxidative DNA damage. Additionally, cells exposed to the same concentrations of ZnO nanoparticles revealed a significant ($p<0.05$) increase in Fpg sensitive sites compared to control cells incubated with Fpg enzyme (Table 4.2). To further confirm the involvement of oxidative stress, the level of Fpg sensitive sites were evaluated in the cells exposed to 20µg/ml ZnO nanoparticles in the presence of NAC. The results revealed a protective effect of NAC on oxidative DNA damage as evident by a reduction in Fpg sensitive sites (Figure 4.6). The protective effect of NAC increased as its concentration increased from 0.75mM to 1mM exhibiting a 26% and 53% reduction respectively in Fpg sensitive sites.

4.3.7. Apoptosis

Flow cytometry analysis was conducted using AnnexinV-FITC/PI staining to investigate the mode of cell death induced by ZnO nanoparticles. HepG2 cells were treated with 14 and 20 µg/ml ZnO nanoparticles for 12h. The

control cells were not stained with AnnexinV-FITC and propidium iodide. However, the cells treated with 14 and 20 µg/ml ZnO nanoparticles for 12h showed 8.1 and 12.8 % apoptotic cells respectively (Figure 4.8A-C). While at 14µg/ml, more cells were in early apoptotic phase (5.93% vs 0.57% in control) then in late phase (2.17% vs 0.27% in control.); at 20µg/ml a noticeable cluster of cells appear in late apoptotic quadrant (7.57%) compared to early apoptotic populations (5.23%). This is due to a high intensity of cell death at the high concentration leading to shifting of cells from early apoptotic phase to late apoptotic phase.

The apoptosis was further confirmed by employing Hoechst 33342 staining. Stained control and ZnO nanoparticles treated cells were examined for nuclear morphology. The control cells had round and homogenously stained nuclei but cells treated with ZnO nanoparticles (14 and 20 µg/ml) for 12h showed marked DNA condensation and apoptotic bodies, characteristic of apoptosis (Figure 4.9).

4.3.8. Mitochondrial membrane potential ($\Delta\psi_m$) analysis

The cells treated with ZnO nanoparticles for 12h showed a marked decrease in $\Delta\psi_m$ evident by a shift in JC-1 fluorescence from red to green (Figure 4.10). This decrease in $\Delta\psi_m$ was concentration dependent with 15.2 and 18.8 % depolarized cells at 14 and 20µg/ml respectively as compared to control cells (9.7%). When examined by fluorescent microscopy, the control cells showed an intense red fluorescence and weak green fluorescence. However, the ZnO nanoparticles treated cells exhibited a bright green fluorescence with a marked decrease in red fluorescence indicating a loss of MMP (Figure 4.11).

4.3.9. Analysis of key apoptotic and signalling proteins

The levels of key apoptotic and signalling proteins were examined in cells exposed to ZnO nanoparticles for 9h by western blotting (Figure 4.12A-C). The cells showed modulation of Bax and Bcl2 protein expression levels with an increase in Bax levels and a corresponding decrease in Bcl2. A significant decrease in the procaspase 9 levels (0.5 fold) and an appearance of a cleavage product at 37kD was observed. Detection of P53 and phosphorylated $P53^{Ser15}$ levels was also carried out and a 2.4 fold increase in the levels of phospho-$P53^{Ser15}$ was observed without any significant change in the levels of P53. No changes in NF-kβ levels were observed on exposure to ZnO nanoparticles.

4.3.10. Effect of ZnO nanoparticles on MAPK phosphorylation

We examined the effect of ZnO nanoparticles treatment on the phosphorylation state of the extracellular signal-regulating kinase (ERK1/2), stress activated protein kinase (SAPK)/ Jun-N-terminal kinase (JNK), and P38 kinase in HepG2 cells by western blotting (Figure 4.13). A 1.8-2.2 fold increase in the phosphorylated JNK was observed at 20 and 14 µg/ml after 9h but no change was found in JNK proteins. Similarly, there was 1.8-2.4 fold upregulation of phosphorylated P38 expression without any modulation of P38 expression. No changes in phospho-ERK and ERK levels were observed on exposure to ZnO nanoparticles. Interestingly, P38 and JNK phosphorylation was completely abrogated in the presence of NAC (Figure 4.14).

4.3.11. Effect of NAC, SP600125, and SB203580 on ZnO nanoparticle induced toxicity

To determine the role of ROS and other signalling pathways in ZnO nanoparticles induced cell death, HepG2 cells were treated with ZnO nanoparticles (20µg/ml) in the presence of NAC (antioxidant), SP600125 (JNK inhibitor) and SB203580 (P38 inhibitor). The effect on cell viability was measured by the MTT assay (Figure 4.15). The presence of NAC completely abolished the cytotoxic effect of ZnO nanoparticles and showed cell viability similar to control cells even after 24h of exposure. However, addition of SP600125 (JNK inhibitor) and SB203580 (P38 inhibitor) did not provide any protection from ZnO nanoparticles induced cell death in HepG2 cells.

The presence of NAC significantly ($p<0.05$) decreased the number of depolarized cells (Figure 4.16A). AnnexinV-FITC/PI and Hoechst 33342 staining indicated that NAC was able to protect cells from ZnO nanoparticle induced apoptosis (data not shown). Bax/Bcl2 modulation and $P53^{Ser15}$ phosphorylation was also noticeably inhibited by NAC addition (Figure 4.16B).

4.3.12. Analysis of released Zn^{2+} and its cytotoxicity

The cells exposed to ZnO nanoparticle supernatant for 6, 12 and 24h showed same cell viability as that of control cells in MTT assay (Figure 4.17A).

The AAS analysis of the supernatant revealed a Zn^{2+} of 1.2ppm (18.46µM) for all time periods (Figure 4.17B). The cells were further treated with a soluble Zn salt- $ZnCl_2$ at equivalent Zn mass dose (18µM) for 6, 12 and 24h

and the cytotoxicity was assessed by the MTT assay. The assay revealed no decrease in cell viability on 6, 12 and 24h exposure to $ZnCl_2$ (Figure 4.17C).

4.4. Discussion

The present study explores the effects of ZnO nanoparticles on human liver cells and provides significant insight into the possible mechanism through which ZnO nanoparticles exert their toxic effects on these cells. Our results demonstrate the cytotoxic and genotoxic potential of ZnO nanoparticles in human liver cells. Oxidative stress and not dissolution was found to be the underlying mechanism behind ZnO nanoparticle induced DNA damage and cell death. Our data also revealed that the mode of cell death was apoptosis which was mediated by ROS triggered mitochondrial pathway as evidenced by decrease in MMP, modulation of Bax/Bcl2 ratio and cleavage of caspase-9 (Figure 4.18). Finally, we also investigated the status and role of some major signalling molecule like MAPK and P53. Interestingly, JNK and P38 activation was observed, however, with minimal effect on ZnO nanoparticle induced apoptosis.

The interference of some nanomaterials with commonly used cytotoxicity test systems has been well documented in the literature (Monteiro-Riviere et al. 2009). Therefore, it has been suggested that the cytotoxicity of nanomaterials should be assessed with two or more independent test systems for validating the findings (Monteiro-Riviere et al. 2009). We evaluated the cytotoxicity of ZnO nanoparticles by three different assay systems viz. the MTT assay, NR uptake and LDH release assay to increase the reliability of the data. The assays revealed a cytotoxic potential of ZnO nanoparticles at 14 and 20 µg/ml after 12 and 24h exposure in HepG2 cells.

The concentration dependence of ZnO nanoparticle toxicity showed a steep response. This steep dose response pattern of ZnO nanoparticle toxicity is in agreement with the studies of Wang et al. (2008) and Lin et al. (2009) carried out on Chinese hamster ovary (CHO) cells and human alveolar epithelial (A549) cells respectively.

Oxidative stress is the most discussed paradigm for the toxicity of nanoparticles. This has been attributed to their small size and hence large surface area which is generally thought to elicit ROS generation and oxidative stress (Xia et al. 2006). The ZnO nanoparticles in our study were also found to be capable of generating intracellular ROS when examined by the cell permeable dye DCFH-DA. This observation is consistent with the earlier studies of Yin et al (2010) and Yang et al (2009a) who observed similar effects on WIL2-NS human lymphoblastoid cells and primary mouse embryo fibroblast cells respectively. We also observed an increase in lipid peroxides in HepG2 cells on exposure to ZnO nanoparticles, which represents another marker of oxidative stress. Lipid peroxidation can further give rise to more free radicals and damage biomolecules like DNA, protein and lipids in conjunction with ROS. It also causes injury to the cell membrane as indicated by an increased LDH release. Different ways for ROS generation by engineered nanoparticles have been proposed (Song et al. 2009; Xia et al. 2006). The nanoparticles can lead to spontaneous ROS generation at their surface owing to their chemical and surface characteristics. They can also lead to the generation of free radicals after their interaction with cellular components e.g. mitochondrial damage. One more way of ROS production is the activation of NADPH-oxidase enzyme

which is responsible for O_2^- production in the membrane of phagocytic cells. In case of ZnO nanoparticles, the generation of ROS has been attributed to their semiconductor and nanolevel characteristic which leads to ROS generation even in the absence of light. This has already been explained in detail by Rasmussen et al (2010) (Rasmussen et al. 2010). The quality of ZnO nanocrystal decreases with decreasing nanoparticle size and results in increased interstitial zinc ions and oxygen vacancies (Nel et al. 2006; Sharma et al. 2009). These crystal defects can lead to a large number of electron-hole pairs which can migrate to the nanoparticle surface and contribute to the ROS generation. The electron and holes can react with the oxygen and hydroxyl ions respectively present in the ZnO nanoparticles aqueous environments. This produces highly reactive free radical compounds including the superoxide anion radical (from electrons) and the hydroxyl radical (from holes) (Rasmussen et al. 2010). When in contact with the cellular environment, these radicals can oxidize and reduce macromolecules (DNA, lipids, proteins) resulting in significant oxidative damage to cell.

Some nanoparticles owing to their small size are capable of reaching the nucleus and might attack DNA (Chen and Mikecz 2005). They may also exhibit an indirect effect on DNA through their ability to generate reactive oxygen species. This DNA damage may either lead to carcinogenesis or cell death, thus disrupting normal cell functions. We observed the genotoxic potential of ZnO nanoparticles in HepG2 cells in the alkaline Comet assay which is capable of detecting single as well as double DNA strand breaks and alkali labile sites even at low levels of DNA damage (Collins 2004). Our

earlier studies have also revealed the DNA damaging potential of these nanoparticles in somatic cells (skin cells, lymphocytes) and germ cells (Gopalan et al. 2009). As ROS is known to react with DNA molecules causing damage to both purine and pyrimidine bases as well as DNA backbone (Martinez et al. 2003), we investigated the link between oxidative stress and DNA damage in HepG2 cells via the Fpg modified Comet assay. The bacterial enzyme Fpg recognizes specifically the most common marker for DNA oxidation- 8-oxo-7, 8-dihydroguanine (8-oxoGua). In the present study, the levels of Fpg-sensitive sites (oxidised purines) increased as compared to the levels of direct single strand breaks as observed in standard Comet assay. Moreover, NAC was able to give protection against these ZnO nanoparticle induced DNA strand breaks and oxidative DNA damage. This confirms oxidative stress as the mediator of ZnO nanoparticles induced DNA damage. These results are in agreement with the findings of Karlsson et al (2008) who observed oxidative DNA lesions in cultured A549 cells after exposure to 20 μg/cm^2 (40 μg/mL) and 40 μg/cm^2 (80 μg/mL) ZnO nanoparticles for 4h.

The ZnO nanoparticle induced cell death observed in this study can occur by two distinct modes- apoptosis and necrosis which can be distinguished by morphological and biochemical features. While necrosis is usually induced by pathological and accidental damage to cells, apoptosis accounts for most of the physiological cell death and is a tightly regulated process controlled by a complex set of molecules (Elmore 2007). To know the mode of ZnO nanoparticles induced cell death, ZnO nanoparticles treated cells were incubated with AnnexinV-FITC/PI and analyzed by flow cytometry.

AnnexinV/PI staining of ZnO nanoparticle treated HepG2 cells resulted in an increase in AnnexinV$^+$/PI$^-$ and AnnexinV$^+$/PI$^+$ cells compared to the control (AnnexinV$^-$/PI$^-$) indicating apoptosis as a possible mode of cell death. To further confirm that ZnO induced cell death represented apoptosis we examined the cells stained with Hoechst 33342 and found nuclear condensation and fragmentation which is another morphological hallmark of apoptosis.

Apoptosis can be mediated by different routes, out of which one major pathway is mitochondrial pathway (also known as the intrinsic pathway) which is triggered by a wide range of stimuli. The intrinsic pathway is regulated by the proteins of the Bcl-2 family. The relative expression levels of the pro-apoptotic (Bax) and the anti-apoptotic proteins (Bcl-2) decides the fate of the cell towards programmed death. In order to examine the role of the Bcl-2 family in ZnO nanoparticle induced apoptosis, the effects of ZnO nanoparticles on Bax and Bcl-2 protein levels were analyzed by Western blotting and an increase in Bax levels with a corresponding decrease in Bcl-2 levels was observed. Another key event in the intrinsic pathway is disruption of the mitochondrial trans-membrane potential. This leads to osmotic mitochondrial swelling with subsequent rupture of the outer mitochondrial membrane, resulting in the release of pro-apoptotic proteins (e.g cytochrome c, apoptosis inducing factor) from the mitochondrial inter-membrane space into the cytoplasm. Cytochrome c induces the formation of apoptosome which binds to downstream caspases, such as procaspase-9, and processes them into proteolytically active forms. Active caspase-9 further mediates activation of effector caspases resulting in apoptosis. We

analyzed this crucial step of mitochondrial membrane depolarization in ZnO nanoparticle treated cells and found a collapse of $\Delta\Psi_m$ following treatment with ZnO nanoparticles. We also observed the activation of caspase-9 as proved by a decrease in the pro-caspase level accompanied by an appearance of 37kD cleavage product. Our results clearly demonstrate the role of mitochondria mediated pathway (intrinsic pathway) in ZnO nanoparticle induced apoptosis.

Investigating the effect of ZnO nanoparticles on MAPK and their importance in ZnO induced apoptosis was another important part of this study. MAPK is a common signalling pathway activated in response to various cellular stimuli such as oxidative stress (Chang and Karin 2001). The MAPK pathways consist of three main members, the extracellular signal-regulating kinase (ERK1/2), stress activated protein kinase (SAPK)/ Jun-N-terminal kinase (JNK), and the P38 pathways, which govern important cellular activities like proliferation, differentiation, stress responses etc. The JNK pathway has been identified as a direct activator of the mitochondrial death machinery providing a molecular linkage from oxidative stress to the mitochondrial apoptosis machinery. It is known to cause the release of cytochrome c and AIF by selective permeabilization of the outer mitochondrial membrane (Aoki et al. 2002). Anti-apoptotic Bcl-2 family proteins, namely Bcl-2 and $Bclx_L$ were found to be phosphorylated by JNK suppressing their anti-apoptotic function (Maundrell et al. 1997). Therefore, we evaluated the link of MAPK with ROS production and apoptosis. We demonstrated that treatment of HepG2 cells with ZnO nanoparticles caused JNK and P38 activation, however, the status of ERK remained unaltered. In

addition, P38 and JNK activation was completely abolished in the presence of NAC suggesting that there is a ROS-dependent induction of JNK and p38 by ZnO nanoparticles. These results point to the possibility that ROS - evoked JNK and P38 activation triggered the mitochondrial-dependent cell death pathway based on the well established role of these kinases in ROS mediated apoptosis (Aoki et al. 2002). Interestingly, Inhibition of JNK and P-38 pathway by using their specific inhibitors (SP600125 and SB203580 respectively) failed to protect cells from apoptosis. This shows that JNK and P38 kinases play no direct role in the apoptosis induced by ZnO nanoparticles. However, their activation by ZnO nanoparticle generated reactive oxygen species might be explained as an adaptive response to bypass the stress injury (El-Najjar et al. 2010). The importance of MAPK cascade in nanoparticles induced cellular responses has not been explored much despite their multifunctional role in cell signalling especially under various stress conditions (Chang and Karin 2001).

It has been shown that tumor suppressor protein P53 is involved in cell cycle arrest, DNA repair and apoptosis in response to genotoxic and oxidative stress (Liu et al. 2008). P53 downregulates anti-apoptotic Bcl2 proteins and trans-activates puma, noxa and pro-apoptotic Bax to trigger the mitochondrial pathway of apoptosis (Pietenpol and Stewart 2002). Various stress stimuli leads to phosphorylation of P53 at different sites which stabilizes and activates it. DNA damage induces phosphorylation of P53 at ser^{15} (Shieh et al. 1997). We therefore investigated activation of P53; link between ROS and P53 activation; and whether it is required for ZnO nanoparticle induced apoptosis. We observed an enhanced phosphorylation

of P53 at ser^{15} in HepG2 cells on exposure to ZnO nanoparticles. This phosphorylation could be abrogated by NAC demonstrating an oxidative stress induced P53 activation. This activation may also be explained as a response to DNA damage which is caused by ZnO nanoparticles induced ROS. We also sought to investigate the status of NFκB in HepG2 cells exposed to ZnO nanoparticles and found no modulation in its expression. NFκB is an important transcription factor controlling many important functions such as immunity. inflammation, and apoptosis (Gilmore 1999). However, a better approach to moniter the activity of this transcription factor is to study its translocation to the nucleus as the increase in the NFκB expression in response to any external factor may be too minimal to be detected by Western blotting.

To decipher the link between oxidative stress and ZnO nanoparticle induced toxicity in HepG2 cells, the cells treated with ZnO nanoparticles in the presence of NAC. NAC completely abolished ZnO nanoparticle induced apoptosis. It was also evaluated whether ROS targeted the mitochondria and thereby decreased the $\Delta\Psi_m$ in ZnO nanoparticle-treated HepG2 cells. We observed that a loss of MMP and increased Bax/Bcl-2 ratio induced by ZnO nanoparticle could also be inhibited in the presence of NAC. These results indicated that ROS caused the $\Delta\Psi_m$ loss, Bax/Bcl-2 modulation and caspases activation, which accounted for the ZnO nanoparticle induced HepG2 apoptosis. A direct link between ROS and apoptosis is possible as ROS production causes dimerisation of Bax in the cytosol. This changes conformation of Bax exposing its mitochondrial docking motif leading to translocation of Bax to mitochondria, channel formation and release of

cytochrome c (Neuzil et al. 2006). These results are supported by the findings of Heng et al. (2010) who demonstrated that initial exposure of human bronchial epithelial cells (BEAS-2B) to oxidative stress increased their sensitivity to the cytotoxic potential of ZnO nanoparticles.

Some studies have raised doubt in ascribing the ZnO nanoparticles toxicity to ROS or nanoparticles *per se* and observed dissolution as the main cause (Franklin et al. 2007). Moreover, the phenomenon of dissolution is expected to become more prominent in case of nanoparticles due to its dependency on the surface area. The toxicity of resulting metal ions is well known and accepted. Brunner et al (2006) observed that more soluble nanoparticles like ZnO and FeO showed greater cytotoxicity then insoluble nanoparticles such as CeO_2 and TiO_2 in human mesothelioma MSTO-211H and rodent 3T3 fibroblast cells, however, any correlation with the phenomenon of dissolution was not demonstrated experimentally. Therefore, we addressed the probability of released Zn^{2+} contribution towards toxicity in our study by two different ways. We incubated cell culture media containing nanoparticles at 37^{o}C for 6, 12 and 24h while mimicking the cell exposure conditions. The supernatant from this media did not result in toxicity at any time period discarding any contribution of released Zn^{2+} towards toxicity. To further understand the dissolution process taking place in our experimental conditions, we measured the Zn content in supernatant by AAS. We found that the [Zn^{2+}] reached a level of 1.2 ppm in 6h and remained constant for 12 and 24h. Therefore, the maximum extent of dissolution that we got resulted in 6h itself and remained constant for next 24h showing that the liberation of Zn^{2+} from nanoparticles is independent of time, in given conditions. We also

attempted to answer the issue of dissolution by exposing cells to an appropriate reference material- $ZnCl_2$ at the Zn mass dose (18uM) equimolar to Zn content in supernatant. No decrease in cell viability was observed at 6, 12 and 24h and this corroborated our results that the impact of Zn^{2+} release on toxicity is insignificant. This finding suggests that although the nanoparticles release Zn^{2+} in the media but this amount is insufficient to cause toxicity. Therefore, the observed toxic responses on exposure to ZnO nanoparticles are due to the nanoparticles *per se* rather than the ions released from them. Our results are in agreement with those of Lin et al. (2009a) and Gojova et al. (2007) who demonstrated that there is no ionic toxicity on ZnO nanoparticles exposure, although it was done in different cellular systems and exposure conditions.

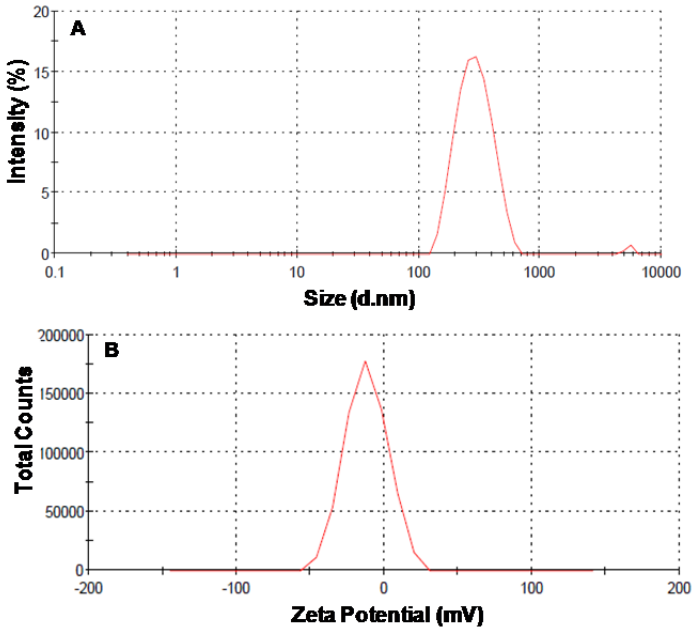

Figure 4.2. Characterization of ZnO NPs; (A) Hydrodynamic diameter; (B) Zeta potential.

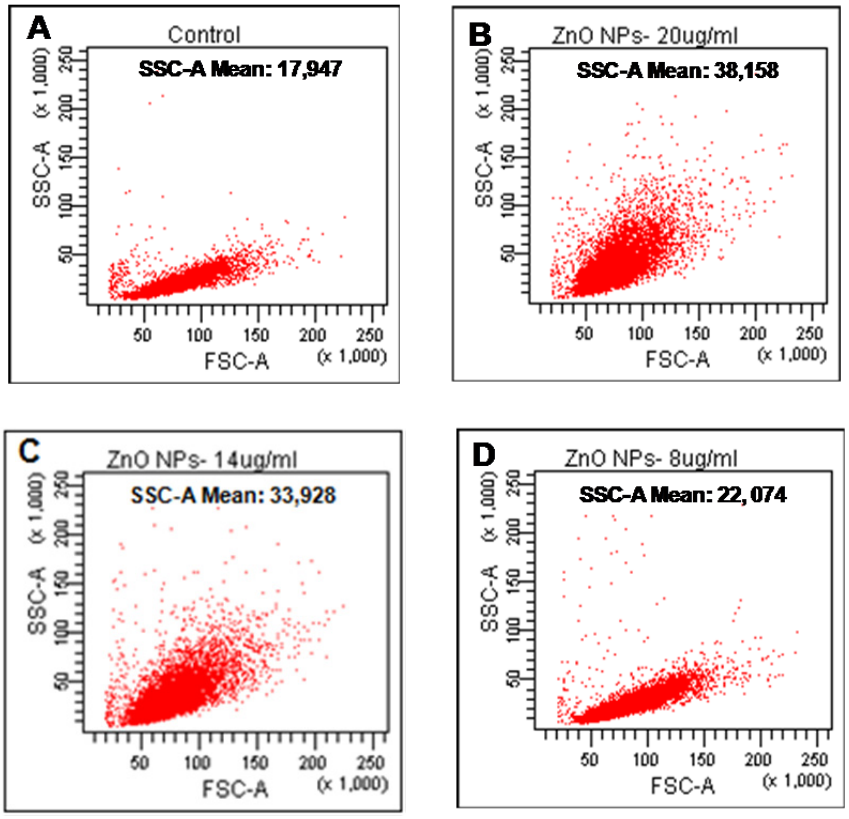

Figure 4.3. Cellular uptake of ZnO NPs in HepG2 cells as assessed by the flow cytometry (A) Control (B-D) ZnO NPs exposed cells.

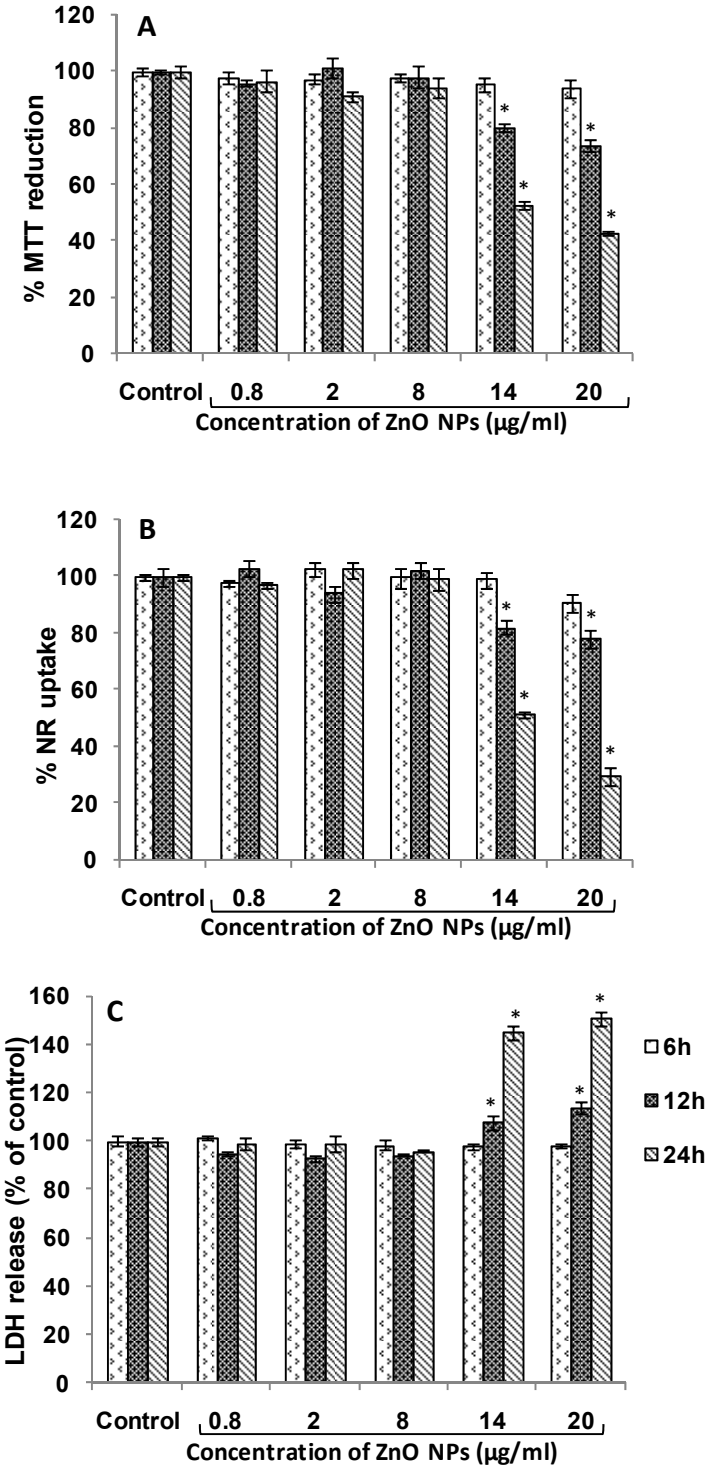

Figure 4.4. Cytotoxic effect of ZnO NPs in HepG2 cells as assessed by (A) MTT assay; (B) Neutral red uptake assay; (C) Lactate dehydrogenase release assay. Data are expressed as the percentage viability of cells exposed to ZnO NPs relative to control cells and are mean ± S.E.M. of triplicates.*$p < 0.05$, compared to control.

Table 4.1. Effect of ZnO NPs on the ROS generation and lipid peroxidation in HepG2 cells after 6h exposure.

Concentrations	ROS generation (% of control)	Hydroperoxide concentration (nmol)
Control	**100 ± 7**	**1.5 ± 0.05**
ZnO NPs (8 µg/ml)	**102 ± 5**	**1.4 ± 0.08**
ZnO NPs (14 µg/m	**116 ± 8**	**1.8 ± 0.04**
ZnO NPs (20 µg/m	**131 ± 5***	**2.6 ± 0.03***

Values represent mean ± S.E. of three experiments.

* $p < 0.05$ when compared to control using one way ANOVA

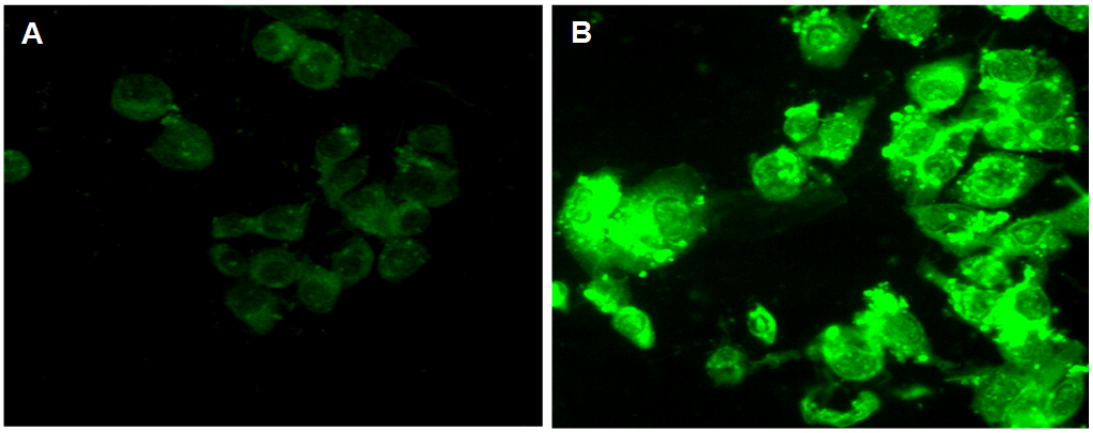

Figure 4.5. Photomicrographs showing generation of the intracellular reactive oxygen species using DCFDA dye in HepG2 cells (A) Control cells; (B) Cells exposed to ZnO NPs for 6h showing increase in fluorescence (Magnification X200).

Table 4.2. Induction of DNA strand breaks and oxidative DNA damage in human liver cells after 6h exposure to ZnO nanoparticles as evident by the Comet parameters.

Concentrations	OTM (arbitrary unit)		Tail DNA (%)	
	Fpg (-)	Fpg (+)	Fpg (-)	Fpg (+)
Control	0.87±0.14	1.21±0.15	5.75±0.88	7.19±0.46
ZnO NPs (8 µg/ml)	1.00±0.08	1.32±0.19	6.80±0.38	8.62±0.79
ZnO NPs (14 µg/m	1.68±0.19*	2.25±0.15* $^{\alpha}$	8.90±0.76*	11±0.62*
ZnO NPs (20 µg/m	2.17±0.20*	4.09±0.05*$^{\alpha}$	11.15±0.11*	14.51±0.55* $^{\alpha}$

Values represent mean ± S.E. of three experiments.
* $p < 0.05$ when compared to control using one way ANOVA
$^{\alpha}$ $p < 0.05$ when compared to Fpg (-) at the same concentration using Student 't' test.

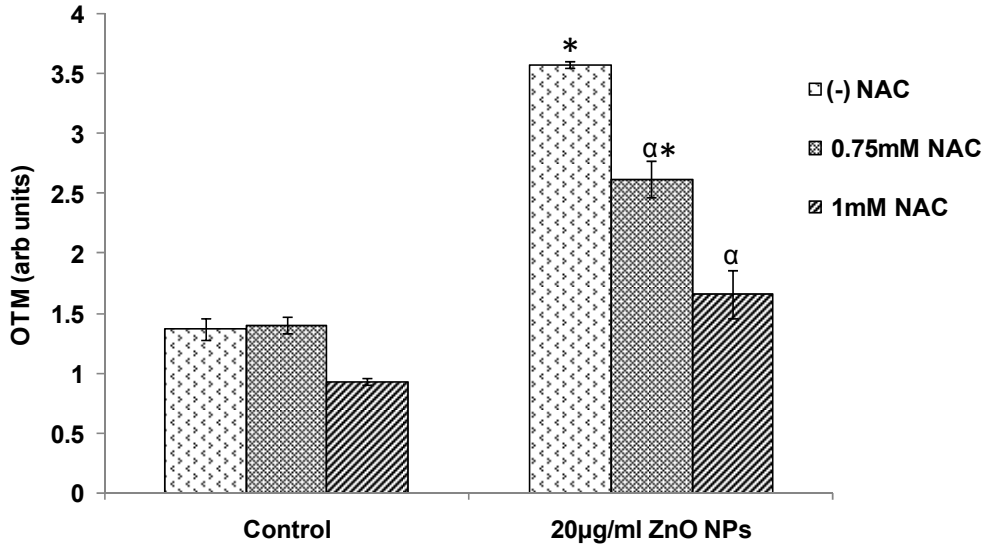

Figure 4.6. Effect of N-acetyl cysteine (NAC) on ZnO NP induced oxidative DNA damage in HepG2 cells; Data represents mean ± S.E.M. of three experiments.*$p < 0.05$ when compared to control using one way ANOVA in Fpg-modified Comet assay. $^{\alpha}p < 0.05$ using when compared to "(-) NAC" at the same concentration using the Student 't' test.

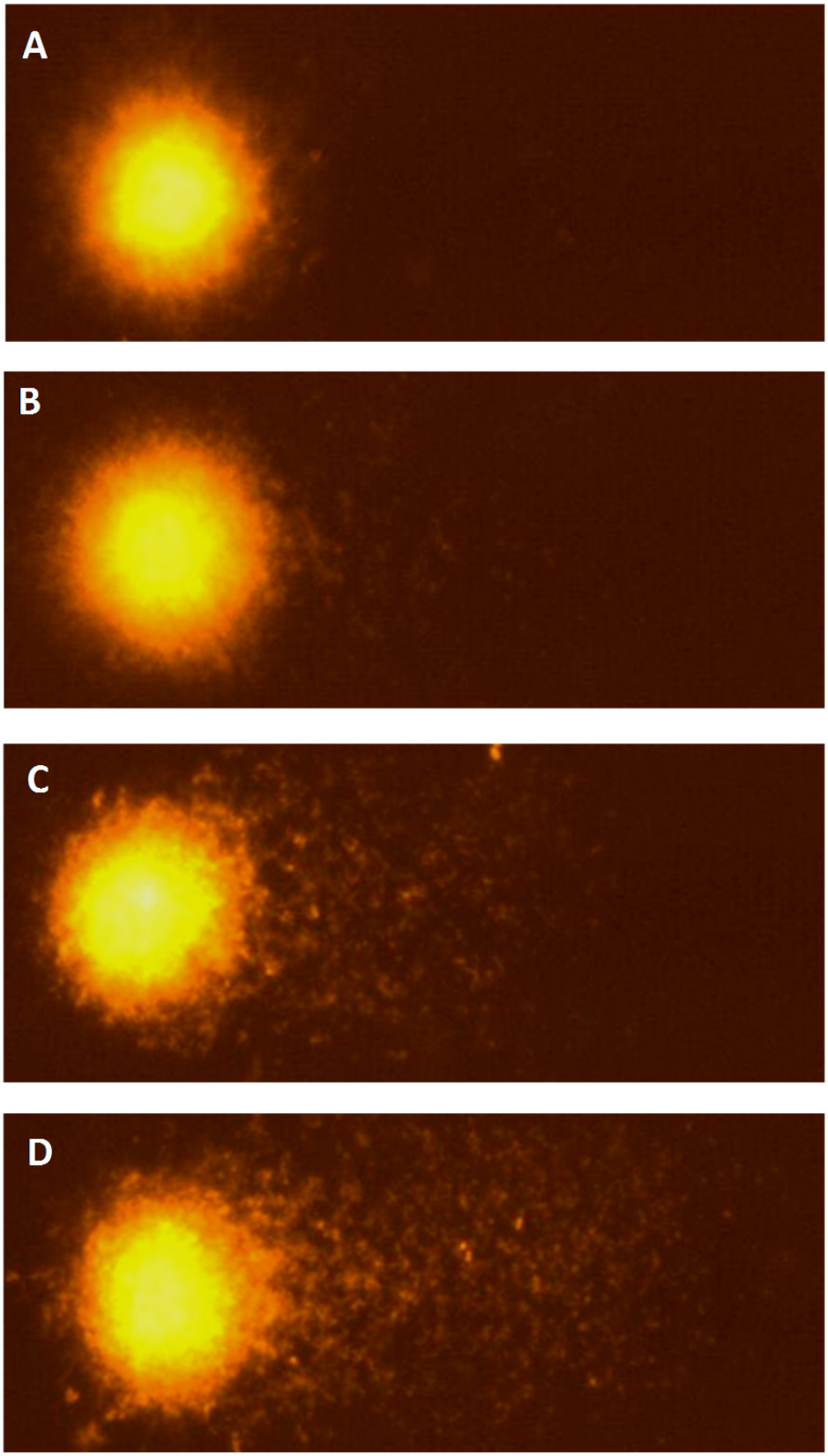

Figure 4.7. HepG2 cells treated with ZnO NPs showing oxidative DNA damage (magnification X400) (A) Control cells in standard alkaline Comet assay; (B) Control cells in Fpg-modified Comet assay; (C) ZnO NPs (20µg/ml) treated HepG2 cell in standard Comet assay; (D) ZnO NPs (20µg/ml) treated HepG2 cell in Fpg-modified Comet assay.

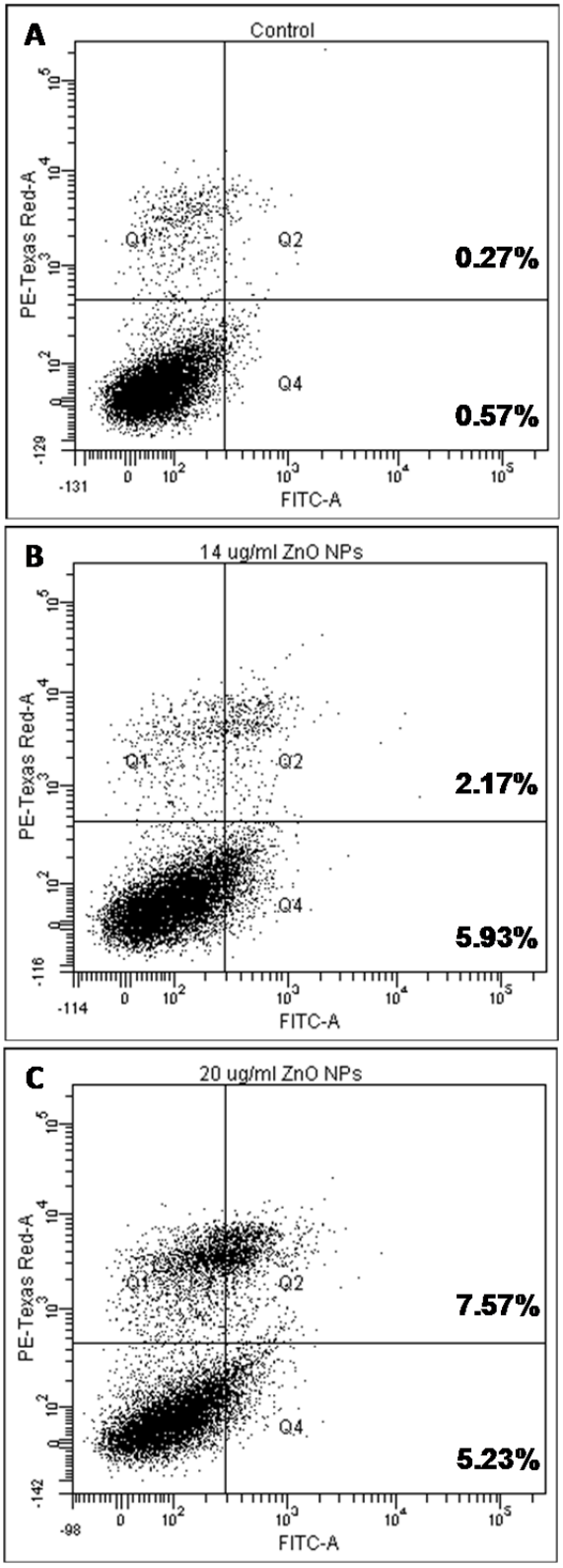

Figure 4.8. ZnO NPs induced apoptosis in HepG2 cells - (A) Control cells; (B) Cells treated with 14µg/ml ZnO NPs; (C) Cells treated with 20µg/ml ZnO NPs. Quadrants: Q1- necrotic cells; Q2- necrotic cells or late phase of apoptotic cells; Q3- unstained live cells, Q4- Early apoptotic cells. Representative dot plots of three independent experiments are presented. Data represent mean ± S.E.M. of three experiments.

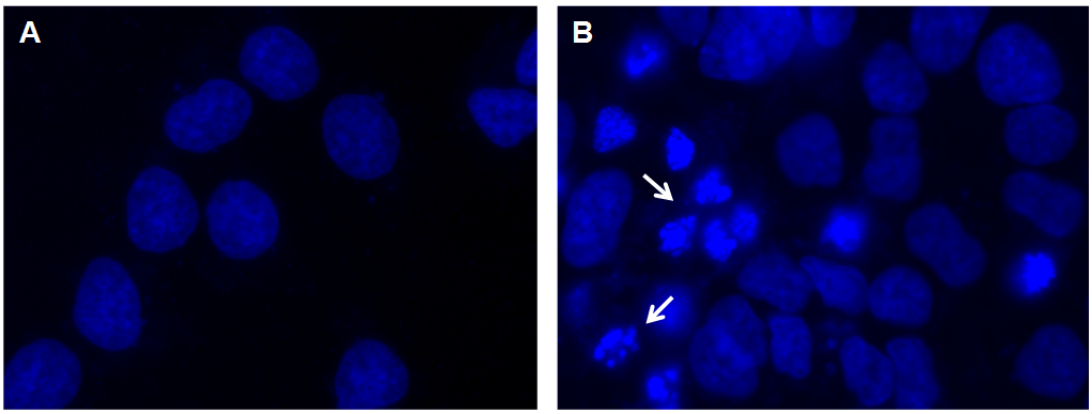

Figure 4.9. Fluorescence images of cells stained with Hoechst 33342. ZnO NP treated cells show apoptotic cells with condensed or fragmented nuclei (indicated by arrows).

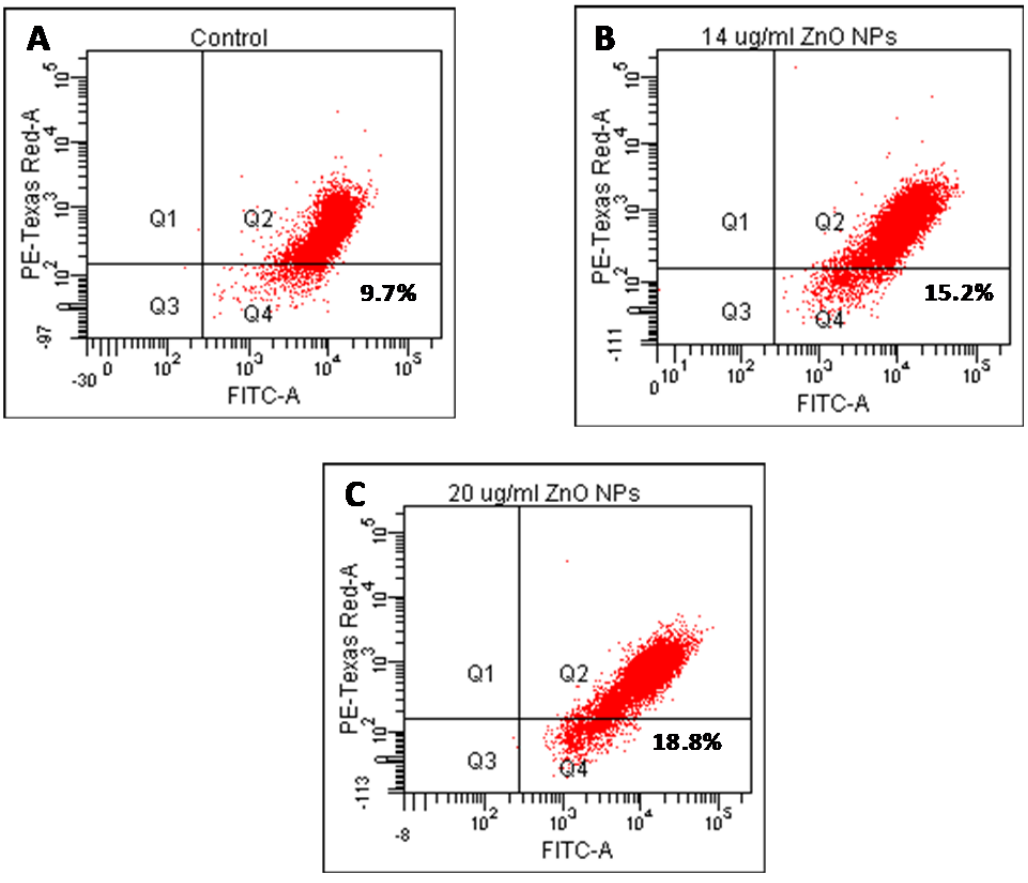

Figure 4.10. ZnO NPs induced mitochondrial membrane potential (MMP) changes in HepG2 cells - (A) Control cells; (B) Cells exposed to 14µg/ml ZnO NPs; (C) Cells exposed to 20µg/ml ZnO NPs.

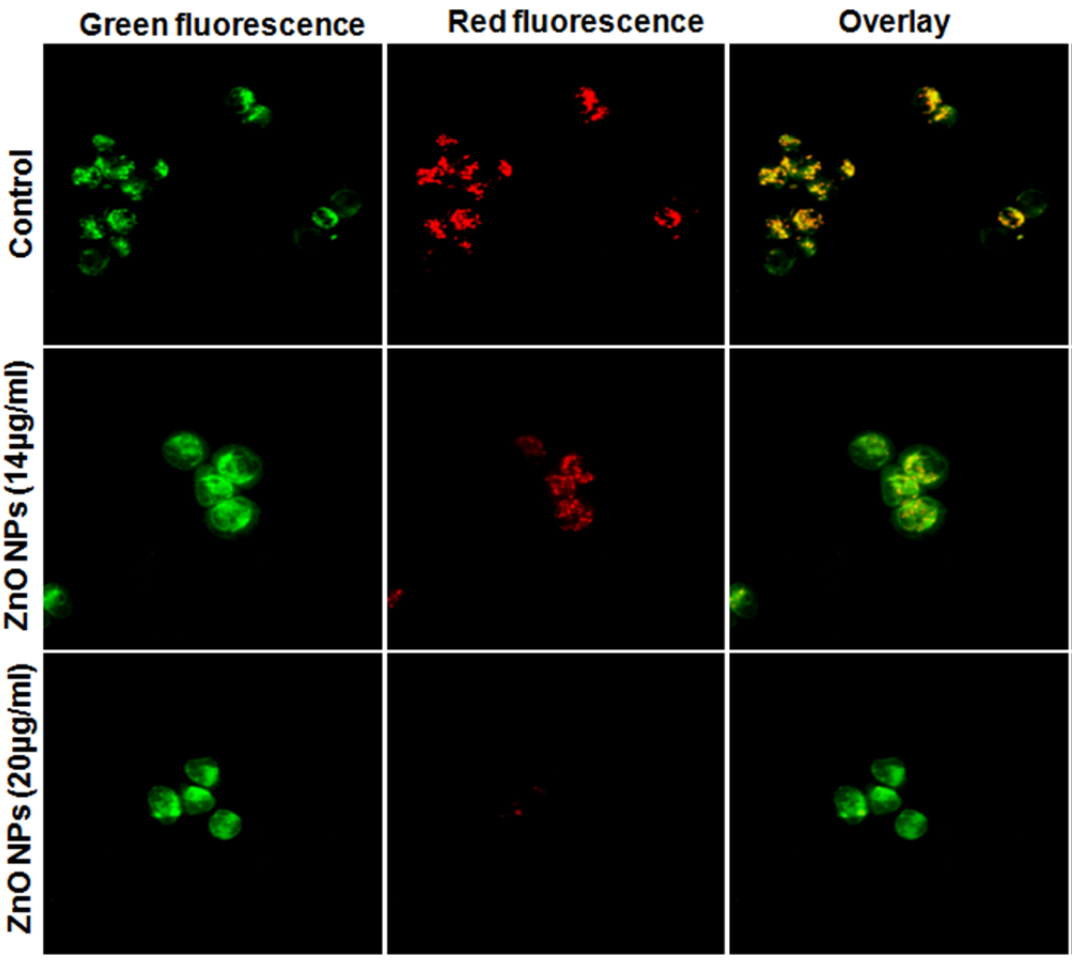

Figure 4.11. Fluorescence images of ZnO NP induced changes in MMP in HepG2 cells. The first (extreme left) column showing only green fluorescence (aggregated form of JC-1), the second (middle) column showing only red fluorescence (monomeric form of JC-1), the third (extreme right) column showing overlay (red-green fluorescence).

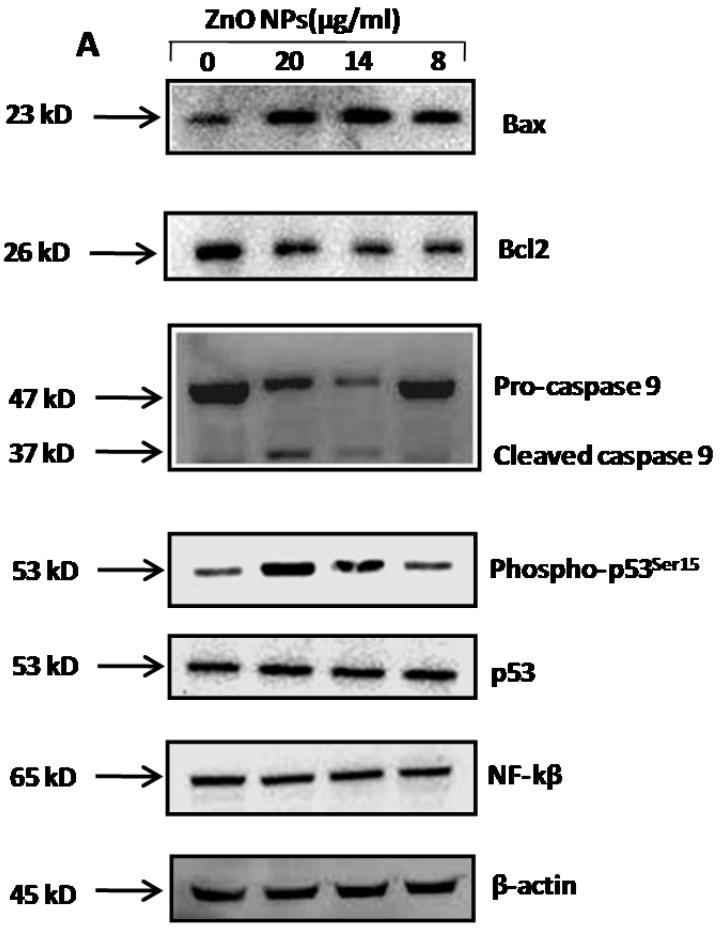
A
ZnO NPs(µg/ml)
0
20
14
8
23 kD
Bax
26 kD
Bcl2
47 kD
37 kD
Pro-caspase 9
Cleaved caspase 9
53 kD
Phospho-p53Ser15
53 kD
p53
65 kD
NF-kβ
45 kD
β-actin

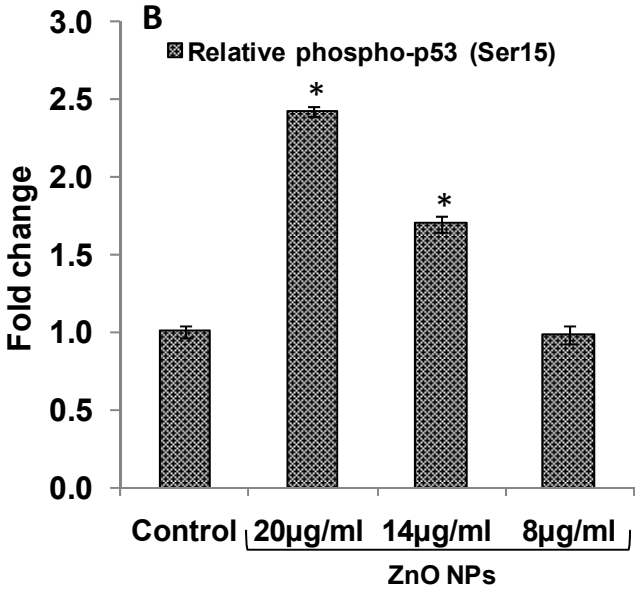
B
Relative phospho-p53 (Ser15)
Fold change
3.0
2.5
2.0
1.5
1.0
0.5
0.0
*
*
Control
20µg/ml
14µg/ml
8µg/ml
ZnO NPs

C

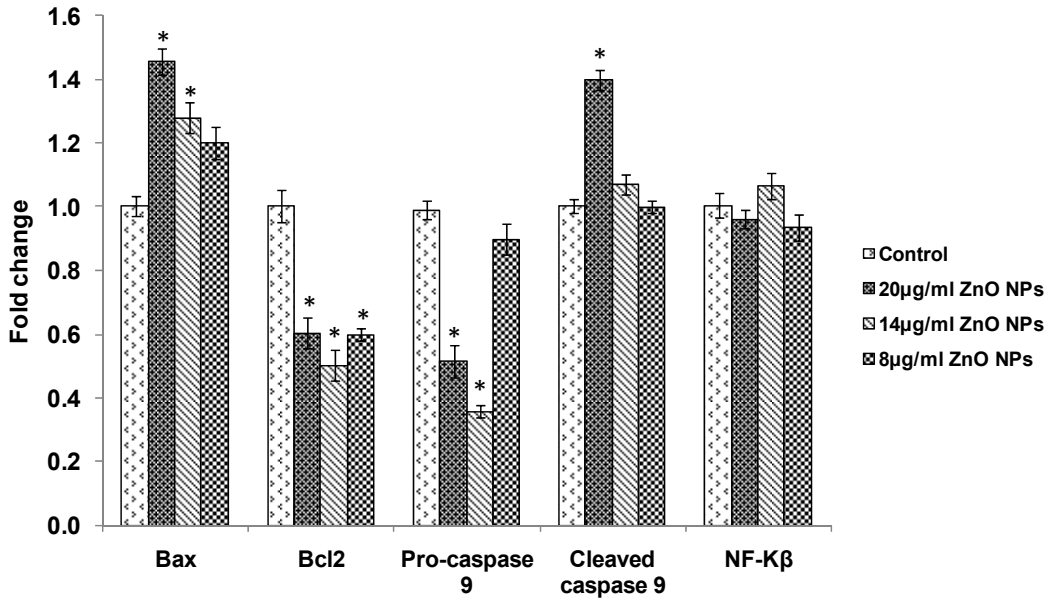

Figure 4.12. Western blot analysis of proteins involved in apoptosis: (A) Bax, Bcl2, NF-kβ expression levels, caspase-9 activation and $p53^{Ser15}$ phosphorylation. β-actin was used as internal control to normalize the data. (B-C) Relative quantification of protein expression levels. Data represent mean ± S.E.M. of three experiments.*$p < 0.05$, compared to control.

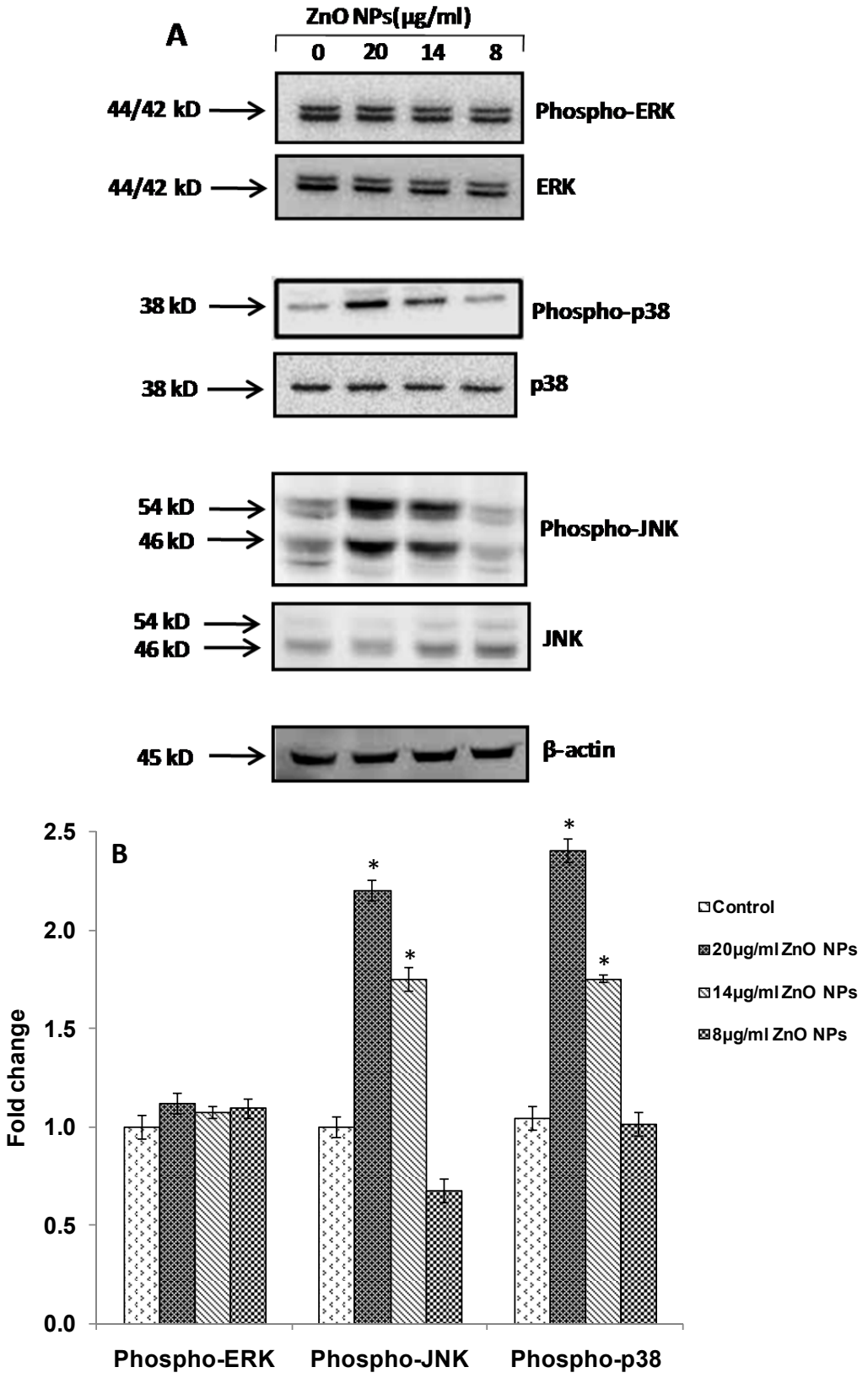

Figure 4.13. Western blot analysis of proteins involved in MAPK signalling in HepG2 cells - (A) Effect of ZnO NPs exposure. (B) Relative quantification of protein expression levels. Quantification was done using scion image software. Data represent mean ± S.E.M of three experiments.*$p < 0.05$, compared to control.

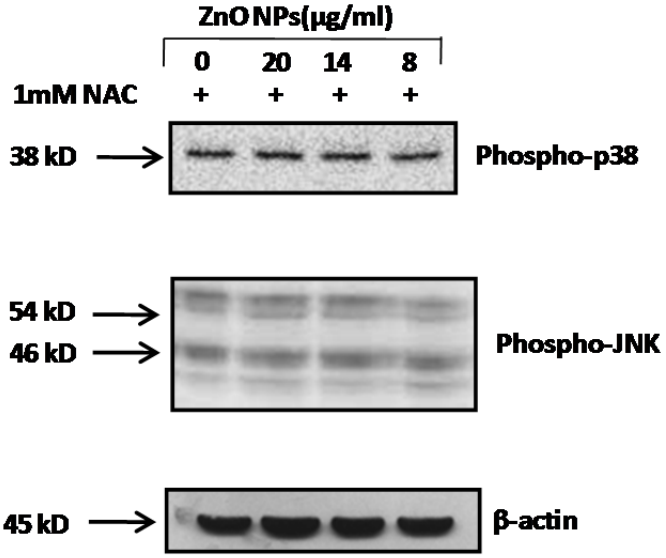

Figure 4.14. Effect of NAC on ZnO NP induced MAPK signalling.

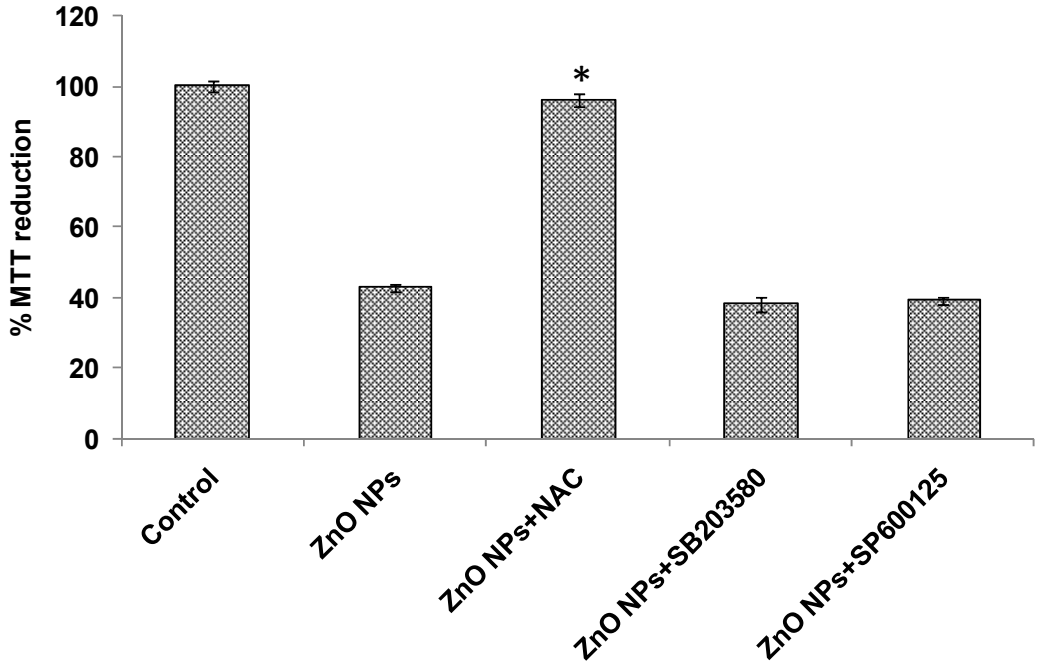

Figure 4.15. Effect of MAPK inhibition and N-acetylcysteine on ZnO NPs induced cytotoxicity in HepG2 cells. Data represent mean±S.E.M. of three experiments.*$p < 0.05$, compared to cell treated with ZnO NPs only.

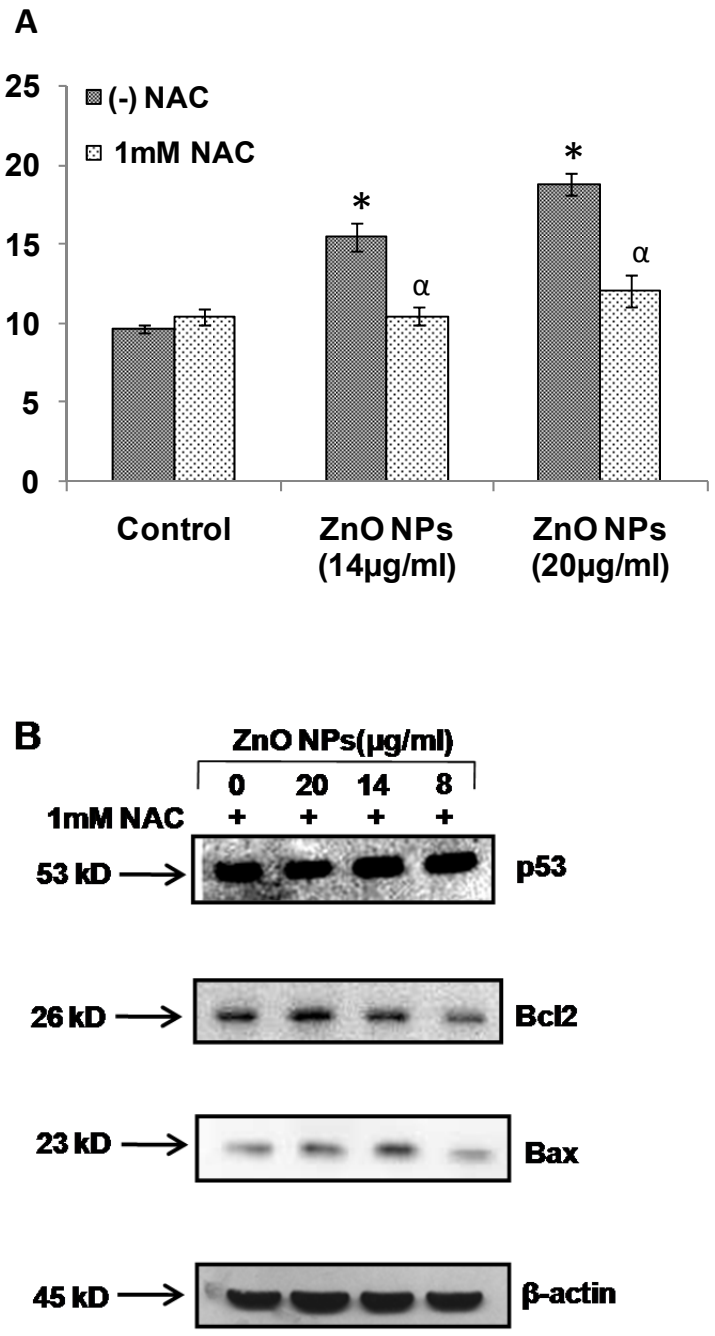

Figure 4.16. Effect of N-acetylcysteine on mitochondrial mediated apoptosis (A) Effect of N-acetylcysteine on ZnO NPs induced loss of MMP. Data represent mean ± S.E.M. of three experiments. *p<0.05 when compared to control. $^{\alpha}$p<0.05 using when compared to "without NAC" at the same concentration. (B) Effect of N-acetylcysteine on ZnO NPs induced Bax, Bcl_2 and p53 phosphorylation. β-actin was used as internal control to normalize the data. Blots shown are representative of three different experiments.

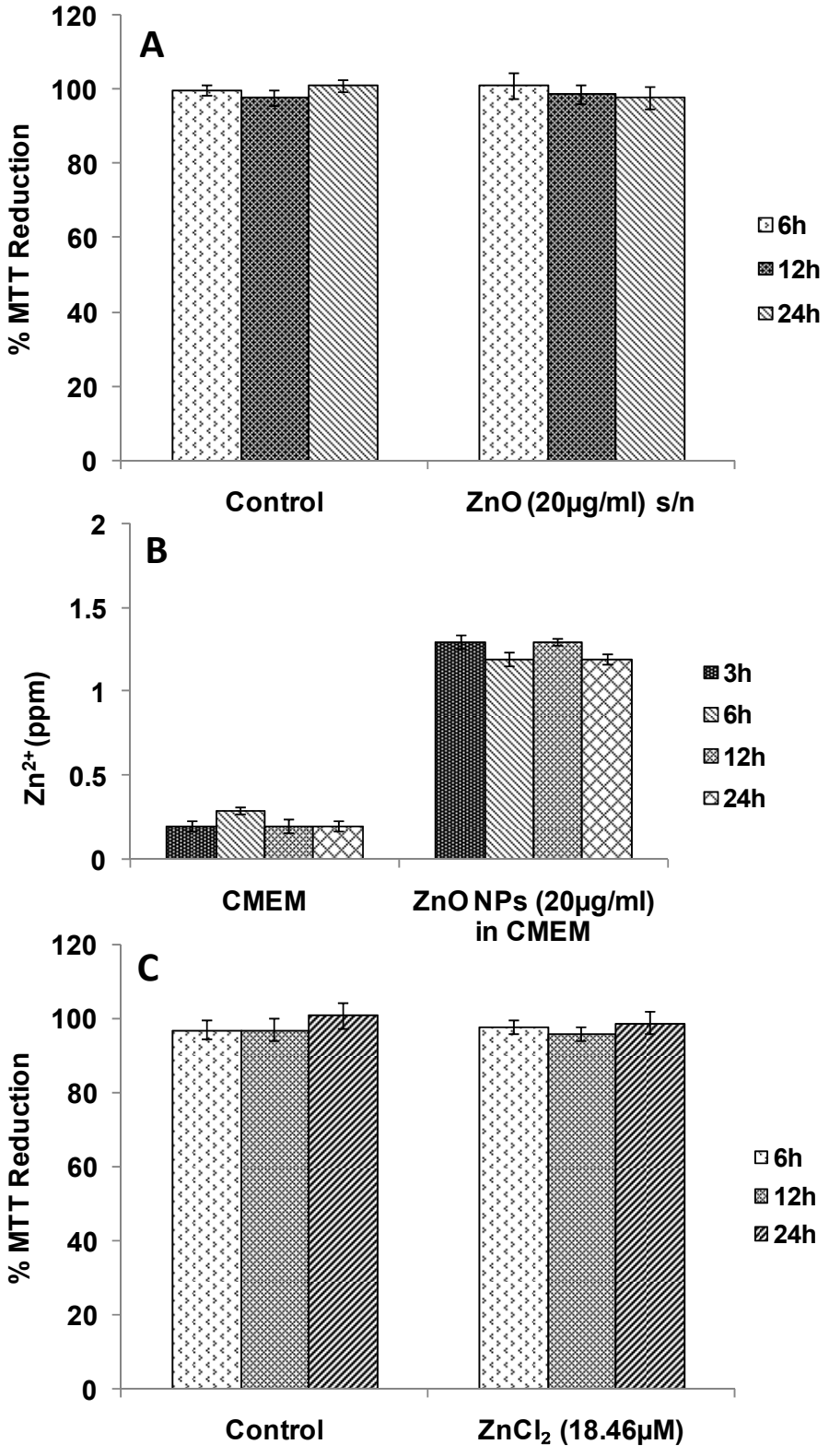

Figure 4.17. Effect of dissolution on ZnO NPs induced cytotoxicity (A) Assessment of cytotoxicity of Zn^{2+} released into the medium from ZnO NPs. (B) Assessment of Zn^{2+} released from ZnO NPs. (C) Assessment of cytotoxicity of released Zn^{2+} using $ZnCl_2$ as the reference standard. The cytotoxicity was assessed by the MTT assay after 6, 12, and 24h exposure. Data represent mean ± S.E.M. of three experiments.

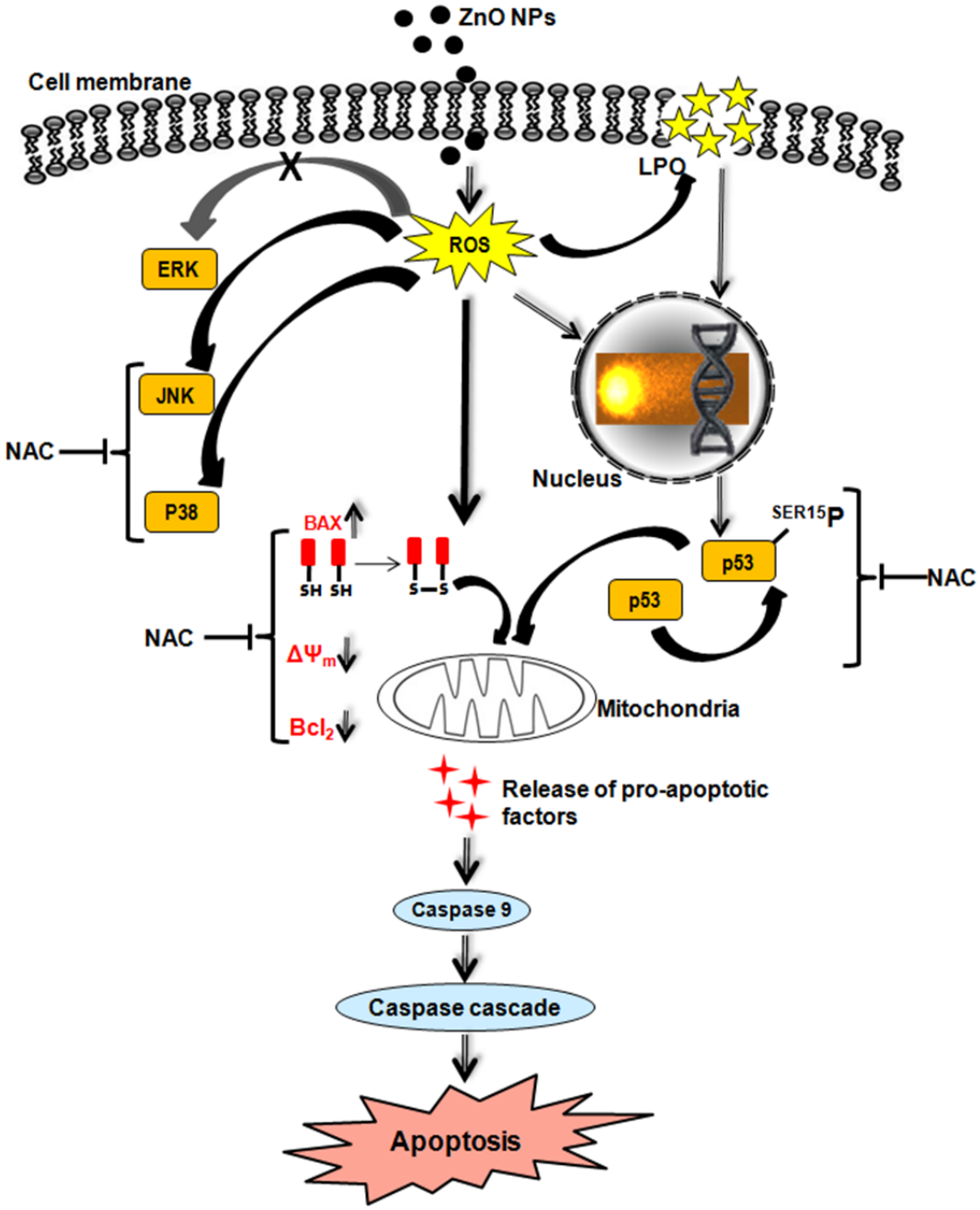

Figure 4.18. Possible mechanisms involved in ZnO NPs induced toxicity in human liver cells.

CHAPTER – 5

In vivo toxicity of ZnO nanoparticles in mice

5.1. Introduction

The toxicity assessment of any novel entity in the *in vivo* systems is always desirable. This is due to the complex cell-cell, cell-matrix interactions, diversity of cell types, hormonal effects that are hard to mimic in the *in vitro* systems. In addition, studying long term chronic effects of the test compound is also not possible without *in vivo* experiments. The importance of the *in vivo* studies in the area of nanomaterial toxicology has already been highlighted (Fischer and Chan 2007).

There are no existing guidelines and standard methodologies for risk assessment of nanomaterials. However, the “committees on toxicity (COT), mutagenicity (COM) and carcinogenicity (COC) of chemicals in food, consumer products and the environment, UK” have suggested extrapolating the *in vitro* nanotoxicity findings to *in vivo* experiments and confirm the results (COT;COM;COC 2005).The same committees (COT, COM and COC) have also advised to consider appropriate route of exposure in the *in vivo* experiments. In case of engineered nanoparticles, the exposure and uptake can occur through different routes. For ZnO nanoparticles, the oral exposure and uptake through the gastrointestinal route needs to be considered. This is keeping in view the fact that ZnO nanoparticles can be ingested directly when used in food, food packaging, drug delivery and cosmetics. Workers involved in ZnO nanoparticles synthesis can be exposed by unintentional hand-to-mouth transfer of nanomaterials. When discharged into the environment accidently, these nanoparticles may enter the human body through food chain. In addition, some of the nanoparticles can be swallowed into the gastrointestinal tract when they are expelled from the

mucociliary system of the lungs after inhalation exposure (Hussain et al. 2001; Oberdorster et al. 2005). Nanoparticles could be then translocated from the lumen of the intestinal tract and blood into different organs like liver. Earlier studies have shown that nano forms of different particles are more toxic then their micro-counterparts after acute exposure via oral route (Chen et al. 2006; Meng et al. 2007; Wang et al. 2007). Biodistribution experiments have revealed liver, kidney and spleen as the target organs for engineered nanoparticles after uptake by gastrointestinal tract (Chen et al. 2006; Cui et al. 2011; Wang et al. 2007). For ZnO nanoparticles, only a few *in vivo* studies are available and most of them are focused on respiratory tract exposure (Sayes et al. 2007; Warheit et al. 2009). A previous study evaluated the acute oral toxicity of ZnO nanoparticles at a high dose range (1-5g/kg body weight) and found a decrease in liver, spleen and pancreas damage with the increase in nanoparticle dose (Wang et al. 2008a). They attributed this pattern to increased agglomeration at higher doses and suggested the need to study ZnO nanoparticle induced oral toxicity at low doses. Moreover, these studies revolve around the general toxicity parameters and have not considered the genotoxic potential of ZnO nanoparticles as well as investigating the mechanism of its toxicity.

Therefore, the present study was undertaken to investigate the acute oral toxicity of ZnO nanoparticle including its genotoxicity and the mechanism of toxicity involved. In addition, we also sought to evaluate if the toxic responses and the mechanism of toxicity involved *in vitro* studies are also being observed in the *in vivo* scenario. For this we exposed mice to ZnO nanoparticles via the oral route according to the OECD guidelines (OECD-

420 2001) and the distribution of nanoparticles in different tissues was investigated. The effects of nanoparticles on body/tissue weight and serum biochemical parameters were also examined. Additionally, we analyzed the genotoxic effects of these particles by *in vivo* comet assay and the organ damage by histopathology. To understand the mechanism of cell death, we measured the oxidative damage by lipid peroxidation and Fpg-modified Comet assay. TUNEL assay was also done in the target organ to understand the mode of cell death.

5.2. Materials and methods

5.2.1. Animals and treatment

All animal-handling procedures were carried out following the regulations of Institutional Animal Ethics Committee and with their prior approval for using the animals. Male Swiss albino mice (~6-week-old, 20 ± 2 g) were obtained from the Indian Institute of Toxicology Research (Lucknow, India) animal breeding colony and were housed in a 12h day and light cycle environment with *ad libitum* availability of diet and water, at the controlled temperature of 23 ± ^{o}C, humidity of 55 ± 5%. The animals were divided into 3 groups containing 25 mice each: Group 1- vehicle control (water); Group 2- ZnO nanoparticles (300mg/Kg body weight); Group 3- ZnO nanoparticles (50mg/Kg body weight). The animals were treated daily through gavage for 14 consecutive days according to the fixed dose procedure (OECD-420 2001).

All animals were weighed at the beginning and end of each treatment. After the treatments, the animals were sacrificed by cervical dislocation. Organs were taken out immediately for isolation of single cells.

5.2.2. Zn content analysis in tissues

This has been described in Chapter 2 (2.11.2).

5.2.3. Biochemical assay of serum

This has been described in Chapter 2 (2.11.3).

5.2.4. Lipid peroxidation (LPO) assay

A 10% homogenate of tissues (liver, kidney and brain) was made in ice cold buffer comprising 0.1 M Na_2HPO_4, 0.1M NaH_2PO_4 and 0.1M KCl, using a Polytron PT 1600 E (KINEMATICA, Switzerland). The homogenate was then centrifuged at 9000 x g for 10min and the supernatant was used for the enzymatic assay. LPO was measured using the method of Utley et al (1976) as described in Chapter 2 (2.11.4.).

5.2.5. Histopathology

The mouse organs were fixed in 10% formalin for 24-48h at room temperature and the tissues were processed for histopathology as described in Chapter 2 (2.11.5.).

5.2.6. Single cell gel electrophoresis/ Comet assay

The tissues from mouse organ (liver and kidney) was minced and suspended in chilled Hank's balanced salt solution with 20mM EDTA. The cell suspension was then mixed with equal amount of 1% LMPA and the slides were prepared and the comet assay performed as previously described in Chapter 2 (2.7).

5.2.7. TUNEL assay

The method of the TUNEL assay has been described before in Chapter 2 (2.11.6).

5.3. Results

5.3.1. Body and organ weights of mice

The three groups of mice did not show any significant difference in the body weights. Similarly, no obvious difference was observed in the organ weights (liver, kidney and brain) of control mice and ZnO nanoparticles treated mice (Table 5.1).

5.3.2. Zn content analysis

A significant ($p<0.05$) increase in the Zn content was found in the liver of mice treated with 300mg/Kg ZnO NPs for 14 days compared to the control mice. In contrast, there was no difference in Zn content in the brain of treated and control mice. The kidney showed a slight increase in the Zn content but it was not statistically significant (Figure 5.1).

5.3.3. Biochemical assays in serum

The mice orally exposed to ZnO nanoparticles at a dose of 300mg/Kg showed a significantly ($p < 0.05$) higher levels of alanine aminotransferase (ALT) and alkaline phosphatase (ALP) compared to control mice (Table 5.2). The levels of bilirubin, blood urea nitrogen (BUN) and creatinine were found to be similar in both the groups.

5.3.4. Lipid peroxidation assay

A significant ($p<0.05$) induction in the lipid peroxidation was observed at the higher dose (300mg/Kg) in the liver and kidney of ZnO nanoparticles exposed mice compared to the control group (Table 5.3). The brain showed no increase in lipid peroxidation on nanoparticle exposure.

5.3.5. Histopathological changes

The liver and kidney of mice exposed orally to ZnO nanoparticles (300mg/Kg) for 14 consecutive days showed pathological alterations. The liver revealed hepatocellular necrosis and accumulation of inflammatory cells around necrotic area (Figure 5.2A-B). Kidney depicted cystic dilation of tubules along with hypertrophied tubules (Figure 5.2C-D).

5.3.6. Oxidative DNA damage

The oxidative DNA damage in the liver and kidney cells of mice was evaluated by the Fpg- modified Comet assay after an acute oral exposure to ZnO nanoparticles.

Cell viability for all the samples was found to be more than 90% in every experiment (data not shown).

A statistically significant ($p<0.05$) increase in the oxidative DNA damage was observed in the liver of mouse exposed to ZnO NPs at the higher dose (300 mg/Kg) as was evident by an increase in the Olive tail moment (arbitrary units) and Tail DNA (%) (Table 5.4). However, no significant DNA damage was observed in the mice administered with the lower dose of ZnO NPs (50 mg/kg).

There was no significant difference in the Comet parameters in the kidney cells of control and ZnO NPs exposed mice.

5.3.7. TUNEL assay

TUNEL assay was done to detect the apoptotic cells in the liver of control mice and ZnO NPs exposed mice. An increase in the TUNEL positive (green fluorescence) cells scattered throughout the liver section was observed in the liver of mice treated with higher dose of ZnO NPs (300 mg/Kg) compared

to control mice (Figure 5.3). However, only few TUNEL positive cells were visible in the liver section of lower dose group (50 mg/Kg) and control group.

5.4. Discussion

In the present study, the acute oral toxicity and genotoxicity of ZnO nanoparticles (300 and 50mg/Kg) in mice was investigated after an exposure of 14 consecutive days. The oral route was selected as the route of exposure for mice. This is because the ZnO nanoparticles are being used in food packaging and may gain entry into the body directly. Even when used in other consumer products like coating and dermatological applications, there is a risk of ingestion during use. Moreover, they may gain entry into the gastrointestinal tract after their accidental release into the environment. The doses at which humans may be exposed to ZnO nanoparticles in these scenarios are yet to be found. We chose to work with the doses that are suggested by OECD guidelines for investigating the acute oral toxicity of any new substance (OECD-420 2001). These doses do not necessarily reflect the actual concentrations of ZnO nanoparticles found in the real environments, however, they can be used to assess the health risks from prolonged exposure to ZnO nanoparticles. The mice were chosen as the *in vivo* model of exposure because of their similarity with human metabolic, biochemical and physiological pathways (Argmann et al. 2005).

The nanoparticles when ingested into the body can be distributed to different regions because of their small size. They can cross small intestine and further distribute into the blood, brain, lung, heart, kidney, spleen, liver, intestine and stomach (Hillyer and Albrecht 2001). Jani et al. (1990) have shown that polystyrene latex nanoparticles when administerated orally can

be absorbed across the gastrointestinal tract, and pass through the mesentery lymph supply and lymph node to liver and spleen. So it is important to find out the information about their bio-distribution. The ZnO nanoparticles were mainly found to be retained in the liver after 14 day acute exposure in our studies. This was not surprising as the liver is the primary organ of metabolism for xenobiotics and the nanoparticles have been reported to reach the liver when administrated through the gastro-intestinal route (Chen et al. 2006; Cui et al. 2011).

The targeting of liver by orally administrated ZnO nanoparticles led to the liver damage as revealed by the histopathological examination which showed hepatocellular necrosis. This was also supported by the ALT and ALP levels in the serum. The levels of these enzymes rise in serum when the liver is damaged. The unaltered levels of creatinine, blood urea nitrogen and bilirubin in the present study indicated normal renal functions in the ZnO nanoparticle exposed group. These results support the findings of Wang et al. (2008a) who demonstrated liver damage by the acute oral exposure of ZnO nanoparticles for 14 consecutive days although at a higher dose of 5000mg/Kg. However, the genotoxic and oxidative stress potential of the nanoparticles was not examined. Moreover, an increased agglomeration at these doses is a problem so the study of toxic responses at lower doses was suggested by the authors (Wang et al. 2008a).

There was absence of mortality in the ZnO nanoparticle exposed groups and no difference in the body/organ weights was observed compared to control group. This suggests that the exposure did not exert any major visible impairment in the health status of animals.

In our *in vitro* toxicity studies, we observed oxidative stress and subsequent oxidative DNA damage in HepG2 cells on exposure to ZnO nanoparticles. Therefore, the condition of oxidative stress was also investigated in our *in vivo* experiments by measuring lipid peroxidation in the liver, kidney and brain of mice. An increased lipid peroxidation levels were observed in the liver of higher dose exposed group compared to the control group indicating ZnO nanoparticle induced oxidative stress in the liver. This oxidative stress also led to the DNA damage in liver as indicated by a significant increase in the Fpg sites in the ZnO nanoparticle exposed group.

The mechanism of cell death suggested by the *in vitro* studies was found to be oxidative stress induced mitochondria mediated apoptosis. Therefore, the phenomenon of apoptosis was also explored in the liver of higher dose (300 mg/Kg) group by employing TUNEL assay. A significant number of cells undergoing apoptosis were found in the mice liver of treated mice compared to the control group suggesting that the oxidative stress might also lead to apoptosis during the *in vivo* exposure.

Although, liver was found to be the target organ of ZnO nanoparticles, the kidney also depicted cystic dilation of tubules along with hypertrophied tubules. An increased lipid peroxidation in the kidney also demonstrated that the ZnO nanoparticle intake also adversely affects the kidney. This suggests that nanoparticle may be transported from blood to kidney and a more obvious and severe damage in kidney may be expected from a longer duration of exposure. Burns et al. (2009) have reported that smaller sized nanoparticles (3-6nm) can be effectively cleared out of the animal by renal excretion while the bigger sized (approximately 30nm) may be retained in

the liver. The glomerular filtration in kidney, which is primarily dependent on the size of metabolites, is ineffective in their clearance. For larger metabolites, the preferred route of excretion is via hepatobilliary mechanism which is a slower mechanism and subsequent long term retention in the organ can lead to organ toxicity (Kumar et al. 2010).

In conclusion, the acute oral exposure of ZnO nanoparticles at 300 mg/Kg for 14 consecutive days leads to accumulation of nanoparticles in liver and significant liver damage. This was evident by the elevated ALT and ALP serum levels and pathological alterations in the liver. The ZnO nanoparticles were also found to induce oxidative stress and oxidative DNA damage in the liver cells. The hepatocyte apoptosis was also observed which might be mediated by the oxidative stress induced mitochondrial pathway as demonstrated in our *in vitro* studies earlier. No damage to the brain of ZnO nanoparticle exposed mice was observed.

Table 5.1. Body weights and organ weights of mice after oral exposure to ZnO nanoparticles.

Groups	Body weight (g)		Liver (mg/g)	Kidney (mg/g)	Brain (mg/g)
	Before	After			
Control	20.5± 0.57	23.9± 0.93	48.2± 0.05	13.1± 0.02	16.23± 0.01
ZnO NPs (50mg/Kg)	20.3± 0.67	23.3± 0.88	51.63± 0.05	13± 0.04	16.86± 0.01
ZnO NPs (300mg/Kg)	20± 0.48	23± 0.92	51.3± 0.03	13.91± 0.01	17.39± 0.02

Values represent mean± SEM of ten animals

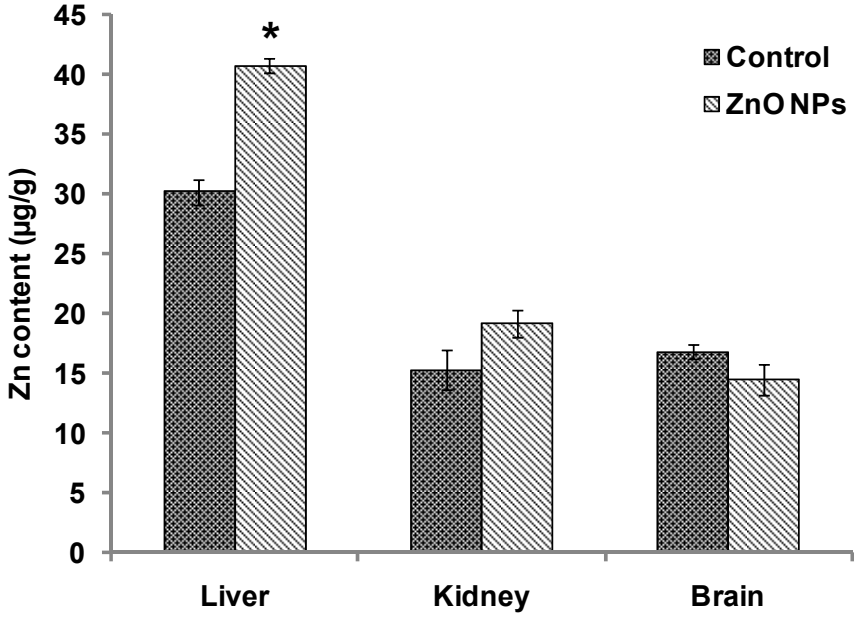

Figure 5.1. Zinc content in selected tissue of the mice (n=5) after oral administration of ZnO NPs (300mg/Kg) for 14 consecutive days. Data represent mean ± S.E.M. of five animals.*$p < 0.05$, compared to control.

Table 5.2. Serum biochemistry parameters in mice after oral exposure to ZnO nanoparticles (300mg/kg) for 14 consecutive days.

Parameters	Groups	
	Control	Treated
ALT (U/L)	55± 5	98± 8.2*
ALP (U/L)	103± 7.3	624± 14.6**
Bilirubin (mg/dl)	0.24± 0.01	0.26± 0.03
BUN (mg/dl)	31± 0.76	26± 3.4
Creatinine (mg/dl)	0.43± 0.03	0.42± 0.04

Values represent mean ± S.E of five animals.
* $p < 0.05$; ** $p < 0.01$ when compared to control.

Table 5.3. Effect of ZnO NPs on lipid peroxidation (LPO)[a] in different organs of mouse.

Organs	Control	ZnO NPs (50mg/Kg.b.wt.)	ZnO NPs (300mg/Kg.b.wt.)
Liver	0.42± 0.01	0.43± 0.02	0.62± 0.01*
Kidney	0.27± 0.02	0.29± 0.01	0.90± 0.01*
Brain	1.19± 0.03	1.09± 0.02	1.25± 0.01

Values represent mean ± S.E of five animals.
[a] LPO expressed as nmol MDA formed/h/g tissue.
*p<0.05, significant when compared to the control group.

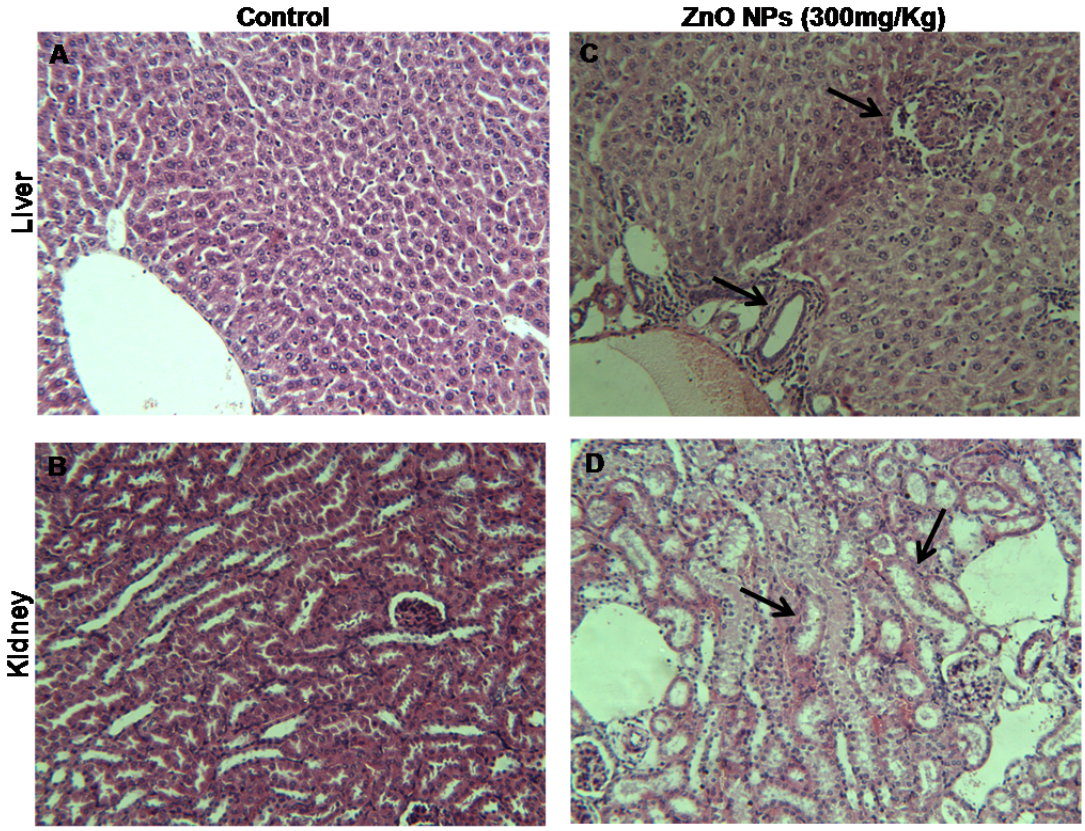

Figure 5.2. Histopathology of liver and kidney tissues in mice treated with ZnO NPs for 14 consecutive days (A-B) Control group showing normal liver and kidney (B-C) Pathological alterations in the liver (hepatocellular necrosis) and kidney (hypertrophied tubules) of ZnO NPs (300mg/Kg) treated group (indicated by arrow); Magnification (X200).

Table 5.4. Effect of ZnO NPs on Comet parameters in liver and kidney cells of mice after oral exposure to ZnO nanoparticles for 14 consecutive days.

Liver	**OTM (arbitrary unit)**		**Tail DNA (%)**	
	Fpg (-)	**Fpg (+)**	**Fpg (-)**	**Fpg (+)**
Control	1.2± 0.1	1.38± 0.12	11.43± 0.92	13.12± 0.31
ZnO NPs (50 mg/Kg)	1.38± 0.08	1.19± 0.06	12.6± 1.02	11.88± 0.66
ZnO NPs (300 mg/Kg)	1.15± 0.04	2.13± 0.13$^{*\alpha}$	11.02± 0.77	16.15± 1.56$^{\alpha}$
Kidney	**OTM (arbitrary unit)**		**Tail DNA (%)**	
	Fpg (-)	**Fpg (+)**	**Fpg (-)**	**Fpg (+)**
Control	0.97± 0.13	1.33± 0.09	9.91± 1.28	11.91± 1.54
ZnO NPs (50 mg/Kg)	1.25± 0.11	1.37± 0.23	12.56± 1.51	11.76± 1.54
ZnO NPs (300 mg/Kg)	1.17± 0.03	1.27± 0.18	11.04± 0.93	10.89± 0.54

Values represent mean ± S.E.M of five animals.
* $p < 0.05$ when compared to control using one way ANOVA
$^{\alpha}$ $p < 0.05$ when compared to Fpg (-) at the same dose using Student 't' test.

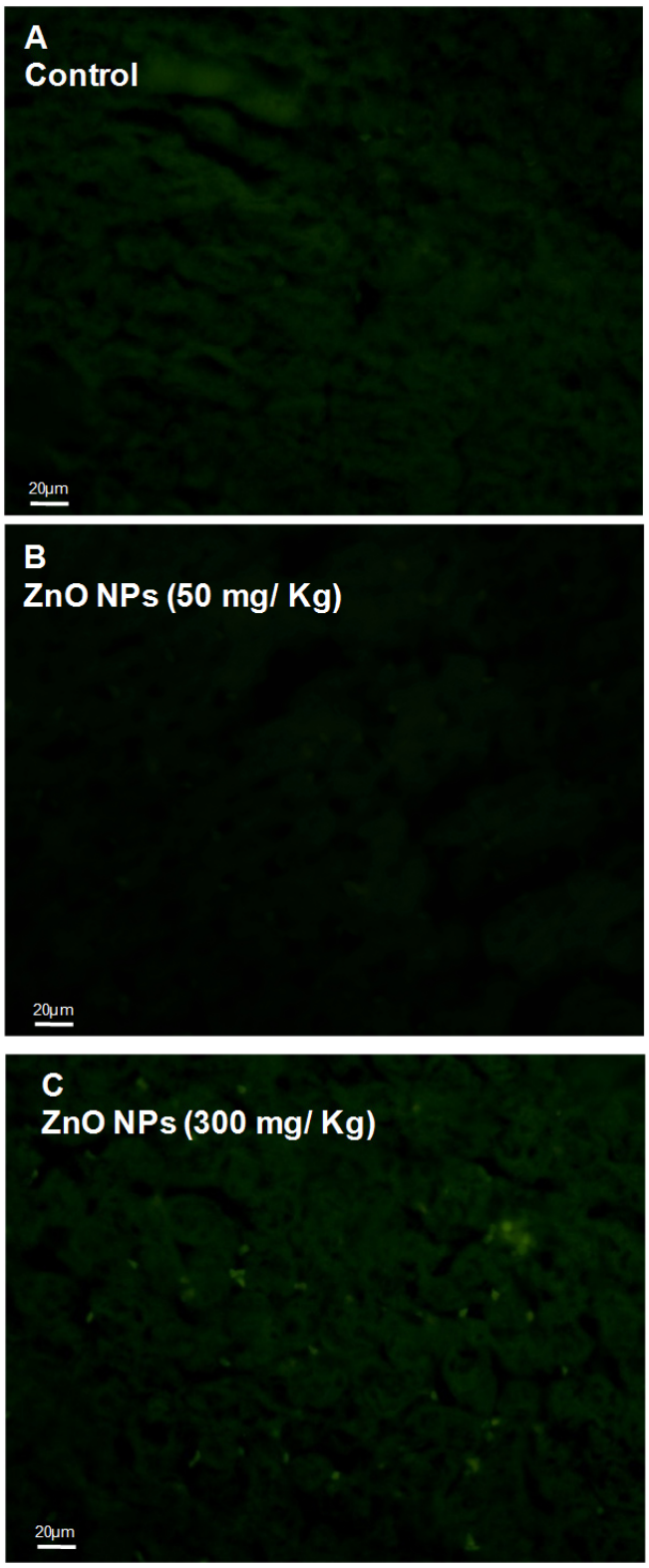

Figure 5.3. ZnO NPs induced apoptosis in the liver cells of mice as detected by the TUNEL assay. Representative images (X400) of TUNEL positive cells (green fluorescence) in the liver sections of (A) Control mice (B-C) Mice exposed to ZnO NPs (300 and 50 mg/Kg) through oral route for 14 consecutive days.

GENERAL DISCUSSION

6.1. General discussion

The lack of information regarding the safety/ toxicity of nanomaterials poses environmental health and safety (EHS) issues. Therefore it is necessary that researchers in toxicology and chemistry as well as other related scientific fields analyze the potential toxic effects of engineered nanoparticles along with their positive aspects.

ZnO nanoparticle is one such widely used enginered nanoparticle in the world consumer market. This makes human beings more prone to ZnO nanoparticle exposure and its adverse effects. In the present study, an attempt was made to evaluate the *in vitro* and *in vivo* toxicity of ZnO nanoparticles in the mammalian system and to elucidate the possible mechanism of its toxicity. The human epidermal cells (A431 cells and primary human epidermal keratinocytes) and human liver cells (HepG2) were selected for assessing ZnO nanoparticle toxicity keeping in view the fact that ZnO nanoparticle are used in cosmetics and food packaging. The results demonstrate that ZnO nanoparticles have cytotoxic and genotoxic potential in both *in vitro* and *in vivo* mammalian systems. The concentrations of ZnO nanaoparticles inducing cytotoxicity were found to be different in different cell types (A431 cells, primary human epidermal keratinocytes and HepG2 cells). This difference can be attributed to the dissimilarties between the growth properties and the biochemical characteristics of these cells. For instance, the concentrations of ZnO nanoparticles that lead to cytotoxicity in HepG2 cells were found to be higher compared to the cytotoxic concentations in A431 cells. This is due to the fact that the liver cells

(HepG2) are metabolically more active and resistant than the skin cells (A431).

ZnO nanoparticle exposure leads to reactive oxygen species (ROS) generation and lipid peroxidation (LPO). The ROS triggered decrease in mitochondrial membrane potential and increase in ratio of Bax/Bcl2 leading to mitochondria mediated pathway involved in apoptosis. In addition, ZnO nanoparticles activated JNK, P38 and induced $P53^{ser15}$ phosphorylation, however, the apoptosis was found to be independent of JNK and P38 pathways. The data also suggests that the nanoparticle dissolution does not play a significant role in ZnO nanoparticle induced toxicity. DNA damage was also found to be mediated by the oxidative stress as evidenced by increase in Fpg sensitive sites in the DNA.

The *in vitro* findings were further extrapolated to the *in vivo* experiments in mice. The mice were exposed to ZnO nanoparticles (300mg/Kg and 50mg/Kg) via the oral route for 14 consecutive days according to the OECD guidelines. The ZnO nanoparticles were mainly retained in the liver and caused lipid peroxidation and oxidative DNA damage. The hepatic cells of mice exposed to higher dose showed apoptosis compared to the control mice.

The results from the present study provide significant data regarding the toxicity of ZnO nanoparticles as well as the underlying molecular mechanism involved. The results also stress upon the need of a thorough toxicity assessment of any novel engineered nanomaterial before their arrival into the world consumer market. This will ensure that the society fully benefits from the nanotechnology while avoiding its potential adverse effects.

6.2. Future work

The study could be further improved by the following:

1. Determining the role of TNF alpha and extrinsic apoptotic pathway in ZnO nanoparticle induced apoptosis.
2. Investigating the effect of different sizes of ZnO nanoparticles on cellular responses.
3. Elucidating the changes in gene expression and metabolic profile of ZnO nanoparticles exposed cells.

References:

Ahamed, M., Posgai, R., Gorey, T.J., Nielsen, M., Hussain, S.M. and Rowe, J.J. (2010) Silver nanoparticles induced heat shock protein 70, oxidative stress and apoptosis in Drosophila melanogaster. Toxicol Appl Pharmacol 242, 263-269.

Alkilany, A.M. and Murphy, C.J. (2010) Toxicity and cellular uptake of gold nanoparticles: what we have learned so far? J Nanopart Res 12, 2313-2333.

Allabashi, R., Stach, W., de la Escosura-Muniz, A., Liste-Calleja, L. and Merkoci, A. (2009) ICP-MS: a powerful technique for quantitative determination of gold nanoparticles without previous dissolving. Journal of Nanoparticle Research 11, 2003-2011.

Aoki, H., Kang, P.M., Hampe, J., Yoshimura, K., Noma, T., Matsuzaki, M. and Izumo, S. (2002) Direct activation of mitochondrial apoptosis machinery by c-Jun N-terminal kinase in adult cardiac myocytes. J Biol Chem 277, 10244-10250.

Argmann, C.A., Chambon, P. and Auwerx, J. (2005) Mouse phenogenomics: the fast track to "systems metabolism". Cell Metab 2, 349-360.

Asharani, P.V., Serina, N.G., Nurmawati, M.H., Wu, Y.L., Gong, Z. and Valiyaveettil, S. (2008) Impact of multi-walled carbon nanotubes on aquatic species. J Nanosci Nanotechnol 8, 3603-3609.

Asharani, P.V., Hande, M.P. and Valiyaveettil, S. (2009a) Anti-proliferative activity of silver nanoparticles. BMC Cell Biol 10, 65.

AshaRani, P.V., Low Kah Mun, G., Hande, M.P. and Valiyaveettil, S. (2009b) Cytotoxicity and genotoxicity of silver nanoparticles in human cells. ACS Nano 3, 279-290.

Ayene, I.S., Koch, C.J. and Krisch, R.E. (2007) DNA strand breakage by bivalent metal ions and ionizing radiation. Int J Radiat Biol 83, 195-210.

Bajpayee, M., Pandey, A.K., Parmar, D., Mathur, N., Seth, P.K. and Dhawan, A. (2005) Comet assay responses in human lymphocytes are not influenced by the menstrual cycle: a study in healthy Indian females. Mutat Res 565, 163-172.

Balbus, J.M., Maynard, A.D., Colvin, V.L., Castranova, V., Daston, G.P., Denison, R.A., Dreher, K.L., Goering, P.L., Goldberg, A.M., Kulinowski, K.M., Monteiro-Riviere, N.A., Oberdorster, G., Omenn, G.S., Pinkerton, K.E., Ramos, K.S., Rest, K.M., Sass, J.B., Silbergeld, E.K. and Wong, B.A. (2007) Meeting report: hazard assessment for nanoparticles--report from an interdisciplinary workshop. Environ Health Perspect 115, 1654-1659.

Bar-Ilan, O., Albrecht, R.M., Fako, V.E. and Furgeson, D.Y. (2009) Toxicity assessments of multisized gold and silver nanoparticles in zebrafish embryos. Small 5, 1897-1910.

Baroli, B., Ennas, M.G., Loffredo, F., Isola, M., Pinna, R. and Lopez-Quintela, M.A. (2007) Penetration of metallic nanoparticles in human full-thickness skin. J Invest Dermatol 127, 1701-1712.

Baroli, B. (2009) Penetration of nanoparticles and nanomaterials in the skin: Fiction or reality? J Pharm Sci.

Bassing, C.H., Chua, K.F., Sekiguchi, J., Suh, H., Whitlow, S.R., Fleming, J.C., Monroe, B.C., Ciccone, D.N., Yan, C., Vlasakova, K., Livingston, D.M., Ferguson, D.O., Scully, R. and Alt, F.W. (2002) Increased ionizing radiation sensitivity and genomic instability in the absence of histone H2AX. Proc Natl Acad Sci U S A 99, 8173-8178.

Bastian, S., Busch, W., Kuhnel, D., Springer, A., Meissner, T., Holke, R., Scholz, S., Iwe, M., Pompe, W., Gelinsky, M., Potthoff, A., Richter, V., Ikonomidou, C. and Schirmer, K. (2009) Toxicity of tungsten carbide and cobalt-doped tungsten carbide nanoparticles in mammalian cells in vitro. Environ Health Perspect 117, 530-536.

Berhanu, D., Dybowska, A., Misra, S.K., Stanley, C.J., Ruenraroengsak, P., Boccaccini, A.R., Tetley, T.D., Luoma, S.N., Plant, J.A. and Valsami-Jones, E. (2009) Characterisation of carbon nanotubes in the context of toxicity studies. Environ Health 8 Suppl 1, S3.

Bihari, P., Holzer, M., Praetner, M., Fent, J., Lerchenberger, M., Reichel, C.A., Rehberg, M., Lakatos, S. and Krombach, F. (2010) Single-walled carbon nanotubes activate platelets and accelerate thrombus formation in the microcirculation. Toxicology 269, 148-154.

Biswas, S.K. and Rahman, I. (2009) Environmental toxicity, redox signaling and lung inflammation: the role of glutathione. Mol Aspects Med 30, 60-76.

Bockmann, J., Lahl, H., Eckert, T. and Unterhalt, B. (2000) Blood titanium levels before and after oral administration titanium dioxide. Pharmazie 55, 140-143.

Borenfreund, E. and Puerner, J.A. (1985) Toxicity determined in vitro by morphological alterations and neutral red absorption. Toxicol Lett 24, 119-124.

Borm, P., Klaessig, F., Landry, T., Moudgil, B., Pauluhn, J., Thomas, K., Trottier, R. and Wood, S. (2006) Research strategies for safety evaluation of nanomaterials. Part V: Role of dissolution in biological fate and effects of nanoscale particles. Toxicolog Sci 90, 23-32.

Boulton, T.G. and Cobb, M.H. (1991) Identification of multiple extracellular signal-regulated kinases (ERKs) with antipeptide antibodies. Cell Regul 2, 357-371.

Bradford, M.M. (1976) A rapid and sensitive method for the quantitation of microgram quantities of protein utilizing the principle of protein-dye binding. Anal Biochem 72, 248-254.

Brunet, L., Lyon, D.Y., Hotze, E.M., Alvarez, P.J. and Wiesner, M.R. (2009) Comparative photoactivity and antibacterial properties of C60 fullerenes and titanium dioxide nanoparticles. Environ Sci Technol 43, 4355-4360.

Brunner, T.J., Wick, P., Manser, P., Spohn, P., Grass, R.N., Limbach, L.K., Bruinink, A. and Stark, W.J. (2006) In vitro cytotoxicity of oxide nanoparticles: comparison to asbestos, silica, and the effect of particle solubility. Environ Sci Technol 40, 4374-4381.

Budihardjo, I., Oliver, H., Lutter, M., Luo, X. and Wang, X. (1999) Biochemical pathways of caspase activation during apoptosis. Annu Rev Cell Dev Biol 15, 269-290.

Buffle, J. (2006) The key role of environmental colloids/nanoparticles for the sustainability of life. Environmental Chemistry 3, 155-158.

Burns, A.A., Vider, J., Ow, H., Herz, E., Penate-Medina, O., Baumgart, M., Larson, S.M., Wiesner, U. and Bradbury, M. (2009) Fluorescent silica nanoparticles with efficient urinary excretion for nanomedicine. Nano Lett 9, 442-448.

Cadet, J., Douki, T. and Ravanat, J.L. (2010) Oxidatively generated base damage to cellular DNA. Free Radic Biol Med 49, 9-21.

Cai, R., Van, G., Aw, P. and Itoh, K. (2006) Solar-driven self-cleaning coating for a painted surface. Comptes Rendus Chimie 9, 829-835.

Canesi, L., Ciacci, C., Vallotto, D., Gallo, G., Marcomini, A. and Pojana, G. (2010) In vitro effects of suspensions of selected nanoparticles (C60 fullerene, TiO2, SiO2) on Mytilus hemocytes. Aquat Toxicol 96, 151-158.

Catala, A. (2010) A synopsis of the process of lipid peroxidation since the discovery of the essential fatty acids. Biochem Biophys Res Commun 399, 318-323.

Chang, L. and Karin, M. (2001) Mammalian MAP kinase signalling cascades. Nature 410, 37-40.

Chaudhary, P., Sharma, R., Sharma, A., Vatsyayan, R., Yadav, S., Singhal, S.S., Rauniyar, N., Prokai, L., Awasthi, S. and Awasthi, Y.C. (2010) Mechanisms of 4-hydroxy-2-nonenal induced pro- and anti-apoptotic signaling. Biochemistry 49, 6263-6275.

Chavan, H., Oruganti, M. and Krishnamurthy, P. (2011) The ATP-Binding Cassette Transporter ABCB6 Is Induced by Arsenic and Protects against Arsenic Cytotoxicity. Toxicol Sci 120, 519-528.

Chen, C., Xing, G., Wang, J., Zhao, Y., Li, B., Tang, J., Jia, G., Wang, T., Sun, J., Xing, L., Yuan, H., Gao, Y., Meng, H., Chen, Z., Zhao, F., Chai, Z. and Fang, X. (2005) Multihydroxylated [Gd@C82(OH)22]n nanoparticles: antineoplastic activity of high efficiency and low toxicity. Nano Lett 5, 2050-2057.

Chen, M. and Mikecz, A.V. (2005) Formation of nucleoplasmic protein aggregates impairs nuclear function in response to SiO2 nanoparticles. Exp Cell Res 305, 51-62.

Chen, M. and Mikecz, A.V. (2007) Uptake and cytotoxicity of nanoparticles. Nanotoxicology, Edited by Y. Zhao and H.S. Nalwa. American Scientific Publishers, USA.

Chen, Y.C., Hsiao, J.K., Liu, H.M., Lai, I.Y., Yao, M., Hsu, S.C., Ko, B.S., Yang, C.S. and Huang, D.M. (2010) The inhibitory effect of superparamagnetic iron oxide nanoparticle (Ferucarbotran) on osteogenic differentiation and its signaling mechanism in human mesenchymal stem cells. Toxicol Appl Pharmacol 245, 272-279.

Chen, Z., Meng, H., Xing, G., Chen, C., Zhao, Y., Jia, G., Wang, T., Yuan, H., Ye, C., Zhao, F., Chai, Z., Zhu, C., Fang, X., Ma, B. and Wan, L. (2006) Acute toxicological effects of copper nanoparticles in vivo. Toxicol Lett 163, 109-120.

Cheng, C., Muller, K.H., Koziol, K.K., Skepper, J.N., Midgley, P.A., Welland, M.E. and Porter, A.E. (2009a) Toxicity and imaging of multi-walled carbon nanotubes in human macrophage cells. Biomaterials 30, 4152-4160.

Cheng, J., Chan, C.M., Veca, L.M., Poon, W.L., Chan, P.K., Qu, L., Sun, Y.P. and Cheng, S.H. (2009b) Acute and long-term effects after single loading of functionalized multi-walled carbon nanotubes into zebrafish (Danio rerio). Toxicol Appl Pharmacol 235, 216-225.

Chithrani, B.D. and Chan, W.C. (2007) Elucidating the mechanism of cellular uptake and removal of protein-coated gold nanoparticles of different sizes and shapes. Nano Lett 7, 1542-1550.

Cho, M., Fortner, J.D., Hughes, J.B. and Kim, J.H. (2009a) Escherichia coli inactivation by water-soluble, ozonated C60 derivative: kinetics and mechanisms. Environ Sci Technol 43, 7410-7415.

Cho, S.J., Maysinger, D., Jain, M., Roder, B., Hackbarth, S. and Winnik, F.M. (2007) Long-term exposure to CdTe quantum dots causes functional impairments in live cells. Langmuir 23, 1974-1980.

Cho, W.S., Cho, M., Jeong, J., Choi, M., Cho, H.Y., Han, B.S., Kim, S.H., Kim, H.O., Lim, Y.T. and Chung, B.H. (2009b) Acute toxicity and pharmacokinetics of 13 nm-sized PEG-coated gold nanoparticles. Toxicol Appl Pharmacol 236, 16-24.

Choi, J.E., Kim, S., Ahn, J.H., Youn, P., Kang, J.S., Park, K., Yi, J. and Ryu, D.Y. (2009a) Induction of oxidative stress and apoptosis by silver nanoparticles in the liver of adult zebrafish. Aquat Toxicol.

Choi, S.J., Oh, J.M. and Choy, J.H. (2009b) Toxicological effects of inorganic nanoparticles on human lung cancer A549 cells. J Inorg Biochem 103, 463-471.

Chu, M., Wu, Q., Yang, H., Yuan, R., Hou, S., Yang, Y., Zou, Y., Xu, S., Xu, K., Ji, A. and Sheng, L. (2010) Transfer of quantum dots from pregnant mice to pups across the placental barrier. Small 6, 670-678.

Circu, M.L. and Aw, T.Y. (2010) Reactive oxygen species, cellular redox systems, and apoptosis. Free Radic Biol Med 48, 749-762.

Collins, A.R. (2004) The comet assay for DNA damage and repair: principles, applications, and limitations. Mol Biotechnol 26, 249-261.

Collins, A.R. (2009) Investigating oxidative DNA damage and its repair using the comet assay. Mutat Res 681, 24-32.

COT;COM;COC. (2005) Joint statement on nanomaterial toxicology. http://cot.food.gov.uk/pdfs/cotstatements2005nanomats.pdf.

Coulthard, L.R., White, D.E., Jones, D.L., McDermott, M.F. and Burchill, S.A. (2009) p38(MAPK): stress responses from molecular mechanisms to therapeutics. Trends Mol Med 15, 369-379.

Crosera, M., Bovenzi, M., Maina, G., Adami, G., Zanette, C., Florio, C. and Filon Larese, F. (2009) Nanoparticle dermal absorption and toxicity: a review of the literature. Int Arch Occup Environ Health.

Cross, S.E., Innes, B., Roberts, M.S., Tsuzuki, T., Robertson, T.A. and McCormick, P. (2007) Human skin penetration of sunscreen nanoparticles: in-vitro assessment of a novel micronized zinc oxide formulation. Skin Pharmacol Physiol 20, 148-154.

Crouzier, D., Follot, S., Gentilhomme, E., Flahaut, E., Arnaud, R., Dabouis, V., Castellarin, C. and Debouzy, J.C. (2010) Carbon nanotubes induce inflammation but decrease the production of reactive oxygen species in lung. Toxicology 272, 39-45.

Cui, Y., Liu, H., Zhou, M., Duan, Y., Li, N., Gong, X., Hu, R., Hong, M. and Hong, F. (2011) Signaling pathway of inflammatory responses in the mouse liver caused by TiO2 nanoparticles. J Biomed Mater Res A 96, 221-229.

Cveticanin, J., Joksic, G., Leskovac, A., Petrovic, S., Sobot, A.V. and Neskovic, O. (2010) Using carbon nanotubes to induce micronuclei and double strand breaks of the DNA in human cells. Nanotechnology 21, 015102.

D'Alessio, M., De Nicola, M., Coppola, S., Gualandi, G., Pugliese, L., Cerella, C., Cristofanon, S., Civitareale, P., Ciriolo, M.R., Bergamaschi, A., Magrini, A. and Ghibelli, L. (2005) Oxidative Bax dimerization promotes its translocation to mitochondria independently of apoptosis. FASEB J 19, 1504-1506.

Davis, R.R., Lockwood, P.E., Hobbs, D.T., Messer, R.L., Price, R.J., Lewis, J.B. and Wataha, J.C. (2007) In vitro biological effects of sodium titanate materials. J Biomed Mater Res B Appl Biomater 83, 505-511.

Dehn, P.F., White, C.M., Conners, D.E., Shipkey, G. and Cumbo, T.A. (2004) Characterization of the human hepatocellular carcinoma (hepg2) cell line as an in vitro model for cadmium toxicity studies. In Vitro Cell Dev Biol Anim 40, 172-182.

Denault, J.B. and Salvesen, G.S. (2002) Caspases: keys in the ignition of cell death. Chem Rev 102, 4489-4500.

Derfus, A.M., Chan, W.C.W. and Bhatia, S.N. (2004) Probing the cytotoxicity of semiconductor quantum dots. Nano Letters 4, 11-18.

Dhawan, A., Taurozzi, J.S., Pandey, A.K., Shan, W., Miller, S.M., Hashsham, S.A. and Tarabara, V.V. (2006) Stable colloidal dispersions of C60 fullerenes in water: evidence for genotoxicity. Environ Sci Technol 40, 7394-7401.

Dhawan, A., Shanker, R., Das, M. and Gupta, K.C. (2011) Guidance for safe handling of nanomaterials. J Biomed Nanotechnol 7, 218-224.

Driessens, N., Versteyhe, S., Ghaddhab, C., Burniat, A., De Deken, X., Van Sande, J., Dumont, J.E., Miot, F. and Corvilain, B. (2009) Hydrogen peroxide induces DNA single- and double-strand breaks in thyroid cells and is therefore a potential mutagen for this organ. Endocr Relat Cancer 16, 845-856.

Dufour, E.K., Kumaravel, T., Nohynek, G.J., Kirkland, D. and Toutain, H. (2006) Clastogenicity, photo-clastogenicity or pseudo-photo-clastogenicity: Genotoxic

effects of zinc oxide in the dark, in pre-irradiated or simultaneously irradiated Chinese hamster ovary cells. Mutat Res 607, 215-224.

El-Najjar, N., Chatila, M., Moukadem, H., Vuorela, H., Ocker, M., Gandesiri, M., Schneider-Stock, R. and Gali-Muhtasib, H. (2010) Reactive oxygen species mediate thymoquinone-induced apoptosis and activate ERK and JNK signaling. Apoptosis 15, 183-195.

Elgrabli, D., Abella-Gallart, S., Robidel, F., Rogerieux, F., Boczkowski, J. and Lacroix, G. (2008) Induction of apoptosis and absence of inflammation in rat lung after intratracheal instillation of multiwalled carbon nanotubes. Toxicology 253, 131-136.

Ellman, G.L. (1959) Tissue sulfhydryl groups. Arch Biochem Biophys 82, 70-77.

Elmore, S. (2007) Apoptosis: a review of programmed cell death. Toxicol Pathol 35, 495-516.

Eom, H.J. and Choi, J. (2009) Oxidative stress of CeO2 nanoparticles via p38-Nrf-2 signaling pathway in human bronchial epithelial cell, Beas-2B. Toxicol Lett 187, 77-83.

Fahmy, B. and Cormier, S.A. (2009) Copper oxide nanoparticles induce oxidative stress and cytotoxicity in airway epithelial cells. Toxicol In Vitro 23, 1365-1371.

Fairbairn, D.W., Olive, P.L. and O'Neill, K.L. (1995) The comet assay: a comprehensive review. Mutat Res 339, 37-59.

Falck, G.C., Lindberg, H.K., Suhonen, S., Vippola, M., Vanhala, E., Catalan, J., Savolainen, K. and Norppa, H. (2009) Genotoxic effects of nanosized and fine TiO2. Hum Exp Toxicol 28, 339-352.

Farah, A.A., Alvarez-Puebla, R.A. and Fenniri, H. (2008) Chemically stable silver nanoparticle-crosslinked polymer microspheres. J Colloid Interface Sci 319, 572-576.

Farkas, J., Christian, P., Urrea, J.A., Roos, N., Hassellov, M., Tollefsen, K.E. and Thomas, K.V. (2010) Effects of silver and gold nanoparticles on rainbow trout (Oncorhynchus mykiss) hepatocytes. Aquat Toxicol 96, 44-52.

Fischer, H.C. and Chan, W.C. (2007) Nanotoxicity: the growing need for in vivo study. Curr Opin Biotechnol 18, 565-571.

FOE. (2006) Nanomaterials, sunscreens and cosmetics: Small ingredients, big risks. Friends of the Earth, United States. Available at http://www.foe.org.

Foldbjerg, R., Dang, D.A. and Autrup, H. (2010) Cytotoxicity and genotoxicity of silver nanoparticles in the human lung cancer cell line, A549. Arch Toxicol.

Folkmann, J.K., Risom, L., Jacobsen, N.R., Wallin, H., Loft, S. and Moller, P. (2009) Oxidatively damaged DNA in rats exposed by oral gavage to C60 fullerenes and single-walled carbon nanotubes. Environ Health Perspect 117, 703-708.

Forman, H.J. (2010) Reactive oxygen species and alpha,beta-unsaturated aldehydes as second messengers in signal transduction. Ann N Y Acad Sci 1203, 35-44.

Franco, R. and Cidlowski, J.A. (2009) Apoptosis and glutathione: beyond an antioxidant. Cell Death Differ 16, 1303-1314.

Franklin, N.M., Rogers, N.J., Apte, S.C., Batley, G.E., Gadd, G.E. and Casey, P.S. (2007) Comparative toxicity of nanoparticulate ZnO, bulk ZnO, and ZnCl2 to a freshwater microalga (Pseudokirchneriella subcapitata): the importance of particle solubility. Environ Sci Technol 41, 8484-8490.

Gaiser, B.K., Fernandes, T.F., Jepson, M., Lead, J.R., Tyler, C.R. and Stone, V. (2009) Assessing exposure, uptake and toxicity of silver and cerium dioxide nanoparticles from contaminated environments. Environ Health 8 Suppl 1, S2.

Gamer, A.O., Leibold, E. and van Ravenzwaay, B. (2006) The in vitro absorption of microfine zinc oxide and titanium dioxide through porcine skin. Toxicol In Vitro 20, 301-307.

Garcia-Leston, J., Roma-Torres, J., Vilares, M., Pinto, R., Cunha, L.M., Prista, J., Teixeira, J.P., Mayan, O., Pasaro, E., Mendez, J. and Laffon, B. (2011) Biomonitoring of a population of Portuguese workers exposed to lead. Mutat Res 721, 81-88.

George, S., Pokhrel, S., Xia, T., Gilbert, B., Ji, Z., Schowalter, M., Rosenauer, A., Damoiseaux, R., Bradley, K.A., Madler, L. and Nel, A.E. (2009) Use of a rapid cytotoxicity screening approach to engineer a safer zinc oxide nanoparticle through iron doping. ACS Nano 4, 15-29.

Gerloff, K., Albrecht, C., Boots, A.W., Förster, I. and Schins, R.P.F. (2009) Cytotoxicity and oxidative DNA damage by nanoparticles in human intestinal Caco-2 cells. Nanotoxicology 3, 355-364.

Gilmore, T.D. (1999) The Rel/NF-kappaB signal transduction pathway: introduction. Oncogene 18, 6842-6844.

Gocke, E., Burgin, H., Muller, L. and Pfister, T. (2009) Literature review on the genotoxicity, reproductive toxicity, and carcinogenicity of ethyl methanesulfonate. Toxicol Lett 190, 254-265.

Gojova, A., Guo, B., Kota, R.S., Rutledge, J.C., Kennedy, I.M. and Barakat, A.I. (2007) Induction of inflammation in vascular endothelial cells by metal oxide nanoparticles: effect of particle composition. Environ Health Perspect 115, 403-409.

Gopalan, R.C., Osman, I.F., Amani, A., De Matas, M. and Anderson, D. (2009) The effect of zinc oxide and titanium dioxide nanoparticles in the Comet assay with UVA photoactivation of human sperm and lymphocytes. Nanotoxicology 3, 33-39.

Halliwell, B. and Whiteman, M. (2004) Measuring reactive species and oxidative damage in vivo and in cell culture: how should you do it and what do the results mean? Br J Pharmacol 142, 231-255.

Han, S.G., Andrews, R. and Gairola, C.G. (2010) Acute pulmonary response of mice to multi-wall carbon nanotubes. Inhal Toxicol 22, 340-347.

Hardman, R. (2006) A toxicologic review of quantum dots: toxicity depends on physicochemical and environmental factors. Environ Health Perspect 114, 165-172.

Hartmann, A., Agurell, E., Beevers, C., Brendler-Schwaab, S., Burlinson, B., Clay, P., Collins, A., Smith, A., Speit, G., Thybaud, V. and Tice, R.R. (2003) Recommendations for conducting the in vivo alkaline Comet assay. 4th International Comet Assay Workshop. Mutagenesis 18, 45-51.

He, L., Liu, Y., Mustapha, A. and Lin, M. (2010) Antifungal activity of zinc oxide nanoparticles against Botrytis cinerea and Penicillium expansum. Microbiol Res.

Heng, B.C., Zhao, X., Xiong, S., Ng, K.W., Boey, F.Y. and Loo, J.S. (2010) Toxicity of zinc oxide (ZnO) nanoparticles on human bronchial epithelial cells (BEAS-2B) is accentuated by oxidative stress. Food Chem Toxicol 48, 1762-1766.

Herzog, E., Byrne, H.J., Casey, A., Davoren, M., Lenz, A.G., Maier, K.L., Duschl, A. and Oostingh, G.J. (2009) SWCNT suppress inflammatory mediator responses in human lung epithelium in vitro. Toxicol Appl Pharmacol 234, 378-390.

Hillyer, J.F. and Albrecht, R.M. (2001) Gastrointestinal persorption and tissue distribution of differently sized colloidal gold nanoparticles. J Pharm Sci 90, 1927-1936.

Hlavin, E.M., Smeaton, M.B. and Miller, P.S. (2010) Initiation of DNA interstrand cross-link repair in mammalian cells. Environ Mol Mutagen 51, 604-624.

Hoshino, A., Fujioka, K., Oku, T., Suga, M., Sasaki, Y.F., Ohta, T., Yasuhara, M., Suzuki, K. and Yamamoto, K. (2004) Physicochemical properties and cellular toxicity of nanocrystal quantum dots depend on their surface modification. Nano Letters 4, 2163-2169.

Hsieh, M.S., Shiao, N.H. and Chan, W.H. (2009) Cytotoxic Effects of CdSe Quantum Dots on Maturation of Mouse Oocytes, Fertilization, and Fetal Development. Int J Mol Sci 10, 2122-2135.

Hsin, Y.H., Chen, C.F., Huang, S., Shih, T.S., Lai, P.S. and Chueh, P.J. (2008) The apoptotic effect of nanosilver is mediated by a ROS- and JNK-dependent mechanism involving the mitochondrial pathway in NIH3T3 cells. Toxicol Lett 179, 130-139.

Huang, C.C., Aronstam, R.S., Chen, D.R. and Huang, Y.W. (2010) Oxidative stress, calcium homeostasis, and altered gene expression in human lung epithelial cells exposed to ZnO nanoparticles. Toxicol In Vitro 24, 45-55.

Hussain, N., Jaitley, V. and Florence, A.T. (2001) Recent advances in the understanding of uptake of microparticulates across the gastrointestinal lymphatics. Adv Drug Deliv Rev 50, 107-142.

Hussain, S., Thomassen, L.C., Ferecatu, I., Borot, M.C., Andreau, K., Martens, J.A., Fleury, J., Baeza-Squiban, A., Marano, F. and Boland, S. (2010) Carbon black and titanium dioxide nanoparticles elicit distinct apoptotic pathways in bronchial epithelial cells. Part Fibre Toxicol 7, 10.

Hussain, S.P., Schwank, J., Staib, F., Wang, X.W. and Harris, C.C. (2007) TP53 mutations and hepatocellular carcinoma: insights into the etiology and pathogenesis of liver cancer. Oncogene 26, 2166-2176.

Jacobsen, N.R., Pojana, G., White, P., Moller, P., Cohn, C.A., Korsholm, K.S., Vogel, U., Marcomini, A., Loft, S. and Wallin, H. (2008) Genotoxicity, cytotoxicity, and reactive oxygen species induced by single-walled carbon nanotubes and C(60) fullerenes in the FE1-Mutatrade markMouse lung epithelial cells. Environ Mol Mutagen 49, 476-487.

Jan, E., Byrne, S.J., Cuddihy, M., Davies, A.M., Volkov, Y., Gun'ko, Y.K. and Kotov, N.A. (2008) High-content screening as a universal tool for fingerprinting of cytotoxicity of nanoparticles. ACS Nano 2, 928-938.

Jani, P., Halbert, G.W., Langridge, J. and Florence, A.T. (1990) Nanoparticle uptake by the rat gastrointestinal mucosa: quantitation and particle size dependency. J Pharm Pharmacol 42, 821-826.

Jasionek, G., Zhdanov, A., Davenport, J., Blaha, L. and Papkovsky, D.B. (2010) Mitochondrial toxicity of microcystin-LR on cultured cells: application to the analysis of contaminated water samples. Environ Sci Technol 44, 2535-2541.

Jeng, H.A. and Swanson, J. (2006) Toxicity of metal oxide nanoparticles in mammalian cells. J Environ Sci Health A Tox Hazard Subst Environ Eng 41, 2699-2711.

Ji, Z., Zhang, D., Li, L., Shen, X., Deng, X., Dong, L., Wu, M. and Liu, Y. (2009) The hepatotoxicity of multi-walled carbon nanotubes in mice. Nanotechnology 20, 445101.

Jiang, W., Mashayekhi, H. and Xing, B. (2009) Bacterial toxicity comparison between nano- and micro-scaled oxide particles. Environ Pollut 157, 1619-1625.

Jin, T., Sun, D., Su, J.Y., Zhang, H. and Sue, H.J. (2009) Antimicrobial efficacy of zinc oxide quantum dots against Listeria monocytogenes, Salmonella Enteritidis, and Escherichia coli O157:H7. J Food Sci 74, M46-52.

John, S., Marpu, S., Li, J., Omary, M., Hu, Z., Fujita, Y. and Neogi, A. Hybrid zinc oxide nanoparticles for biophotonics. J Nanosci Nanotechnol 10, 1707-1712.

John, S., Marpu, S., Li, J., Omary, M., Hu, Z., Fujita, Y. and Neogi, A. (2010) Hybrid zinc oxide nanoparticles for biophotonics. J Nanosci Nanotechnol 10, 1707-1712.

Jung, H. and Choi, H. (2006) Catalytic decomposition of ozone and para-Chlorobenzoic acid (pCBA) in the presence of nanosized ZnO. Applied Catalysis B: Environmental Chemistry 66, 288-294.

Kang, S., Mauter, M.S. and Elimelech, M. (2008) Physicochemical determinants of multiwalled carbon nanotube bacterial cytotoxicity. Environ Sci Technol 42, 7528-7534.

Kang, S., Mauter, M.S. and Elimelech, M. (2009) Microbial cytotoxicity of carbon-based nanomaterials: implications for river water and wastewater effluent. Environ Sci Technol 43, 2648-2653.

Karlsson, H.L., Cronholm, P., Gustafsson, J. and Moller, L. (2008) Copper oxide nanoparticles are highly toxic: a comparison between metal oxide nanoparticles and carbon nanotubes. Chem Res Toxicol 21, 1726-1732.

Karlsson, H.L., Gustafsson, J., Cronholm, P. and Moller, L. (2009) Size-dependent toxicity of metal oxide particles--a comparison between nano- and micrometer size. Toxicol Lett 188, 112-118.

Karlsson, H.L. (2010) The comet assay in nanotoxicology research. Anal Bioanal Chem 398, 651-666.

Kasemets, K., Ivask, A., Dubourguier, H.C. and Kahru, A. (2009) Toxicity of nanoparticles of ZnO, CuO and TiO2 to yeast Saccharomyces cerevisiae. Toxicol In Vitro 23, 1116-1122.

Kauser, S., Schallreuter, K.U., Thody, A.J., Gummer, C. and Tobin, D.J. (2003) Regulation of human epidermal melanocyte biology by beta-endorphin. J Invest Dermatol 120, 1073-1080.

Kawata, K., Osawa, M. and Okabe, S. (2009) In vitro toxicity of silver nanoparticles at noncytotoxic doses to HepG2 human hepatoma cells. Environ Sci Technol 43, 6046-6051.

Kim, I.S., Baek, M. and Choi, S.J. (2010a) Comparative cytotoxicity of Al2O3, CeO2, TiO2 and ZnO nanoparticles to human lung cells. J Nanosci Nanotechnol 10, 3453-3458.

Kim, J., Park, Y., Yoon, T.H., Yoon, C.S. and Choi, K. (2010b) Phototoxicity of CdSe/ZnSe quantum dots with surface coatings of 3-mercaptopropionic acid or tri-n-octylphosphine oxide/gum arabic in Daphnia magna under environmentally relevant UV-B light. Aquat Toxicol 97, 116-124.

Kuhnel, D., Busch, W., Meissner, T., Springer, A., Potthoff, A., Richter, V., Gelinsky, M., Scholz, S. and Schirmer, K. (2009) Agglomeration of tungsten carbide nanoparticles in exposure medium does not prevent uptake and toxicity toward a rainbow trout gill cell line. Aquat Toxicol 93, 91-99.

Kulmala, M. (2004) Formation and growth rates of ultrafine atmospheric particles: a review of observations. J Aerosol Sci 35, 143-176.

Kumar, R., Roy, I., Ohulchanskky, T.Y., Vathy, L.A., Bergey, E.J., Sajjad, M. and Prasad, P.N. (2010) In vivo biodistribution and clearance studies using multimodal organically modified silica nanoparticles. ACS Nano 4, 699-708.

Kuo, T.R., Wu, C.L., Hsu, C.T., Lo, W., Chiang, S.J., Lin, S.J., Dong, C.Y. and Chen, C.C. (2009) Chemical enhancer induced changes in the mechanisms of transdermal delivery of zinc oxide nanoparticles. Biomaterials 30, 3002-3008.

Lai, J.C., Lai, M.B., Jandhyam, S., Dukhande, V.V., Bhushan, A., Daniels, C.K. and Leung, S.W. (2008) Exposure to titanium dioxide and other metallic oxide nanoparticles induces cytotoxicity on human neural cells and fibroblasts. Int J Nanomedicine 3, 533-545.

Larese, F.F., D'Agostin, F., Crosera, M., Adami, G., Renzi, N., Bovenzi, M. and Maina, G. (2009) Human skin penetration of silver nanoparticles through intact and damaged skin. Toxicology 255, 33-37.

Lasagna-Reeves, C., Gonzalez-Romero, D., Barria, M.A., Olmedo, I., Clos, A., Sadagopa Ramanujam, V.M., Urayama, A., Vergara, L., Kogan, M.J. and Soto, C. Bioaccumulation and toxicity of gold nanoparticles after repeated administration in mice. Biochem Biophys Res Commun 393, 649-655.

Le, H.T., Rao, G.A., Hirko, A.C. and Hughes, J.A. (2010) Polymeric nanoparticles containing conjugated phospholipase A2 for nonviral gene delivery. Mol Pharm 7, 1090-1097.

Lee, H.C. and Wei, Y.H. (2000) Mitochondrial role in life and death of the cell. J Biomed Sci 7, 2-15.

Leonov, A.P., Zheng, J., Clogston, J.D., Stern, S.T., Patri, A.K. and Wei, A. (2008) Detoxification of gold nanorods by treatment with polystyrenesulfonate. ACS Nano 2, 2481-2488.

Li, J.J., Hartono, D., Ong, C.N., Bay, B.H. and Yung, L.Y. (2010) Autophagy and oxidative stress associated with gold nanoparticles. Biomaterials 31, 5996-6003

Li, K.G., Chen, J.T., Bai, S.S., Wen, X., Song, S.Y., Yu, Q., Li, J. and Wang, Y.Q. (2009) Intracellular oxidative stress and cadmium ions release induce cytotoxicity of unmodified cadmium sulfide quantum dots. Toxicol In Vitro 23, 1007-1013.

Li, N., Sioutas, C., Cho, A., Schmitz, D., Misra, C., Sempf, J., Wang, M., Oberley, T., Froines, J. and Nel, A. (2003) Ultrafine particulate pollutants induce oxidative stress and mitochondrial damage. Environ Health Perspect 111, 455-460.

Lin, W., Xu, Y., Huang, C., Ma, Y., Shannon, K.B., Chen, D. and Huang, Y. (2009a) Toxicity of nano- and micro-sized ZnO particles in human lung epithelial cells. J Nanopart Res 11, 25-39.

Lin, W.S., Xu, Y., Huang, C.C., Ma, Y.F., Shannon, K.B., Chen, D.R. and Huang, Y.W. (2009b) Toxicity of nano- and micro-sized ZnO particles in human lung epithelial cells. Journal of Nanoparticle Research 11, 25-39.

Lindberg, H.K., Falck, G.C., Suhonen, S., Vippola, M., Vanhala, E., Catalan, J., Savolainen, K. and Norppa, H. (2009) Genotoxicity of nanomaterials: DNA damage and micronuclei induced by carbon nanotubes and graphite nanofibres in human bronchial epithelial cells in vitro. Toxicol Lett 186, 166-173.

Liu, B., Chen, Y. and St Clair, D.K. (2008) ROS and p53: a versatile partnership. Free Radic Biol Med 44, 1529-1535.

Liu, W., Wu, Y., Wang, C., Li, H.C., Wang, T., Liao, C.Y., Cui, L., Zhou, Q.F., Yan, B. and Jiang, G.B. (2010) Impact of silver nanoparticles on human cells: effect of particle size. Nanotoxicology 4, 319-330.

Liu, X., Vinson, D., Abt, D., Hurt, R.H. and Rand, D.M. (2009) Differential toxicity of carbon nanomaterials in Drosophila: larval dietary uptake is benign, but adult exposure causes locomotor impairment and mortality. Environ Sci Technol 43, 6357-6363.

Lu, S.C. (2009) Regulation of glutathione synthesis. Mol Aspects Med 30, 42-59.

Ma-Hock, L., Treumann, S., Strauss, V., Brill, S., Luizi, F., Mertler, M., Wiench, K., Gamer, A.O., van Ravenzwaay, B. and Landsiedel, R. (2009) Inhalation toxicity of multiwall carbon nanotubes in rats exposed for 3 months. Toxicol Sci 112, 468-481.

Ma, H., Bertsch, P.M., Glenn, T.C., Kabengi, N.J. and Williams, P.L. (2009) Toxicity of manufactured zinc oxide nanoparticles in the nematode Caenorhabditis elegans. Environ Toxicol Chem 28, 1324-1330.

Mantzaris, M.D., Tsianos, E.V. and Galaris, D. (2011) Interruption of triacylglycerol synthesis in the endoplasmic reticulum is the initiating event for saturated fatty acid-induced lipotoxicity in liver cells. FEBS J 278, 519-530.

Marnett, L.J. (2000) Oxyradicals and DNA damage. Carcinogenesis 21, 361-370.

Marquis, B.J., Love, S.A., Braun, K.L. and Haynes, C.L. (2009) Analytical methods to assess nanoparticle toxicity. Analyst 134, 425-439.

Martinez, G.R., Loureiro, A.P., Marques, S.A., Miyamoto, S., Yamaguchi, L.F., Onuki, J., Almeida, E.A., Garcia, C.C., Barbosa, L.F., Medeiros, M.H. and Di Mascio, P. (2003) Oxidative and alkylating damage in DNA. Mutat Res 544, 115-127.

Mates, J.M., Perez-Gomez, C. and Nunez de Castro, I. (1999) Antioxidant enzymes and human diseases. Clin Biochem 32, 595-603.

Maundrell, K., Antonsson, B., Magnenat, E., Camps, M., Muda, M., Chabert, C., Gillieron, C., Boschert, U., Vial-Knecht, E., Martinou, J.C. and Arkinstall, S. (1997) Bcl-2 undergoes phosphorylation by c-Jun N-terminal kinase/stress-activated protein kinases in the presence of the constitutively active GTP-binding protein Rac1. J Biol Chem 272, 25238-25242.

McCord, J.M. and Fridovich, I. (1969) Superoxide dismutase. An enzymic function for erythrocuprein (hemocuprein). J Biol Chem 244, 6049-6055.

Meng, H., Chen, Z., Xing, G., Yuan, H., Chen, C., Zhao, F., Zhang, C. and Zhao, Y. (2007) Ultrahigh reactivity provokes nanotoxicity: explanation of oral toxicity of nano-copper particles. Toxicol Lett 175, 102-110.

Midander, K., Cronholm, P., Karlsson, H.L., Elihn, K., Moller, L., Leygraf, C. and Wallinder, I.O. (2009) Surface characteristics, copper release, and toxicity of nano- and micrometer-sized copper and copper(II) oxide particles: a cross-disciplinary study. Small 5, 389-399.

Migliore, L., Saracino, D., Bonelli, A., Colognato, R., D'Errico, M.R., Magrini, A., Bergamaschi, A. and Bergamaschi, E. (2010) Carbon nanotubes induce oxidative DNA damage in RAW 264.7 cells. Environ Mol Mutagen 51, 294-303.

Miller, R.J., Lenihan, H.S., Muller, E.B., Tseng, N., Hanna, S.K. and Keller, A.A. (2003) Impacts of metal oxide nanoparticles on marine phytoplankton. Environ Sci Technol 44, 7329-7334.

Miller, R.J., Lenihan, H.S., Muller, E.B., Tseng, N., Hanna, S.K. and Keller, A.A. (2010) Impacts of Metal Oxide Nanoparticles on Marine Phytoplankton. Environ Sci Technol.

Missirlis, D. and Hubbell, J.A. (2009) In vitro uptake of amphiphilic, hydrogel nanoparticles by J774A.1 cells. J Biomed Mater Res A, DOI 10.1002/jbm.a.32648

Mitchell, L.A., Lauer, F.T., Burchiel, S.W. and McDonald, J.D. (2009) Mechanisms for how inhaled multiwalled carbon nanotubes suppress systemic immune function in mice. Nat Nanotechnol 4, 451-456.

Miura, N. and Shinohara, Y. (2009) Cytotoxic effect and apoptosis induction by silver nanoparticles in HeLa cells. Biochem Biophys Res Commun 390, 733-737.

Moller, P. (2005) Genotoxicity of environmental agents assessed by the alkaline comet assay. Basic Clin Pharmacol Toxicol 96 Suppl 1, 1-42.

Monteiro-Riviere, N.A., Inman, A.O. and Zhang, L.W. (2009) Limitations and relative utility of screening assays to assess engineered nanoparticle toxicity in a human cell line. Toxicol Appl Pharmacol 234, 222-235.

Moos, P.J., Chung, K., Woessner, D., Honeggar, M., Cutler, N.S. and Veranth, J.M. (2010) ZnO particulate matter requires cell contact for toxicity in human colon cancer cells. Chem Res Toxicol 23, 733-739.

Mortensen, L.J., Oberdorster, G., Pentland, A.P. and Delouise, L.A. (2008) In vivo skin penetration of quantum dot nanoparticles in the murine model: the effect of UVR. Nano Lett 8, 2779-2787.

Mosmann, T. (1983) Rapid colorimetric assay for cellular growth and survival: application to proliferation and cytotoxicity assays. J Immunol Methods 65, 55-63.

Motskin, M., Wright, D.M., Muller, K., Kyle, N., Gard, T.G., Porter, A.E. and Skepper, J.N. (2009) Hydroxyapatite nano and microparticles: correlation of particle properties with cytotoxicity and biostability. Biomaterials 30, 3307-3317.

Munro, K.L., Mariana, A., Klavins, A.I., Foster, A.J., Lai, B., Vogt, S., Cai, Z., Harris, H.H. and Dillon, C.T. (2008) Microprobe XRF mapping and XAS investigations of the intracellular metabolism of arsenic for understanding arsenic-induced toxicity. Chem Res Toxicol 21, 1760-1769.

Murray, A.R., Kisin, E., Leonard, S.S., Young, S.H., Kommineni, C., Kagan, V.E., Castranova, V. and Shvedova, A.A. (2009) Oxidative stress and inflammatory response in dermal toxicity of single-walled carbon nanotubes. Toxicology 257, 161-171.

Narayanan, D.L., Saladi, R.N. and Fox, J.L. (2010) Ultraviolet radiation and skin cancer. Int J Dermatol 49, 978-986.

Navarro, R., Busnadiego, I., Ruiz-Larrea, M.B. and Ruiz-Sanz, J.I. (2006) Superoxide anions are involved in doxorubicin-induced ERK activation in hepatocyte cultures. Ann N Y Acad Sci 1090, 419-428.

NCPI. (2011) Nanotechnology consumer products inventory. Available at http://www.nanotechproject.org.

Negre-Salvayre, A., Auge, N., Ayala, V., Basaga, H., Boada, J., Brenke, R., Chapple, S., Cohen, G., Feher, J., Grune, T., Lengyel, G., Mann, G.E., Pamplona, R., Poli, G., Portero-Otin, M., Riahi, Y., Salvayre, R., Sasson, S., Serrano, J., Shamni, O., Siems, W., Siow, R.C., Wiswedel, I., Zarkovic, K. and Zarkovic, N. (2010) Pathological aspects of lipid peroxidation. Free Radic Res 44, 1125-1171.

Nel, A., Xia, T., Madler, L. and Li, N. (2006) Toxic potential of materials at the nanolevel. Science 311, 622-627.

Nemmar, A., Melghit, K., Al-Salam, S., Zia, S., Dhanasekaran, S., Attoub, S., Al-Amri, I. and Ali, B.H. (2011) Acute respiratory and systemic toxicity of pulmonary exposure to rutile Fe-doped TiO(2) nanorods. Toxicology 279, 167-175.

Neuzil, J., Wang, X.F., Dong, L.F., Low, P. and Ralph, S.J. (2006) Molecular mechanism of 'mitocan'-induced apoptosis in cancer cells epitomizes the multiple roles of reactive oxygen species and Bcl-2 family proteins. FEBS Lett 580, 5125-5129.

Nielsen, J.B., Nielsen, F. and Sorensen, J.A. (2007) Defense against dermal exposures is only skin deep: significantly increased penetration through slightly damaged skin. Arch Dermatol Res 299, 423-431.

NNI. (2004) National Nanotechnology Initiative. What is nanotechnology? Available at: http://www.nano.gov/html/facts/whatIsNano.html.

Nordberg, J. and Arner, E.S. (2001) Reactive oxygen species, antioxidants, and the mammalian thioredoxin system. Free Radic Biol Med 31, 1287-1312.

Nowack, B. and Bucheli, T.D. (2007) Occurrence, behavior and effects of nanoparticles in the environment. Environ Pollut 150, 5-22.

NRC. (1983) National Research Counil. Risk Assessment in the Federal Government: Managing the Process. Washington, DC:National Academy Press.

Nygaard, U.C., Hansen, J.S., Samuelsen, M., Alberg, T., Marioara, C.D. and Lovik, M. (2009) Single-walled and multi-walled carbon nanotubes promote allergic immune responses in mice. Toxicol Sci 109, 113-123.

Oberdorster, G., Ferin, J. and Lehnert, B.E. (1994) Correlation between particle size, in vivo particle persistence, and lung injury. Environ Health Perspect 102 Suppl 5, 173-179.

Oberdorster, G., Oberdorster, E. and Oberdorster, J. (2005) Nanotoxicology: an emerging discipline evolving from studies of ultrafine particles. Environ Health Perspect 113, 823-839.

OECD-420. (2001) OECD Guideline for the testing of chemicals; Acute oral toxicity-fixed dose procedure.

OECD-473. (1997) Guideline for the testing of chemicals- In Vitro Mammalian Chromosome Aberration Test.

Ogami, A., Morimoto, Y., Myojo, T., Oyabu, T., Murakami, M., Todoroki, M., Nishi, K., Kadoya, C., Yamamoto, M. and Tanaka, I. (2009) Pathological features of different sizes of nickel oxide following intratracheal instillation in rats. Inhal Toxicol 21, 812-818.

Osman, I.F., Baumgartner, A., Cemeli, E., Fletcher, J.N. and Anderson, D. (2010) Genotoxicity and cytotoxicity of zinc oxide and titanium dioxide in HEp-2 cells. Nanomedicine (Lond) 5, 1193-1203.

Pacurari, M., Yin, X.J., Zhao, J., Ding, M., Leonard, S.S., Schwegler-Berry, D., Ducatman, B.S., Sbarra, D., Hoover, M.D., Castranova, V. and Vallyathan, V. (2008) Raw single-wall carbon nanotubes induce oxidative stress and activate MAPKs, AP-1, NF-kappaB, and Akt in normal and malignant human mesothelial cells. Environ Health Perspect 116, 1211-1217.

Pan, Y., Leifert, A., Ruau, D., Neuss, S., Bornemann, J., Schmid, G., Brandau, W., Simon, U. and Jahnen-Dechent, W. (2009) Gold nanoparticles of diameter 1.4 nm trigger necrosis by oxidative stress and mitochondrial damage. Small 5, 2067-2076.

Panyam, J., Zhou, W.Z., Prabha, S., Sahoo, S.K. and Labhasetwar, V. (2002) Rapid endo-lysosomal escape of poly(DL-lactide-co-glycolide) nanoparticles: implications for drug and gene delivery. FASEB J 16, 1217-1226.

Park, E.J., Cho, W.S., Jeong, J., Yi, J., Choi, K. and Park, K. (2009) Pro-inflammatory and potential allergic responses resulting from B cell activation in mice treated with multi-walled carbon nanotubes by intratracheal instillation. Toxicology 259, 113-121.

Park, E.J., Kim, H., Kim, Y., Yi, J., Choi, K. and Park, K. (2010) Carbon fullerenes (C60s) can induce inflammatory responses in the lung of mice. Toxicol Appl Pharmacol 244, 226-233.

PAS71. (2005) Publicly Available Specification. Vocabulary- Nanoparticles. British Standards Institution (BSI).

Patlolla, A., Patlolla, B. and Tchounwou, P. (2010a) Evaluation of cell viability, DNA damage, and cell death in normal human dermal fibroblast cells induced by functionalized multiwalled carbon nanotube. Mol Cell Biochem 338, 225-232.

Patlolla, A.K., Hussain, S.M., Schlager, J.J., Patlolla, S. and Tchounwou, P.B. (2010b) Comparative study of the clastogenicity of functionalized and nonfunctionalized multiwalled carbon nanotubes in bone marrow cells of Swiss-Webster mice. Environ Toxicol.

Pelka, J., Gehrke, H., Esselen, M., Turk, M., Crone, M., Brase, S., Muller, T., Blank, H., Send, W., Zibat, V., Brenner, P., Schneider, R., Gerthsen, D. and Marko, D. (2009) Cellular uptake of platinum nanoparticles in human colon carcinoma cells and their impact on cellular redox systems and DNA integrity. Chem Res Toxicol 22, 649-659.

Philips, H.J. (1973) Tissue Culture: Methods and Applications. Academic Press, New York pp 406-408.

Pietenpol, J.A. and Stewart, Z.A. (2002) Cell cycle checkpoint signaling: cell cycle arrest versus apoptosis. Toxicology 181-182, 475-481.

Poland, C.A., Duffin, R., Kinloch, I., Maynard, A., Wallace, W.A., Seaton, A., Stone, V., Brown, S., Macnee, W. and Donaldson, K. (2008) Carbon nanotubes introduced into the abdominal cavity of mice show asbestos-like pathogenicity in a pilot study. Nat Nanotechnol 3, 423-428.

Porter, D.W., Hubbs, A.F., Mercer, R.R., Wu, N., Wolfarth, M.G., Sriram, K., Leonard, S., Battelli, L., Schwegler-Berry, D., Friend, S., Andrew, M., Chen, B.T., Tsuruoka, S., Endo, M. and Castranova, V. (2010) Mouse pulmonary dose- and time course-responses induced by exposure to multi-walled carbon nanotubes. Toxicology 269, 136-147.

Powers, K., Palazuelos, M., Moudgil, B. and Roberts, S. (2007) Characterization of the size, shape and state of dispersion of nanoparticles for toxicological studies. Nanotoxicology 1, 42-51.

Rahman, M.F., Wang, J., Patterson, T.A., Saini, U.T., Robinson, B.L., Newport, G.D., Murdock, R.C., Schlager, J.J., Hussain, S.M. and Ali, S.F. (2009) Expression of genes related to oxidative stress in the mouse brain after exposure to silver-25 nanoparticles. Toxicol Lett 187, 15-21.

Rakhorst, H.A., Tra, W.M., Posthumus-Van Sluijs, S.T., Hovius, S.E., Levendag, P.C., Kanaar, R. and Hofer, S.O. (2006) Quantitative analysis of radiation-induced DNA break repair in a cultured oral mucosal model. Tissue Eng 12, 3395-3403.

Rasmussen, J.W., Martinez, E., Louka, P. and Wingett, D.G. (2010) Zinc oxide nanoparticles for selective destruction of tumor cells and potential for drug delivery applications. Expert Opin Drug Deliv 7, 1063-1077.

Ravichandran, P., Periyakaruppan, A., Sadanandan, B., Ramesh, V., Hall, J.C., Jejelowo, O. and Ramesh, G.T. (2009) Induction of apoptosis in rat lung epithelial cells by multiwalled carbon nanotubes. J Biochem Mol Toxicol 23, 333-344.

Reddy, A.R., Reddy, Y.N., Krishna, D.R. and Himabindu, V. (2010) Multi wall carbon nanotubes induce oxidative stress and cytotoxicity in human embryonic kidney (HEK293) cells. Toxicology 272, 11-16.

Reddy, K.M., Feris, K., Bell, J., Wingett, D.G., Hanley, C. and Punnoose, A. (2007) Selective toxicity of zinc oxide nanoparticles to prokaryotic and eukaryotic systems. Appl Phys Lett 90, 2139021-2139023.

Rejman, J., Oberle, V., Zuhorn, I.S. and Hoekstra, D. (2004) Size-dependent internalization of particles via the pathways of clathrin- and caveolae-mediated endocytosis. Biochem J 377, 159-169.

Ringwood, A.H., Levi-Polyachenko, N. and Carroll, D.L. (2009a) Fullerene exposures with oysters: embryonic, adult, and cellular responses. Environ Sci Technol 43, 7136-7141.

Ringwood, A.H., McCarthy, M., Bates, T.C. and Carroll, D.L. (2009b) The effects of silver nanoparticles on oyster embryos. Mar Environ Res.

Roberts, P.J. and Der, C.J. (2007) Targeting the Raf-MEK-ERK mitogen-activated protein kinase cascade for the treatment of cancer. Oncogene 26, 3291-3310.

Roberts, R.A., Smith, R.A., Safe, S., Szabo, C., Tjalkens, R.B. and Robertson, F.M. (2010) Toxicological and pathophysiological roles of reactive oxygen and nitrogen species. Toxicology 276, 85-94.

Roh, J.Y., Sim, S.J., Yi, J., Park, K., Chung, K.H., Ryu, D.Y. and Choi, J. (2009) Ecotoxicity of silver nanoparticles on the soil nematode Caenorhabditis elegans using functional ecotoxicogenomics. Environ Sci Technol 43, 3933-3940.

Romero, G., Estrela-Lopis, I., Zhou, J., Rojas, E., Franco, A., Espinel, C.S., Fernandez, A.G., Gao, C., Donath, E. and Moya, S.E. (2010) Surface Engineered Poly(lactide-co-glycolide) Nanoparticles for Intracellular Delivery: Uptake and Cytotoxicity-A Confocal Raman Microscopic Study. Biomacromolecules.

Rouas, C., Bensoussan, H., Suhard, D., Tessier, C., Grandcolas, L., Rebiere, F., Dublineau, I., Taouis, M., Pallardy, M., Lestaevel, P. and Gueguen, Y. (2010) Distribution of Soluble Uranium in the Nuclear Cell Compartment at Subtoxic Concentrations. Chem Res Toxicol.

Rouse, J.G., Haslauer, C.M., Loboa, E.G. and Monteiro-Riviere, N.A. (2008) Cyclic tensile strain increases interactions between human epidermal keratinocytes and quantum dot nanoparticles. Toxicol In Vitro 22, 491-497.

RS/RAE. (2004) The Royal Society and the Royal Academy of Engineering. Nanoscience and Nanotechnologies: Opportunities and Uncertainties. Royal Society Policy Document 19/04. .

Rupper, A. and Cardelli, J. (2001) Regulation of phagocytosis and endo-phagosomal trafficking pathways in Dictyostelium discoideum. Biochim Biophys Acta 1525, 205-216.

Ryman-Rasmussen, J.P., Riviere, J.E. and Monteiro-Riviere, N.A. (2006) Penetration of intact skin by quantum dots with diverse physicochemical properties. Toxicol Sci 91, 159-165.

Ryman-Rasmussen, J.P., Riviere, J.E. and Monteiro-Riviere, N.A. (2007) Surface coatings determine cytotoxicity and irritation potential of quantum dot nanoparticles in epidermal keratinocytes. J Invest Dermatol 127, 143-153.

Sager, T., Porter, D., Robinson, V., Lindsley, W., Schwegler-, Berry, D. and Castranova, V. (2008) Improved method to disperse nanoparticles for in vitro and in vivo investigation of toxicity. Nanotoxicology 1, 118-129.

Sayes, C.M., Reed, K.L. and Warheit, D.B. (2007) Assessing toxicity of fine and nanoparticles: comparing in vitro measurements to in vivo pulmonary toxicity profiles. Toxicol Sci 97, 163-180.

Sayes, C.M. and Warheit, D.B. (2009) Characterization of nanomaterials for toxicity assessment. Wiley Interdiscip Rev Nanomed Nanobiotechnol 1, 660-670.

SCCP. (2007) Scientific Committee on Consumer Products. Opinion on safety of nanomaterials in cosmetic products. European Commission. SCCP/1147/07.

SCENIHR. (2009) European Commission Scientific Committee on Emerging and Newly Identified Health Risks. Risk Assessment of Products of Nanotechnologies.

Schilling, K., Bradford, B., Castelli, D., Dufour, E., Nash, J.F., Pape, W., Schulte, S., Tooley, I., van den Bosch, J. and Schellauf, F. (2010) Human safety review of "nano" titanium dioxide and zinc oxide. Photochem Photobiol Sci 9, 495-509.

Schulz, J., Hohenberg, H., Pflucker, F., Gartner, E., Will, T., Pfeiffer, S., Wepf, R., Wendel, V., Gers-Barlag, H. and Wittern, K.P. (2002) Distribution of sunscreens on skin. Adv Drug Deliv Rev 54 Suppl 1, S157-163.

Scown, T.M., Santos, E.M., Johnston, B.D., Gaiser, B., Baalousha, M., Mitov, S., Lead, J.R., Stone, V., Fernandes, T.F., Jepson, M., van Aerle, R. and Tyler, C.R. (2010) Effects of aqueous exposure to silver nanoparticles of different sizes in rainbow trout. Toxicol Sci 115, 521-534.

Sharma, H.S., Hussain, S., Schlager, J., Ali, S.F. and Sharma, A. (2010) Influence of nanoparticles on blood-brain barrier permeability and brain edema formation in rats. Acta Neurochir Suppl 106, 359-364.

Sharma, S.K., Pujari, P.K., Sudarshan, K., Dutta, D., Mahapatra, M., Godbole, S.V., Jayakumar, O.D. and Tyagi, A.K. (2009) Positron annihilation studies in ZnO nanoparticles. Solid State Communications 149, 550-554.

Shieh, S.Y., Ikeda, M., Taya, Y. and Prives, C. (1997) DNA damage-induced phosphorylation of p53 alleviates inhibition by MDM2. Cell 91, 325-334.

Shukla, R.K., Sharma, V., Pandey, A.K., Singh, S., Sultana, S. and Dhawan, A. (2011) ROS-mediated genotoxicity induced by titanium dioxide nanoparticles in human epidermal cells. Toxicol In Vitro 25, 231-241.

Simonelli, A., Miraglia, N., Basilicata, P., Pieri, M., Loredana, C., Genovese, G., Guadagni, R., Acampora, A. and Sannolo, N. (2007) Interactions between nanoparticles and living organisms: Mechanisms and health effects. Nanotoxicology, Edited by Y. Zhao and H.S. Nalwa. American Scientific Publishers, USA.

Singh, N., Manshian, B., Jenkins, G.J., Griffiths, S.M., Williams, P.M., Maffeis, T.G., Wright, C.J. and Doak, S.H. (2009) NanoGenotoxicology: the DNA damaging potential of engineered nanomaterials. Biomaterials 30, 3891-3914.

Singh, N.P., McCoy, M.T., Tice, R.R. and Schneider, E.L. (1988) A simple technique for quantitation of low levels of DNA damage in individual cells. Exp Cell Res 175, 184-191.

Sinha, R., Karan, R., Sinha, A. and Khare, S.K. (2010) Interaction and nanotoxic effect of ZnO and Ag nanoparticles on mesophilic and halophilic bacterial cells. Bioresour Technol.

Skebo, J.E., Grabinski, C.M., Schrand, A.M., Schlager, J.J. and Hussain, S.M. (2007) Assessment of metal nanoparticle agglomeration, uptake, and interaction using high-illuminating system. Int J Toxicol 26, 135-141.

Slamenova, D., Kovacikova, I., Horvathova, E., Wsolova, L. and Navarova, J. (2010) Carboxymethyl chitin-glucan (CM-CG) protects human HepG2 and HeLa cells against oxidative DNA lesions and stimulates DNA repair of lesions induced by alkylating agents. Toxicol In Vitro 24, 1986-1992.

Smith, C.C., O'Donovan, M.R. and Martin, E.A. (2006) hOGG1 recognizes oxidative damage using the comet assay with greater specificity than FPG or ENDOIII. Mutagenesis 21, 185-190.

Sonavane, G., Tomoda, K., Sano, A., Ohshima, H., Terada, H. and Makino, K. (2008) In vitro permeation of gold nanoparticles through rat skin and rat intestine: effect of particle size. Colloids Surf B Biointerfaces 65, 1-10.

Song, M.M., Song, W.J., Bi, H., Wang, J., Wu, W.L., Sun, J. and Yu, M. (2010) Cytotoxicity and cellular uptake of iron nanowires. Biomaterials 31, 1509-1517.

Song, W., Zhang, J., Guo, J., Ding, F., Li, L. and Sun, Z. (2009) Role of the dissolved zinc ion and reactive oxygen species in cytotoxicity of ZnO nanoparticles. Toxicol Lett 199, 389-397.

Speit, G. and Hartmann, A. (2006) The comet assay: a sensitive genotoxicity test for the detection of DNA damage and repair. Methods Mol Biol 314, 275-286.

Stap, J., Krawczyk, P.M., Van Oven, C.H., Barendsen, G.W., Essers, J., Kanaar, R. and Aten, J.A. (2008) Induction of linear tracks of DNA double-strand breaks by alpha-particle irradiation of cells. Nat Methods 5, 261-266.

Su, Y., He, Y., Lu, H., Sai, L., Li, Q., Li, W., Wang, L., Shen, P., Huang, Q. and Fan, C. (2009) The cytotoxicity of cadmium based, aqueous phase - synthesized, quantum dots and its modulation by surface coating. Biomaterials 30, 19-25.

Suzuki, H., Toyooka, T. and Ibuki, Y. (2007) Simple and easy method to evaluate uptake potential of nanoparticles in mammalian cells using a flow cytometric light scatter analysis. Environ Sci Technol 41, 3018-3024.

Tang, J., Xiong, L., Wang, S., Wang, J., Liu, L., Li, J., Yuan, F. and Xi, T. (2009) Distribution, translocation and accumulation of silver nanoparticles in rats. J Nanosci Nanotechnol 9, 4924-4932.

Tang, M., Xing, T., Zeng, J., Wang, H., Li, C., Yin, S., Yan, D., Deng, H., Liu, J., Wang, M., Chen, J. and Ruan, D.Y. (2008) Unmodified CdSe quantum dots induce elevation of cytoplasmic calcium levels and impairment of functional properties of sodium channels in rat primary cultured hippocampal neurons. Environ Health Perspect 116, 915-922.

Tao, X., Fortner, J.D., Zhang, B., He, Y., Chen, Y. and Hughes, J.B. (2009) Effects of aqueous stable fullerene nanocrystals (nC60) on Daphnia magna: evaluation of sub-lethal reproductive responses and accumulation. Chemosphere 77, 1482-1487.

Tarantola, M., Schneider, D., Sunnick, E., Adam, H., Pierrat, S., Rosman, C., Breus, V., Sonnichsen, C., Basche, T., Wegener, J. and Janshoff, A. (2009) Cytotoxicity of metal and semiconductor nanoparticles indicated by cellular micromotility. ACS Nano 3, 213-222.

Teeguarden, J., Hinderliter, P., Orr, G., Thrall, B. and Pounds, J. (2007) Particokinetics in vitro: Dosimetry considerations for in vitro nanoparticles toxicity assessments. Toxicol Sci 95, 300-312.

Thakor, A.S., Paulmurugan, R., Kempen, P., Zavaleta, C., Sinclair, R., Massoud, T.F. and Gambhir, S.S. (2011) Oxidative stress mediates the effects of Raman-active gold nanoparticles in human cells. Small 7, 126-136.

Thannickal, V.J. and Fanburg, B.L. (2000) Reactive oxygen species in cell signaling. Am J Physiol Lung Cell Mol Physiol 279, L1005-1028.

Theng, B.K.G. and Yuan, G. (2008) Nanoparticles in the soil environment. Elements 4, 395-399.

Tice, R.R., Agurell, E., Anderson, D., Burlinson, B., Hartmann, A., Kobayashi, H., Miyamae, Y., Rojas, E., Ryu, J.C. and Sasaki, Y.F. (2000) Single cell gel/comet assay: guidelines for in vitro and in vivo genetic toxicology testing. Environ Mol Mutagen 35, 206-221.

Tinkle, S.S., Antonini, J.M., Rich, B.A., Roberts, J.R., Salmen, R., DePree, K. and Adkins, E.J. (2003) Skin as a route of exposure and sensitization in chronic beryllium disease. Environ Health Perspect 111, 1202-1208.

Torchilin, V.P., Rammohan, R., Weissig, V. and Levchenko, T.S. (2001) TAT peptide on the surface of liposomes affords their efficient intracellular delivery even at low temperature and in the presence of metabolic inhibitors. Proc Natl Acad Sci U S A 98, 8786-8791.

Toyokuni, S. (1998) Oxidative stress and cancer: the role of redox regulation. Biotherapy 11, 147-154.

Trop, M., Novak, M., Rodl, S., Hellbom, B., Kroell, W. and Goessler, W. (2006) Silver-coated dressing acticoat caused raised liver enzymes and argyria-like symptoms in burn patient. J Trauma 60, 648-652.

Tsaousi, A., Jones, E. and Case, C.P. (2010) The in vitro genotoxicity of orthopaedic ceramic (Al2O3) and metal (CoCr alloy) particles. Mutat Res 697, 1-9.

USEPA. (2007) Nanotechnology White Paper. Science Policy Council. United States Environmental Protection Agency. EPA 100/B-07/ 001.

Utley, H., Bernheim, F. and Hochstein, P. (1976) Effect of sulfhydryl reagents on peroxidation in microsomes. Arch Biochem Biophys 118, 29-32.

Van Bladeren, P.J. (2000) Glutathione conjugation as a bioactivation reaction. Chem Biol Interact 129, 61-76.

Vigneron, A. and Vousden, K.H. (2010) p53, ROS and senescence in the control of aging. Aging (Albany NY) 2, 471-474.

Vlasits, J., Jakopitsch, C., Bernroitner, M., Zamocky, M., Furtmuller, P.G. and Obinger, C. (2010) Mechanisms of catalase activity of heme peroxidases. Arch Biochem Biophys 500, 74-81.

Vucic, D. and Fairbrother, W.J. (2007) The inhibitor of apoptosis proteins as therapeutic targets in cancer. Clin Cancer Res 13, 5995-6000.

Walker, V.G., Li, Z., Hulderman, T., Schwegler-Berry, D., Kashon, M.L. and Simeonova, P.P. (2009) Potential in vitro effects of carbon nanotubes on human aortic endothelial cells. Toxicol Appl Pharmacol 236, 319-328.

Wan, C.P., Myung, E. and Lau, B.H. (1993) An automated micro-fluorometric assay for monitoring oxidative burst activity of phagocytes. J Immunol Methods 159, 131-138.

Wang, B., Feng, W., Wang, M., Wang, T., Gu, T., Zhu, M., Ouyang, H., Shi, J., Zhang, F., Zhao, Y., Chai, Z., Wang, H. and Wang, J. (2008a) Acute toxicological impact of nano- and submicro-scaled zinc oxide powder on healthy adult mice. J Nanopart Res 10, 263-276.

Wang, H.J., Growcock, A.C., Tang, T.H., O'Hara, J., Huang, Y.W. and Aronstam, R.S. (2010a) Zinc oxide nanoparticle disruption of store-operated calcium entry in a muscarinic receptor signaling pathway. Toxicol In Vitro 24, 1953-1961.

Wang, J., Zhou, G., Chen, C., Yu, H., Wang, T., Ma, Y., Jia, G., Gao, Y., Li, B., Sun, J., Li, Y., Jiao, F., Zhao, Y. and Chai, Z. (2007) Acute toxicity and biodistribution of different sized titanium dioxide particles in mice after oral administration. Toxicol Lett 168, 176-185.

Wang, L., Nagesha, D.K., Selvarasah, S., Dokmeci, M.R. and Carrier, R.L. (2008b) Toxicity of CdSe Nanoparticles in Caco-2 Cell Cultures. J Nanobiotechnology 6, 11.

Wang, L., Mercer, R.R., Rojanasakul, Y., Qiu, A., Lu, Y., Scabilloni, J.F., Wu, N. and Castranova, V. (2010b) Direct fibrogenic effects of dispersed single-walled carbon nanotubes on human lung fibroblasts. J Toxicol Environ Health A 73, 410-422.

Wang, Y. and Wu, W. (2006) In situ evading of phagocytic uptake of stealth solid lipid nanoparticles by mouse peritoneal macrophages. Drug Deliv 13, 189-192.

Warheit, D.B., Brock, W.J., Lee, K.P., Webb, T.R. and Reed, K.L. (2005) Comparative pulmonary toxicity inhalation and instillation studies with different TiO2 particle formulations: impact of surface treatments on particle toxicity. Toxicol Sci 88, 514-524.

Warheit, D.B. (2008) How meaningful are the results of nanotoxicity studies in the absence of adequate material characterization? Toxicol Sci 101, 183-185.

Warheit, D.B., Sayes, C.M. and Reed, K.L. (2009) Nanoscale and fine zinc oxide particles: can in vitro assays accurately forecast lung hazards following inhalation exposures? Environ Sci Technol 43, 7939-7945.

Weibel, A., Bouchet, R., Boulc'h, F. and Knauth, P. (2005) The big problem of small particles: A comparison of methods for determination of particle size in nanocrystalline anatase powders. Chemistry of Materials 17, 2378-2385.

Wick, P., Manser, P., Limbach, L.K., Dettlaff-Weglikowska, U., Krumeich, F., Roth, S., Stark, W.J. and Bruinink, A. (2007) The degree and kind of agglomeration affect carbon nanotube cytotoxicity. Toxicol Lett 168, 121-131.

Wiesenthal, A., Hunter, L., Wang, S., Wickliffe, J. and Wilkerson, M. (2011) Nanoparticles: small and mighty. Int J Dermatol 50, 247-254.

Wise, J.P., Sr., Goodale, B.C., Wise, S.S., Craig, G.A., Pongan, A.F., Walter, R.B., Thompson, W.D., Ng, A.K., Aboueissa, A.M., Mitani, H., Spalding, M.J. and Mason, M.D. (2010) Silver nanospheres are cytotoxic and genotoxic to fish cells. Aquat Toxicol 97, 34-41.

Witasp, E., Shvedova, A.A., Kagan, V.E. and Fadeel, B. (2009) Single-walled carbon nanotubes impair human macrophage engulfment of apoptotic cell corpses. Inhal Toxicol 21 Suppl 1, 131-136.

Wiwanitkit, V., Sereemaspun, A. and Rojanathanes, R. (2009) Effect of gold nanoparticles on spermatozoa: the first world report. Fertil Steril 91, e7-8.

Wu, J., Liu, W., Xue, C., Zhou, S., Lan, F., Bi, L., Xu, H., Yang, X. and Zeng, F.D. (2009) Toxicity and penetration of TiO(2) nanoparticles in hairless mice and porcine skin after subchronic dermal exposure. Toxicol Lett.

Wu, J.C., Chye, S.M., Shih, M.K., Chen, C.H., Yang, H.L. and Chen, S.C. (2010) Genotoxicity of dicrotophos, an organophosphorous pesticide, assessed with different assays in vitro. Environ Toxicol.

Xia, L., Lenaghan, S.C., Zhang, M., Zhang, Z. and Li, Q. (2010) Naturally occurring nanoparticles from English ivy: an alternative to metal-based nanoparticles for UV protection. J Nanobiotechnology 8, 12.

Xia, T., Kovochich, M., Brant, J., Hotze, M., Sempf, J., Oberley, T., Sioutas, C., Yeh, J.I., Wiesner, M.R. and Nel, A.E. (2006) Comparison of the abilities of ambient and manufactured nanoparticles to induce cellular toxicity according to an oxidative stress paradigm. Nano Lett 6, 1794-1807.

Xia, T., Kovochich, M., Liong, M., Madler, L., Gilbert, B., Shi, H., Yeh, J.I., Zink, J.I. and Nel, A.E. (2008) Comparison of the mechanism of toxicity of zinc oxide and cerium oxide nanoparticles based on dissolution and oxidative stress properties. ACS Nano 2, 2121-2134.

Xie, G., Sun, J., Zhong, G., Shi, L. and Zhang, D. (2009) Biodistribution and toxicity of intravenously administered silica nanoparticles in mice. Arch Toxicol 84, 183-190.

Xu, A., Chai, Y., Nohmi, T. and Hei, T.K. (2009) Genotoxic responses to titanium dioxide nanoparticles and fullerene in gpt delta transgenic MEF cells. Part Fibre Toxicol 6, 3.

Yadav, A., Prasad, V., Kathe, A.A., Raj, S., Yadav, D., Sundaramoorthy, C. and Vigneshwaran, N. (2006) Functional finishing in cotton fabrics using zinc oxide nanoparticles. Bull. Mater. Sci.

Yang, H., Liu, C., Yang, D., Zhang, H. and Xi, Z. (2009a) Comparative study of cytotoxicity, oxidative stress and genotoxicity induced by four typical nanomaterials: the role of particle size, shape and composition. J Appl Toxicol 29, 69-78.

Yang, S.T., Wang, X., Jia, G., Gu, Y., Wang, T., Nie, H., Ge, C., Wang, H. and Liu, Y. (2008) Long-term accumulation and low toxicity of single-walled carbon nanotubes in intravenously exposed mice. Toxicol Lett 181, 182-189.

Yang, W., Shen, C., Ji, Q., An, H., Wang, J., Liu, Q. and Zhang, Z. (2009b) Food storage material silver nanoparticles interfere with DNA replication fidelity and bind with DNA. Nanotechnology 20, 085102.

Yang, X.Y., Edelmann, R.E. and Oris, J.T. (2009c) Suspended C(60) nanoparticles protect against short-term UV and fluoranthene photo-induced toxicity, but cause long-term cellular damage in Daphnia magna. Aquat Toxicol.

Yin, H., Casey, P.S., McCall, M.J. and Fenech, M. (2010) Effects of surface chemistry on cytotoxicity, genotoxicity, and the generation of reactive oxygen species induced by ZnO nanoparticles. Langmuir 26, 15399-15408.

Yuranova, T., Laub, D. and Kiwi, J. (2007) Synthesis activity and characterization of textiles showing self-cleaning activity under daylight irradiation. Catal Today 122, 109-117.

Zamocky, M., Furtmuller, P.G. and Obinger, C. (2008) Evolution of catalases from bacteria to humans. Antioxid Redox Signal 10, 1527-1548.

Zhang, L.W. and Monteiro-Riviere, N.A. (2008) Assessment of quantum dot penetration into intact, tape-stripped, abraded and flexed rat skin. Skin Pharmacol Physiol 21, 166-180.

Zhang, L.W., Yu, W.W., Colvin, V.L. and Monteiro-Riviere, N.A. (2008) Biological interactions of quantum dot nanoparticles in skin and in human epidermal keratinocytes. Toxicol Appl Pharmacol 228, 200-211.

Zhang, L.W., Yang, J., Barron, A.R. and Monteiro-Riviere, N.A. (2009) Endocytic mechanisms and toxicity of a functionalized fullerene in human cells. Toxicol Lett 191, 149-157.

Zhang, Y., Ali, S.F., Dervishi, E., Xu, Y., Li, Z., Casciano, D. and Biris, A.S. Cytotoxicity effects of graphene and single-wall carbon nanotubes in neural phaeochromocytoma-derived PC12 cells. ACS Nano 4, 3181-3186.

Zhang, Y., Chen, W., Zhang, J., Liu, J., Chen, G. and Pope, C. (2007) In vitro and in vivo toxicity of CdTe nanoparticles. J Nanosci Nanotechnol 7, 497-503.

Zhang, Y. and Dong, C. (2007) Regulatory mechanisms of mitogen-activated kinase signaling. Cell Mol Life Sci 64, 2771-2789.

Zhang, Y., Jiang, L., Geng, C., Li, L., Shao, J. and Zhong, L. (2011) Possible involvement of oxidative stress in potassium bromate-induced genotoxicity in human HepG2 cells. Chem Biol Interact 189, 186-191.

Zhao, J., Xu, L., Zhang, T., Ren, G. and Yang, Z. (2009) Influences of nanoparticle zinc oxide on acutely isolated rat hippocampal CA3 pyramidal neurons. Neurotoxicology 30, 220-230.

Zhao, Y., Meng, H., Chen, Z., Zhao, F. and Chai, Z. (2007) Chapter 1: Biological Activities of Nanomaterials/Nanoparticles. Nanotoxicology, Edited by Y. Zhao and H.S. Nalwa. American Scientific Publishers, USA.

Zhou, P., Gross, S., Liu, J.H., Yu, B.Y., Feng, L.L., Nolta, J., Sharma, V., Piwnica-Worms, D. and Qiu, S.X. (2010) Flavokawain B, the hepatotoxic constituent from

kava root, induces GSH-sensitive oxidative stress through modulation of IKK/NF-kappaB and MAPK signaling pathways. FASEB J 24, 4722-4732.

Zhu, X., Zhu, L., Lang, Y. and Chen, Y. (2008) Oxidative stress and growth inhibition in the freshwater fish Carassius auratus induced by chronic exposure to sublethal fullerene aggregates. Environ Toxicol Chem 27, 1979-1985.

Zhu, X., Wang, J., Zhang, X., Chang, Y. and Chen, Y. (2009) The impact of ZnO nanoparticle aggregates on the embryonic development of zebrafish (Danio rerio). Nanotechnology 20, 195103.

Publications and presentations originating from this study

Publications:

- Alok Dhawan, **Vyom Sharma** and Devendra Parmar. Nanomaterials: A challenge for toxicologists. *Nanotoxicology* **2009,** 3(1): 1-9 (Review).

- **Vyom Sharma**, Ritesh K Shukla, Neha Saxena, Devendra Parmar, Mukul Das and Alok Dhawan. DNA damaging potential of zinc oxide nanoparticles in human epidermal cells. *Toxicology Letters* **2009**, 185; 211-218.[The article featured in the European Commission document "Science for Environment Policy – Nanomaterials", Issue 12, Page 4, April 2009]

- Alok Dhawan and **Vyom Sharma**. Toxicity assessment of nanomaterials: methods and challenges. *Analytical and Bioanalytical Chemistry* **2010,** 398: 589-605 (Review).

- **Vyom Sharma**, Suman K. Singh, Diana Anderson, Desmond J. Tobin and Alok Dhawan. Zinc oxide nanoparticle induced genotoxicity in primary human epidermal keratinocytes. *Journal of Nanoscience and Nanotechnology* **2011,** 11: 3782-3788.

- **Vyom Sharma**, Diana Anderson and Alok Dhawan. Zinc oxide nanoparticles induce oxidative DNA damage and ROS-triggered mitochondria mediated apoptosis in human liver cells (HepG2) (Revised manuscript submitted to *Apoptosis*).

- **Vyom Sharma**, Poonam Singh, Alok K Pandey, Alok Dhawan. Induction of oxidative stress, DNA damage and apoptosis in mice liver after acute oral exposure to zinc oxide nanoparticles (Under review).

Poster presentations:

- **Best Poster Presentation Award: Vyom Sharma**, Diana Anderson and Alok Dhawan. Zinc oxide nanoparticles induce oxidative stress and genotoxicity in human liver cells (HepG2).
  International Symposium on the Safe Use of Nanomaterials (SUN 2011), Indian Institute of Toxicology Research, Lucknow, India, February 1-3, **2011**.

- **Vyom Sharma**, Anshi Shukla, Kavita Seth, Diana Anderson, Alok Dhawan. ZnO nanoparticles induce oxidative DNA damage and JNK-mediated apoptosis in human liver cells (HepG2).
  Nanotoxicology- 2010,
  Edinburgh Napier University, Edinburgh, UK, June 2-4, **2010**.

- **Best Poster Presentation Award: Vyom Sharma**, Ritesh K Shukla, Neha Saxena, Devendra Parmar, Mukul Das and Alok Dhawan. Zinc oxide nanoparticles induce cytotoxicity and DNA damage in human skin epithelial cell line.
  International Conference on Nanomaterial Toxicology (ICONTOX)
  Indian Institute of Toxicology Research, Lucknow, February 5-7, **2008**.

Published abstracts in international journals:

- **Vyom Sharma**, Diana Anderson and Alok Dhawan. Zinc oxide nanoparticles induce oxidative stress and genotoxicity in human liver cells (HepG2). *Journal of Biomedical Nanotechnology* **2011**, 7; 98-99.

- **Vyom Sharma**, Ritesh K Shukla, Neha Saxena, Devendra Parmar, Mukul Das and Alok Dhawan. Zinc oxide nanoparticles induce cytotoxicity and DNA damage in human skin epithelial cell line. *Nanotoxicology* **2008**, 2 (S1); 83.

- Alok Dhawan, **Vyom Sharma** and Devendra Parmar. Nanomaterial: A challenge for toxicologists. *Nanotoxicology* **2008**, 2 (S1); 29.